(7150)

The Loma Prieta, California, Earthquake of October 17, 1989—Earth Structures and Engineering Characterization of Ground Motion

THOMAS L. HOLZER, *Editor*

PERFORMANCE OF THE BUILT ENVIRONMENT
THOMAS L. HOLZER, *Coordinator*

U.S. GEOLOGICAL SURVEY PROFESSIONAL PAPER 1552–D

Prepared in cooperation with the National Science Foundation

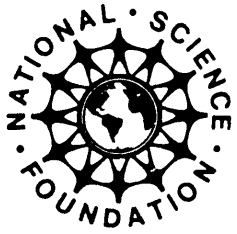

UNITED STATES GOVERNMENT PRINTING OFFICE, WASHINGTON : 1998

DEPARTMENT OF THE INTERIOR

BRUCE BABBITT, *Secretary*

U.S. GEOLOGICAL SURVEY

Charles G. Groat, *Director*

Text and illustrations edited by Jeff Troll

Manuscript approved for publication, January 24, 1997

Library of Congress catalog-card No. 92-32287

For sale by
U.S. Geological Survey, Map Distribution
Box 25286, MS 306, Federal Center
Denver, CO 80225

CONTENTS

EARTH STRUCTURES AND ENGINEERING CHARACTERIZATION OF GROUND MOTION

INTRODUCTION

By Thomas L. Holzer,
U.S. Geological Survey

This chapter contains two papers that summarize the performance of engineered earth structures—dams and stabilized excavations in soil—and two papers that characterize for engineering purposes the attenuation of ground motion with distance during the Loma Prieta earthquake. Documenting the field performance of engineered structures and confirming empirically based predictions of ground motion are critical for safe and cost effective seismic design of future structures as well as the retrofitting of existing ones.

Catastrophic flooding caused by dam failure is a persistent concern in areas with earthquake potential. Harder and others (this chapter) present a valuable compilation of the performance of earth dams during the 1989 earthquake. They estimate that 111 dams, the majority of which were homogenous earth dams, were within 80 km of the seismogenic rupture. Thirty-six of these dams experienced free-field peak horizontal ground accelerations greater than 0.2 *g*, but only one major dam—Austrian—and one minor dam—Soda Lake—suffered moderate damage. The authors conclude that low reservoir levels, which reduced saturation of embankments, was a major contributor to the good performance of these dams. The field performance and strong-motion data provide an opportunity to learn more about how earth and rockfill dams behave during earthquakes at low reservoir levels.

Failures of embankments in soils during earthquakes both disrupt traffic and damage nearby buildings. Vucetic and others (this chapter) evaluate the performance of nine excavations that were stabilized by soil nailing, an in-situ technique used to reinforce existing soil masses during excavation by horizontally drilling and installing passive inclusions. The inclusions, called nails, cause the soil to behave as a composite unit. The 1989 earthquake provided the first seismic loading of earth structures of this type and thus presents a special opportunity to evaluate the performance of nailed walls. None of the nine soil-nailed excavations evaluated by the authors showed any signs of distress or movement even though one in the epicentral regional was strongly shaken. The authors conclude that conservative design and construction are the primary reasons for their good performance.

The most common methods for estimating ground motion in future earthquakes in California are empirical and rely on syntheses of observations from previous earthquakes. Papers by Campbell (this chapter) and Bozorgnia and Niazi (this chapter) build on this tradition. For further discussion of other aspects of strong ground motion during the earthquake, the reader is referred to the 16 papers in Borcherdt (1994) as well as selected papers in Spudich (1996).

Campbell (this chapter) examines the dependence of recorded peak horizontal acceleration, peak horizontal velocity, and Modified Mercalli Intensity on distance from the seismogenic rupture zone, source-to-site azimuth, and site geology. He develops empirical fits to these parameters. He concludes that peak accelerations recorded on alluvium at sites more than 50 km from the seismogenic rupture zone were significantly higher than would have been predicted by existing attenuation relations available at the time of the earthquake. He also notes a strong directional or azimuthal dependence of ground motion and intensity. Significantly higher amplitudes corresponded to azimuths pointed at Santa Cruz, San Francisco, and Oakland than at azimuths to the northeast and east. Local site geology strongly affected ground motion with sites underlain by Holocene San Francisco bay mud typically recording higher accelerations.

Bozorgnia and Niazi (this chapter) study the frequency dependence of the attenuation of ground motion by examining vertical and horizontal response spectra for spectral ordinates at periods ranging from 0.05 to 2 s. They observe that the shape of the response spectra for both vertical and horizontal components of ground motion and their ratio depends on both distance and magnitude. The vertical-to-horizontal spectral ratio at higher frequencies is substantially higher than the two-thirds value commonly used in engineering practice. The ratio is highest near the earthquake source. However, at low frequencies and farther from the earthquake source, the spectral ratio decreases significantly, which implies current design practice is conservative.

REFERENCES CITED

Borcherdt, R.B., ed., 1994, The Loma Prieta, California, earthquake of October 17, 1989—Strong ground motion: U.S. Geological Professional Paper 1551-A, 272 p.

Spudich, P.A., ed., 1996, The Loma Prieta, California, earthquake of October 17, 1989—Main-shock characteristics: U.S. Geological Professional Paper 1550-A, 297 p.

EARTH STRUCTURES AND ENGINEERING CHARACTERIZATION OF GROUND MOTION

PERFORMANCE OF EARTH DAMS DURING THE LOMA PRIETA EARTHQUAKE

By L.F. Harder, Jr., California Department of Water Resources, Sacramento, Calif.;
J.D. Bray, University of California, Berkeley, Calif.;
R.L. Volpe, R.L. Volpe & Associates, Los Gatos, Calif.; and
K.V. Rodda, Wahler Associates, Palo Alto, Calif.

CONTENTS

ABSTRACT

The earthquake shook a large number of earth and rockfill dams. There were more than 100 dams within 50 miles of the fault rupture associated with this event. Although more than half of the dams were less than 60 feet in height, a number of major dams were strongly shaken. In general, the dams performed satisfactory with one major dam and one minor dam developing moderate damage. A small number also developed minor to moderate cracking and required repairs. The great majority, however, sustained no significant damage. Although this result was very encouraging, it should be tempered by the fact that the reservoirs retained by many of these dams were low at the time of the earthquake. In addition, the duration of strong shaking during this earthquake was relatively short. Consequently, the earthquake was not the most critical test of these structures.

INTRODUCTION

The earthquake resulted from a slip on a segment of the San Andreas fault near Santa Cruz, Calif. As summarized by Spudich (1996), slip occurred on a dipping fault surface approximately 22 miles long and was generally confined to depths between 4 and 12 miles. From the hypocenter, slip propagated in both the northwest and southeast directions over a relatively short source duration of approximately 6 to15 s. Most studies suggest that slip in the southeast portion was predominantly strike-slip, whereas slip in the northwest portion also had a significant thrust component.

Most of the slip associated with the main shock is considered to have stopped within 4 miles of the ground surface, although surface cracking observed in the area near the fault may have been associated with zones of compression and extension generated by a tectonically offset basement (Spudich, 1996). The event represents the largest earthquake in the San Francisco/Santa Cruz area since the great 1906 San Francisco earthquake of magnitude 8+. The Loma Prieta fault rupture occurred along a portion of the San Andreas fault segment which ruptured during the 1906 earthquake.

The duration of strong shaking for this earthquake was generally between 7 and 10 s, about half of that usually associated with a magnitude 7 event. It has been speculated that this short duration was a result of the central location of the earthquake's focal point and its bidirectional rupture pattern (see Seed and others, 1990). The highest horizontal ground acceleration recorded was 0.64 *g* and was measured at the Corralitos station located adjacent to the surface projection of the fault rupture and only a few miles from the epicenter. Seismographs in the epicentral area also recorded relatively high vertical accelerations that were comparable to those recorded in the horizontal direction. For example, at

the Capitola recording station, located approximately 9 miles southwest of the epicenter, the peak vertical acceleration was 0.60 *g* whereas the peak horizontal acceleration was 0.54 *g*.

CHARACTERISTICS OF EARTH DAMS CONSIDERED IN THIS STUDY

Presented in figure 1 is a map showing the epicenter and locations of major aftershocks associated with the earthquake. Also shown in this figure are the locations of 111 earth dams situated within 50 miles of the fault rupture zone. The majority of these dams are essentially homogeneous earth dams. The heights and completion dates for these dams are summarized in tables 1 and 2.

Table 3 presents a listing of the number of dams subjected to various levels of ground shaking during the earthquake. The estimates of peak ground acceleration were developed by interpolating between values measured at nearby seismographic stations.

Most of the reservoirs in the affected area were relatively low at the time of the earthquake, with many at less than half their normal heights. Some reservoirs were essentially empty. This was a result of the fact that the earthquake occurred immediately after the irrigation season following 3 years of lower-than-average rainfall.

PRE-1906 EARTH DAMS

Of the 21 dams built prior to the 1906 earthquake, none experienced significant damage as a result of the Loma Prieta earthquake. This is not unexpected, as these dams generally performed satisfactorily during the 1906 earthquake. Because the 1906 earthquake involved a much greater fault rupture and release of energy, all of these older dams had probably been subjected to much greater amplitudes and durations of shaking during that event than during Loma Prieta. Many of these older dams were located relatively close to the 1906 fault rupture and have been estimated to have been shaken by motions having peak accelerations between 0.6 and 0.8 *g* (Seed and others, 1978).

In their examination of the performance of earth dams during earthquakes, Seed and others (1978) attributed the good performance of these older dams during the 1906 earthquake to the fact that they were constructed mostly of clayey soils and built on either clayey or rock foundations. Such materials are generally thought to retain most of their strengths during strong shaking.

Two of these older dams, University Mound N. Basin and Piedmont Dams, were built primarily of sandy soils but were not thought to have been saturated at the time of the 1906 earthquake. These two dams are located more than 45 miles from the Loma Prieta fault-rupture zone and experienced peak ground accelerations of only about 0.1 *g* with no reported damage.

Table 1.—*Maximum heights of earth dams considered in this study*

Maximum height (ft.)	Number of dams
< 10	1
11 - 20	7
20 - 40	31
41 - 60	24
61 - 80	16
81 - 100	8
101 - 150	14
151 - 200	5
201 - 250	4
251 - 300	0
301 - 350	1
Total	111 dams

Table 2.—*Dates of completion for earth dams considered in this study*

Completion dates	Number of dams
1861 - 1906	21
1906 - 1920	2
1921 - 1930	9
1931 - 1940	14
1941 - 1950	10
1951 - 1960	23
1961 - 1970	27
1971 - 1980	4
1981 - 1989	1
Total	111 dams

Table 3.—*Estimates of peak ground accelerations for earth dams considered in this study*

Estimated peak ground acceleration (*g*)	Number of dams
0.05 - 0.10	34
0.11 - 0.20	41
0.21 - 0.30	10
0.31 - 0.40	11
0.41 - 0.50	14
0.51 - 0.60	1
Total	111 dams

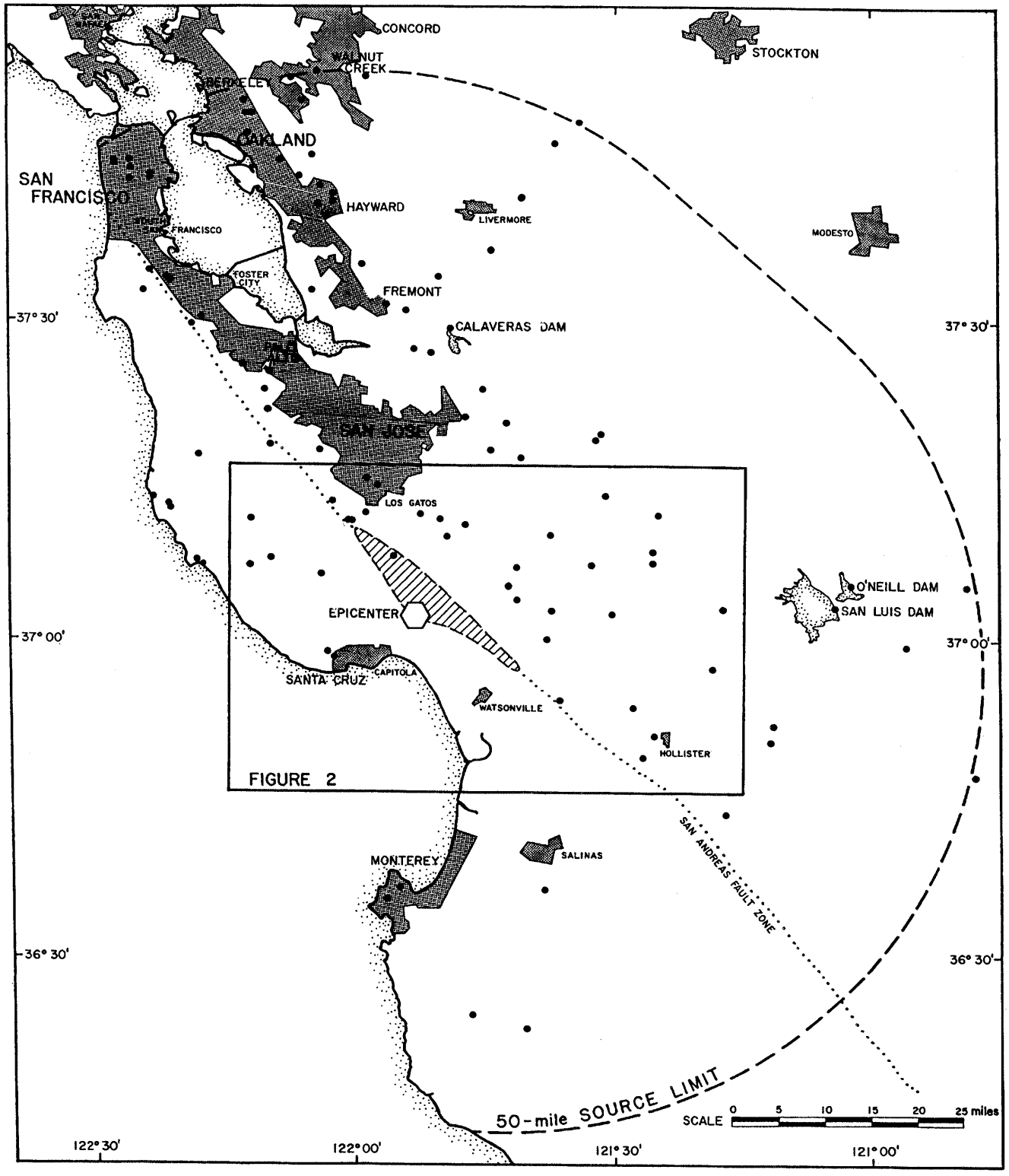

Figure 1.—Locations of 111 earth and rockfill dams within 50 miles of the Loma Prieta fault rupture zone (diagonal line pattern).

HYDRAULIC FILL DAMS

There are five hydraulic fill dams within 50 miles of the fault rupture associated with Loma Prieta: Mill Creek, Chabot, Calaveras, Hawkins, and Old Upper San Leandro.

Chabot Dam is one of the predominantly clayey dams which performed well during the 1906 earthquake. This dam was located about 37 miles from the Loma Prieta fault-rupture zone and experienced a peak ground acceleration of about 0.1 *g* without sustaining significant damage.

The Old Upper San Leandro Dam was replaced in 1977 with a new dam immediately downstream of the previous one. Both structures were located about 41 miles from the Loma Prieta fault-rupture zone and experienced peak ground accelerations of about 0.1 *g* without sustaining significant damage.

The performance of the Calaveras, Mill Creek, and Hawkins Dams is discussed in subsequent sections.

ROCKFILL DAMS

No dams are composed completely of rockfill within 50 miles of the Loma Prieta fault- rupture zone. However, many earth dams in this area were built with substantial zones of rockfill. Even Calaveras Dam, known as a hydraulic fill, was completed with substantial zones of rockfill. The performance of some prominent dams built with zones of rockfill is discussed in later sections.

Table 4.—*Hydraulic fill dams located within 50 miles of the Loma Prieta fault rupture zone*

Dam	Year completed	Max. height (feet)
Mill Creek	1889	76
Chabot	1892	142
Calaveras	1925	210
Hawkins	1928	72
Old Upper San Leandro	--	--

SELECTED CASE HISTORIES OF PERFORMANCE

Information regarding the performance of 35 earth dams located relatively close to the fault rupture is presented in table 5. The locations of these dams are shown in figure 2. Additional details for selected dams are presented in following sections.

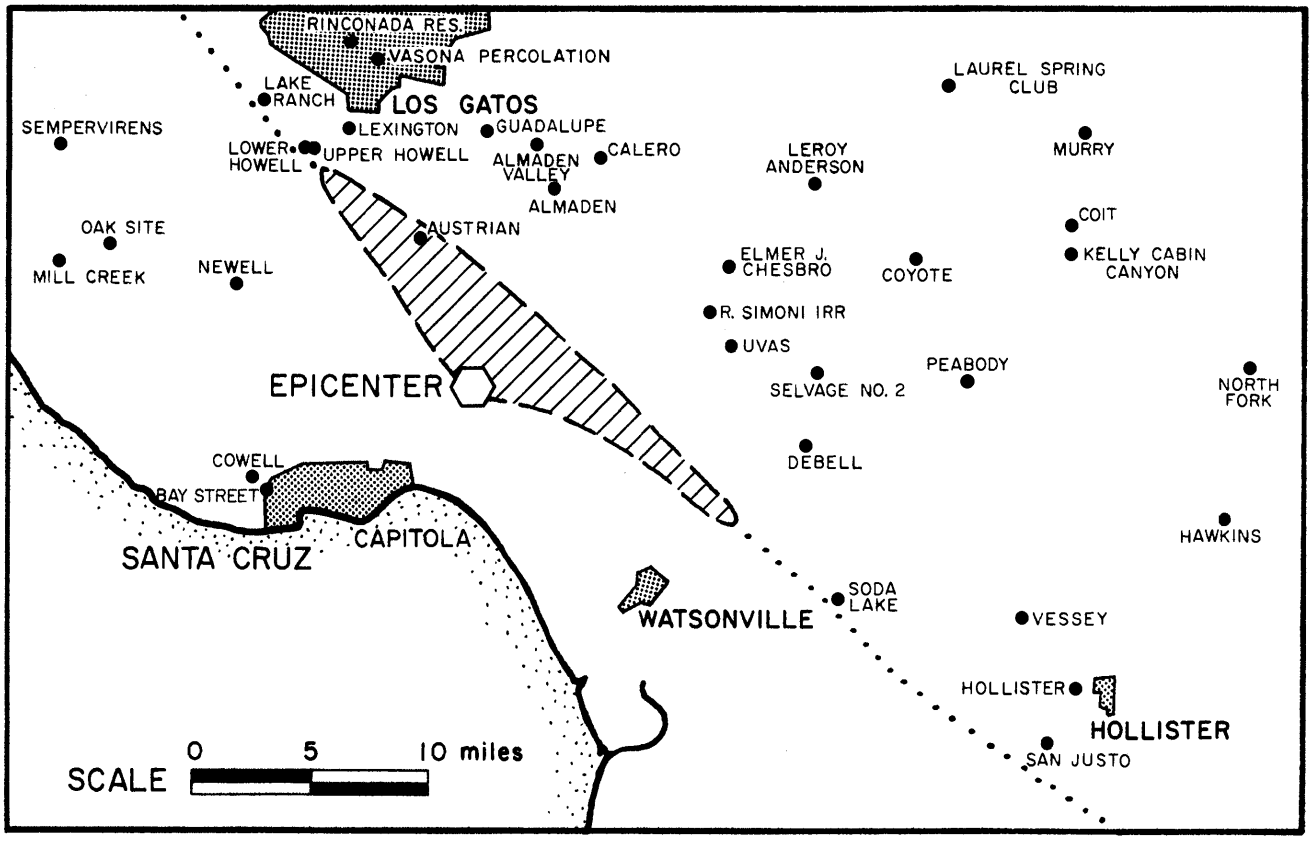

Figure 2.—Locations of earth and rockfill dams in close proximity to the Loma Prieta fault rupture zone.

Table 5.—*Summary of performance for selected case histories during the 1989 Loma Prieta earthquake*

DAM	TYPE	DATE OF COMPLETION	MAX. HEIGHT (feet)	APPROX. SOURCE DISTANCE (miles)	ESTIMATED PGA (g)	DAMAGE
AUSTRIAN	ERTH	1950	185	< 1	0.55 - 0.6	MODERATE SETTLEMENT, TRANSVERSE AND LONGITUDINAL CRACKING, SPILLWAY DAMAGE
COWELL	ERTH	1890	50	11.	0.45 - 0.5	NO REPORTED DAMAGE, RESERVOIR EMPTY
BAY STREET	ERTH	1924	27	10.	0.45 - 0.5	MINOR SURFICIAL CRACKING ON CREST
DEBELL	ERTH	1952	53	4.5	0.45 - 0.5	NO REPORTED DAMAGE
LEXINGTON	ERTH	1953	205	2.	0.45	MODERATE LONGITUDINAL AND TRANSVERSE CRACKING, 0.9 FEET OF SETTLEMENT
LOWER HOWELL	ERTH	1877	39	1.5	0.4 - 0.45	1/4 - INCH LONGITUDINAL CRACK ON CREST
UPPER HOWELL	ERTH	1878	36	1.5	0.4 - 0.45	NO REPORTED DAMAGE
ALMADEN	ERTH	1936	110	6.	0.4 - 0.45	MINOR LONGITUDINAL CRACK AT JUNCTION OF DAM CREST AND U/S CONCRETE FACING
UVAS	ERTH	1957	118	5.5	0.4 - 0.45	NO REPORTED DAMAGE
R SIMONI IRRIGATION	ERTH	1961	44	6.	0.4 - 0.45	NO REPORTED DAMAGE, RESERVOIR VIRTUALLY EMPTY
GUADALUPE	ERTH	1935	142	6.	0.4 - 0.45	MODERATE CRACKING AT TOP OF U/S BERM, SPALLING OF U/S CONCRETE PANELS
LAKE RANCH	ERTH	1877	38	4.	0.4 - 0.45	2 EMBANKMENTS WITH MINOR LONGITUDINAL AND TRANSVERSE CRACKING
NEWELL	ERRK	1960	182	6.	0.4 - 0.45	1 TO 9-INCH WIDE LONGITUDINAL CRACKS IN UPPER U/S SLOPE, INCREASED SEEPAGE
ALMADEN VALLEY	ERTH	1965	38	7.	0.4 - 0.45	NO REPORTED DAMAGE
ELMER J. CHESBRO	ERTH	1955	95	8.	0.4 - 0.45	MODERATE LONGITUDINAL CREST CRACKING, MINOR TRANSVERSE CRACKING AT ABUTMENT
CALERO	ERTH	1935	90	8.	0.35 - 0.4	NO REPORTED DAMAGE
VASONA PERCOLATION	ERTH	1935	34	5.5	0.35 - 0.4	MINOR LONGITUDINAL CREST CRACKING, MINOR TRANSVERSE CRACKING NEAR SPILLWAY
SELVAGE NO. 2	ERTH	1948	42	7.	0.35 - 0.4	NO REPORTED DAMAGE
RINCONADA	ERTH	1969	40	6.	0.35 - 0.4	4 TEARS IN RUBBER LINER SEAMS, CRACKED CONCRETE INTAKE VAULT
VESSEY	ERTH	1945	20	13.	0.3 - 0.35	MINOR LONGITUDINAL CRACKING ON CREST, RESERVOIR EMPTY
OAK SITE	ERTH	1969	43	9.5	0.3 - 0.35	NO REPORTED DAMAGE
SODA LAKE	ERTH	1978	35	5.5	0.3 - 0.35	4 TAILINGS DAMS - LIQUEFACTION OF TAILINGS, SLUMPING OF 10-FT WEST DAM
MILL CREEK	HYDF	1889	76	12.	0.25 - 0.3	MINOR LONGITUDINAL CRACKS ON CREST
SEMPERVIRENS	ERTH	1951	42	12.	0.25 - 0.3	NO REPORTED DAMAGE
HOLLISTER WW PD	ERTH	1972	13	16.	0.25 - 0.3	MODERATE CRACKING, RESERVOIR EMPTY
SAN JUSTO	ERRK	1986	135	17.	0.26	NO REPORTED DAMAGE
LEROY ANDERSON	ERRK	1950	235	13.	0.26	MINOR LONGITUDINAL CRACKING ON NEW CREST FILL
HAWKINS	HYDF	1931	72	21.	0.2 - 0.25	MINOR LONGITUDINAL CRACKS ON CREST AND U/S SLOPE, RESERVOIR EMPTY
PEABODY	ERTH	1950	63	12.	0.2 - 0.25	NO REPORTED DAMAGE
COYOTE	ERRK	1936	140	14.	0.19	NO SIGNIFICANT DAMAGE
KELLY CABIN CANYON	ERTH	1955	32	18.	0.15 - 0.2	NO REPORTED DAMAGE
COIT	ERTH	1956	54	19.	0.15 - 0.2	NO REPORTED DAMAGE
LAUREL SPRING CLUB	ERTH	1968	28	20.	0.15 - 0.2	NO REPORTED DAMAGE
MURRY	ERTH	1957	54	22.	0.1 - 0.15	NO REPORTED DAMAGE
NORTH FORK	ERTH	1939	100	23.	0.1 - 0.15	NO REPORTED DAMAGE, RESERVOIR VIRTUALLY EMPTY

NOTES: ERTH = EARTH, ERRK = EARTH AND ROCKFILL, HYDF = HYDRAULIC FILL

AUSTRIAN DAM

Austrian Dam was the earth dam most heavily damaged by the Loma Prieta earthquake. This dam is located directly above the projected northern segment of the fault rupture and about 7 miles from the epicenter (fig. 2). Because of its proximity to the earthquake, it is also thought to have been the dam to have experienced the largest shaking with peak ground accelerations estimated to have been between 0.55 and 0.6 *g*.

Fortunately, at the time of the earthquake, the reservoir elevation was about 100 feet below the dam crest. In fact, the reservoir level had been depressed during a 3 to 4 year drought prior to the earthquake, and the upper embankment materials were not fully saturated. The damage sustained by the embankment included moderate settlement, downstream movement, and moderate longitudinal and transverse cracking (fig. 3). The concrete spillway located on the right abutment was also heavily damaged. Details of the investigations and remedial construction are described in a report by Wahler Associates (1990). Previous summaries of damage were presented by Bureau and others (1989), Rodda and others (1990), and Seed and others (1990).

Austrian Dam is a 185-foot-high rolled earth fill dam and was completed in 1950. The dam site is situated between the San Andreas and the Sargent faults. The dam is about 4,000 feet southeast of the main intersection of these fault zones, with the trace of the 1906 movement on the San Andreas fault located only 1,700 feet south of the dam. The Sargent fault is located less than 700 feet north of the dam. The dam is founded on rocks typical of the Franciscan Complex, including highly fractured sandstone, graywacke, cobble conglomerate, shale, and serpentine.

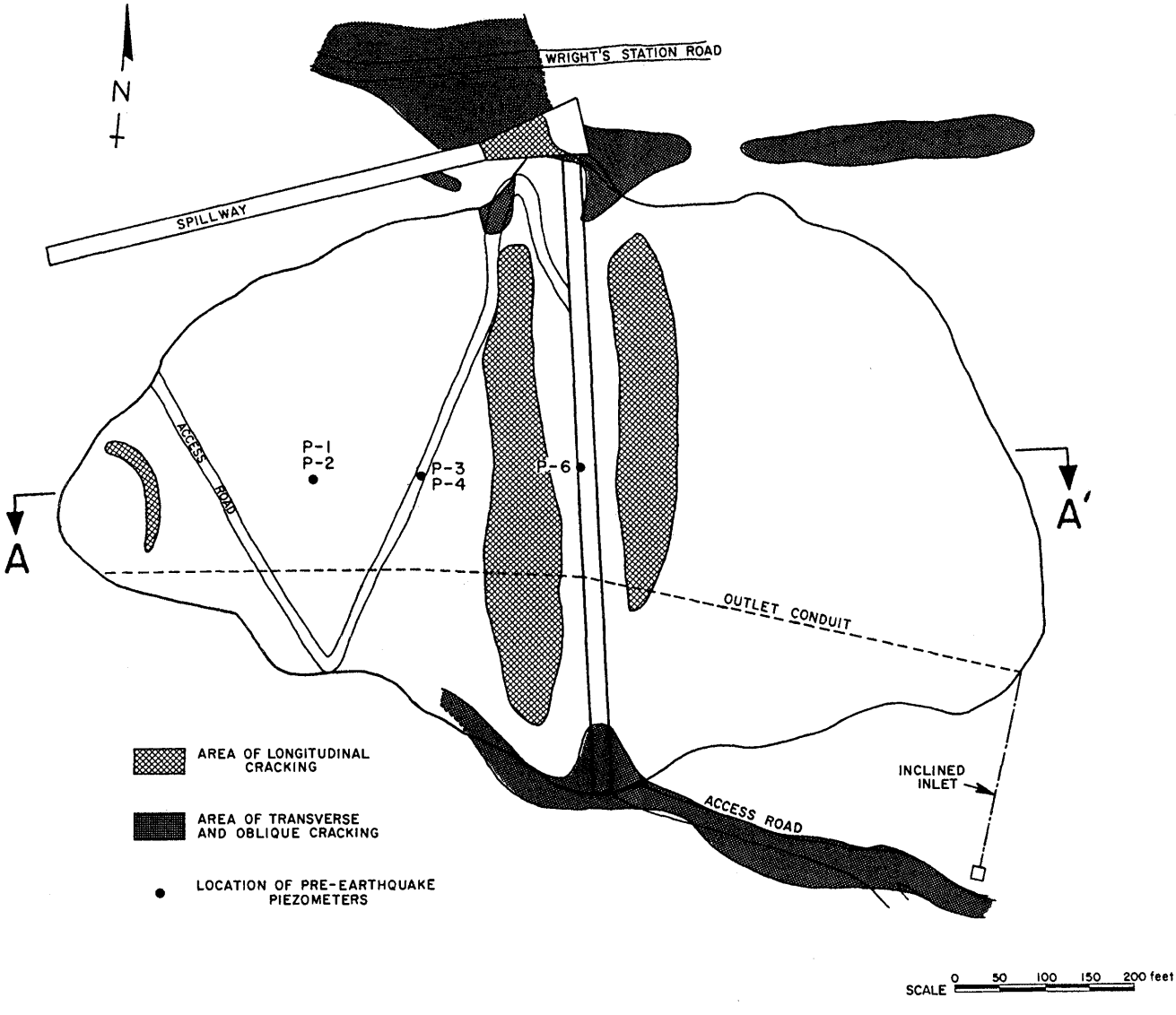

Figure 3.—Plan view of Austrian Dam locating cracks induced by the earthquake—section *A-A'* shown in figure 4 (adapted from Wahler Associates, 1990).

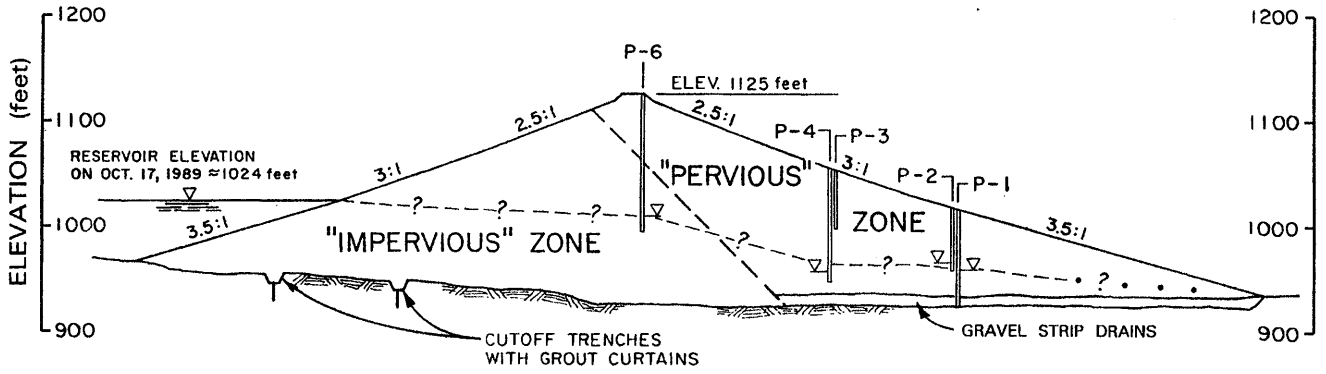

Figure 4.—Maximum cross section of Austrian Dam (section *A-A'* adapted from Wahler Associates, 1990).

The embankment was built by selective borrowing in an attempt to create a more impervious upstream zone in comparison to the downstream half of the embankment. Gravel strip drains were also placed beneath the downstream "pervious" zone. Figure 4 presents a view of the maximum cross section, together with the approximate reservoir and piezometer levels on the day of the earthquake.

Sampling of the embankment materials during earlier studies of the dam and the piezometer readings together indicate that there is not an appreciable difference between the upstream "impervious" and downstream "pervious" zones, and that the gravel drains are not completely effective in relieving downstream seepage pressures. Hence, the dam can be considered to be nearly homogeneous.

Selected embankment material properties are summarized in table 6. This table presents gradation, compacted density, and placement moisture content values from control tests performed during the original construction in 1950, together with dry density results measured in the dam following the earthquake. Table 6 also presents plasticity, shear strength, and K_{2max} values from laboratory tests performed on undisturbed tube samples taken in 1979. During the remedial construction in 1989, the average relative compaction measured in the preexisting upstream shell of the dam (based on a compactive effort of 20,000 ft.-lb/ft^3) was 93 percent. As shown in table 6, the in-situ dry densities of the fill materials in those tests were generally in the upper half of the range of dry densities determined during the 1950 construction control tests.

Significant ground movement in the vicinity of the dam was observed on the downstream right abutment above the spillway chute, on the upstream left abutment between the dam crest and the inclined inlet, and along the right side of the reservoir upstream of the dam (fig. 3).

On the right abutment, a nearly continuous arcuate scarp was observed, extending up to about 200 feet above the dam crest and about 1,000 feet downstream, with maximum vertical and horizontal displacements of about 3 feet. The cracking and movements observed in this area were coincident with topographic features associated with landsliding. Observations in exploration trenches indicated that these cracks split bedrock materials and that the fissures existed prior to the earthquake.

On the left abutment, nearly continuous cracking was observed about 400 feet along an access road from the dam crest to the upstream inlet structure. The cracking generally paralleled the slope, with vertical scarps up to 14 inches in height, and was subsequently determined by exploratory trenching to be the expression of a shallow landslide in loose material overlying graywacke and shale bedrock that had experienced previous, lesser movements. This landslide did not threaten the inclined inlet.

In addition to several small slumps and landslides around the rim of the reservoir, a set of aligned fissures was observed after the earthquake on the right side of the reservoir. These fissures developed along a topographic bench for a distance of about 1,500 feet upstream of the dam (fig. 3). In general, the fissures appeared to correspond to slumping of the ground toward the reservoir, with vertical scarps up to 3 feet being measured. The dam owner's geotechnical consultant excavated borrow and exploration trenches in this area and concluded that the aligned cracking resulted from shaking-

Table 6.—*Characterization of Austrian Dam fill materials*

Engineering property	Range	Mean
USCS Classification	SC, GC, CL	
Gradation: > No. 4 (%)	26.0 - 71.5	46.3
Gradation: < No. 200 (%)	16.0 - 43.7	31.8
Specific Gravity, G_s	2.60 - 2.78	2.70
Liquid Limit	28 - 32	31
Plasticity Index	11 - 15	13
W_c (as compacted ~1950, %)	9.5 - 19.5	14.5
γ_d (as compacted ~1950, pcf)	107.5 - 132.0	121.1
γ_d (in situ-1989, pcf)	121.3 - 131.6	126.6
C' (psf)		0
ϕ' (degrees)		44
C (psf)		290
ϕ (degrees)		21
K_{2max}	106 - 128	122

induced settlement of loose, clayey fill overlying a steep bedrock surface and that the linear orientation of the fissures was most likely a result of excavation and/or shaping of the ground during the initial dam construction (Wahler Associates, 1990).

There remains, however, some disagreement as to the cause of the aligned fissures. In a study by Aydin and others (1992), another set of cracks, located approximately 500 feet upslope of the aligned fissures, was mapped. These higher cracks had offsets commonly between 2 and 8 inches, and the study concluded that they were associated with sympathetic tectonic movements on the primary strand of the Sargent fault during the earthquake. That study went on to suggest that the aligned fissures on the bench along the reservoir might be associated with movements along another strand of the Sargent fault.

Figure 5 presents horizontal and vertical movements for crest monuments measured just prior and after the earthquake. These measurements indicated that the dam crest settled over 2.5 feet along most of its length. In addition, the right end of the dam appeared to move downstream horizontally 1.5 feet relative to the left end. Since the survey monuments were not tied into a stationary benchmark, absolute displacement vectors cannot be calculated. Movements and damage near the toe of the dam suggest that the dam moved primarily downstream.

The strong shaking and ground movements produced extensive cracking in the crest of the dam near both abutments. Near the left end of the crest, predominantly transverse cracks in the embankment were up to about 8 inches in width and 10 feet in depth. However, the most pronounced cracking near the left end of the dam occurred along the embankment-foundation contact, where vertical scarps up to 16 inches were observed at the surface. Subsequent explorations traced open cracks varying from 1/8 inch to as much as 1 1/2 feet in width along this contact to depths of up to about 27 feet. The explorations suggested that the cracks were within old landslide deposits that had been left in place on the upper part of the abutment. The possibility that some undisclosed separations might have occurred at even greater depths led to a subsequent remedial grouting program to further examine the contact at greater depths.

Particularly severe cracking occurred where the right end of the dam abuts onto the concrete spillway. This area of the spillway includes an entrance section from the unlined approach channel, the weir, and a transition section which converges to the chute section. The entrance section includes a wing wall extending upstream along the left side of the approach channel, and a "return" wall coming back in a downstream direction, presumably intended to prevent scour around the upstream end of the wing wall. The two walls thus form a "U" pointing downstream, with the right end of the dam abuting on the outside of the return wall and also backfilling the space between the two walls. Up to 9-inch-wide diagonal cracks occurred in the embankment between the walls. Separations up to 10 inches also developed between the inner faces of the walls and the enclosed embankment. A separation along the outside face of the return wall extended to a depth of about 23 feet (nearly the base of the wall). This would have been particularly dangerous had the reservoir been full, as the normal amount of freeboard was only about 15 feet.

Immediately downstream of the spillway entrance, where the dam abuts the left wall of the transition section, several cutoff collars on the outer (embankment) side of the wall were sheared-off due to upstream-downstream movement of the adjoining embankment relative to the wall.

Extensive damage also occurred in the transition and chute sections of the spillway walls. Up to 3/4-inch-wide tension cracks were observed in the walls and slab of both sections. The cracking in the slab of the chute section was somewhat regularly spaced at about 2 to 4 feet, normal to the axis of the spillway. The 80 feet of chute and transition section farthest upstream was found to have elongated a total of about 7 inches. In the transition section, tension cracks generally paralleled the trend of cracking which occurred in the natural slope above the spillway. Up to 1-inch-wide separations were observed between the bottom of the slab and its highly weathered bedrock foundation along the left wall of the transition section. Subsequent grouting through the slab indicated that these voids developed existed primarily beneath the walls, but not beneath the central part of the slab. This suggested that the spillway walls had been subjected to some sort of rocking action. At the downstream end of the chute, the concrete wingwall on the left side was rotated and torn away from the left wall, while the right wing wall could not be found.

In addition to the damage to the crest and spillway, a series of roughly parallel longitudinal cracks formed in the upstream and downstream faces of the dam. The initial widths of the cracks were relatively small, but ultimately widened within a few weeks to as much as a foot in places. These time-dependent movements may have resulted from major aftershocks, rainfall during this period, soil creep, and/or pore-pressure dissipation and consolidation. Seven days after the main shock, the four longitudinal cracks which formed in the upper 50 feet of the upstream face were approximately 5 to 15 feet deep and 1 to 4 inches wide. A number of longitudinal cracks which were 3 to 8 feet deep and 2 to 6 inches wide formed in the downstream face. The majority of the longitudinal cracks in the downstream face were located near the crest, although some limited cracking also occurred near the toe of the dam. In addition, there was some minor bulging of the downstream toe. Exploration trenches indicated that the longitudinal cracks generally dipped steeply toward the dam crest on both embankment slopes. Hence, the cracks did not appear to result from slope instability, but rather from settlement and rearrangement of the earth embankment.

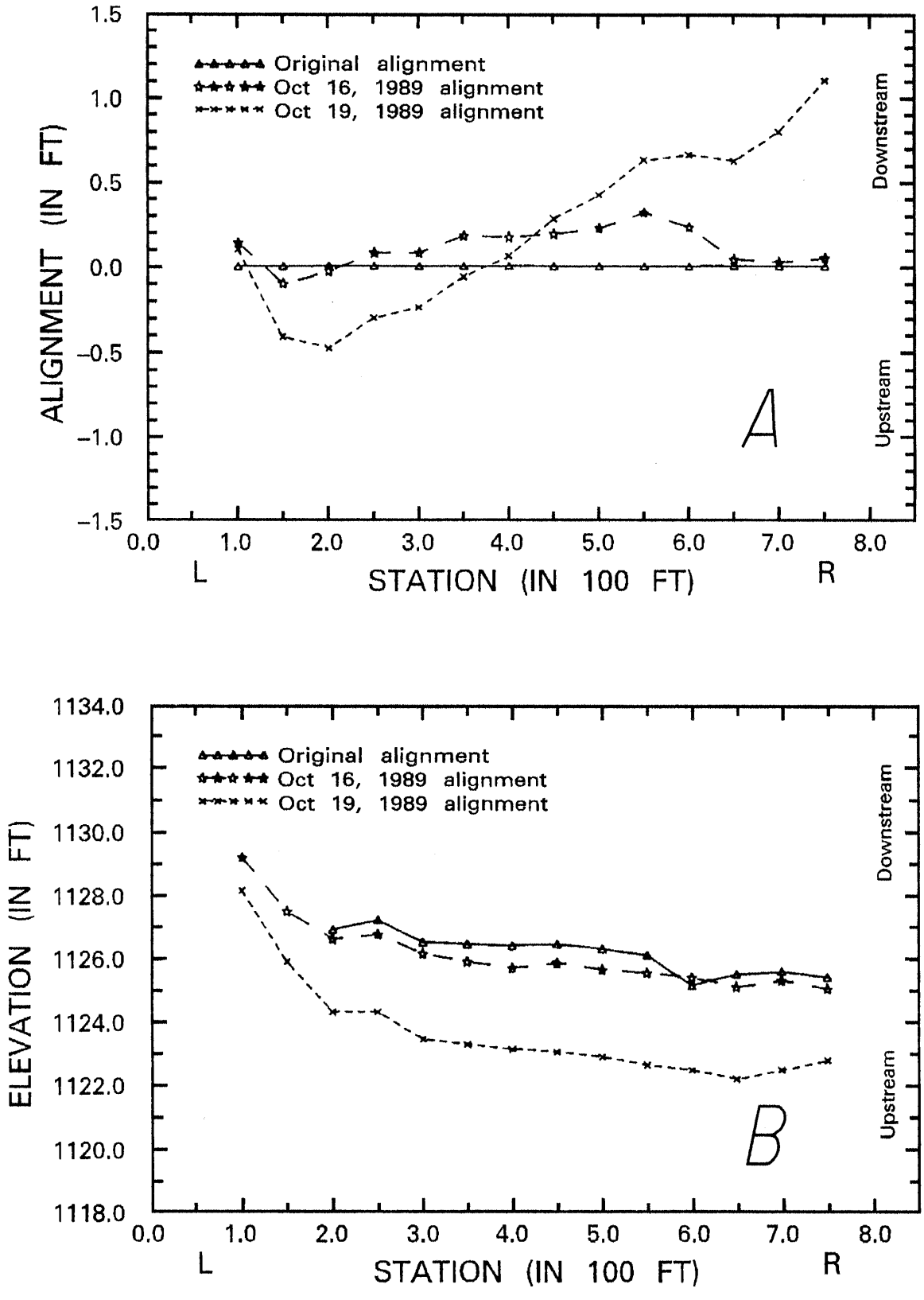

Figure 5.—Horizontal (A) and vertical (B) movements of crest monuments at Austrian Dam (from Seed and others, 1990).

The movements of the embankment were concluded to be due to general settlement and spreading of the fill during the strong earthquake shaking, followed by subsequent downslope creep. Figure 6 presents piezometer measurements made for 5 standpipe piezometers installed prior to the earthquake. These instruments recorded pore-pressure increases between 12 and 54 feet of water. Possibly related to the pore-pressure increases is the fact that some of the trenches excavated across the longitudinal cracks near the crest encountered free water at elevations considerably higher than reservoir levels at the time of the investigation (Wahler Associates, 1990).

The largest pore-pressure increase, 54 feet of water, occurred in piezometer P-1, with its tip located within the downstream "pervious" zone near the bedrock contact. The standpipe for this instrument was found to be significantly deformed between elevations 955 and 960 (about 25 to 30 feet above the bedrock contact). The standpipe for piezometer P-6, which measured an increase in hydraulic head of about 49 feet of water, was also found to be deformed between elevations 1,017 and 1,041 feet (about mid-height of the embankment). These deformations were suggestive of earthquake-induced internal movements corresponding to lateral spreading of the embankment.

The repair of the earthquake damage consisted of (1) excavating and recompacting the fill in the areas of extensive cracking, (2) placing a zoned fill with chimney and blanket drains in the crest fill at both embankment ends, (3) excavating and recompacting the upstream face of the fill to create an impervious blanket, (4) epoxy grouting the cracking in the spillway and cement grouting voids beneath the spillway slabs, and (5) grouting of the rock at the left abutment contact with the fill.

This repair successfully remediated the earthquake-induced damage to the embankment and was accomplished within 8 weeks following the earthquake. Details of the repair can be found in Wahler Associates (1990). Due to the severity of damage to the concrete spillway and concern about potential future landslides in the right abutment, a new spillway was later constructed on the left abutment of the dam in 1993-1994.

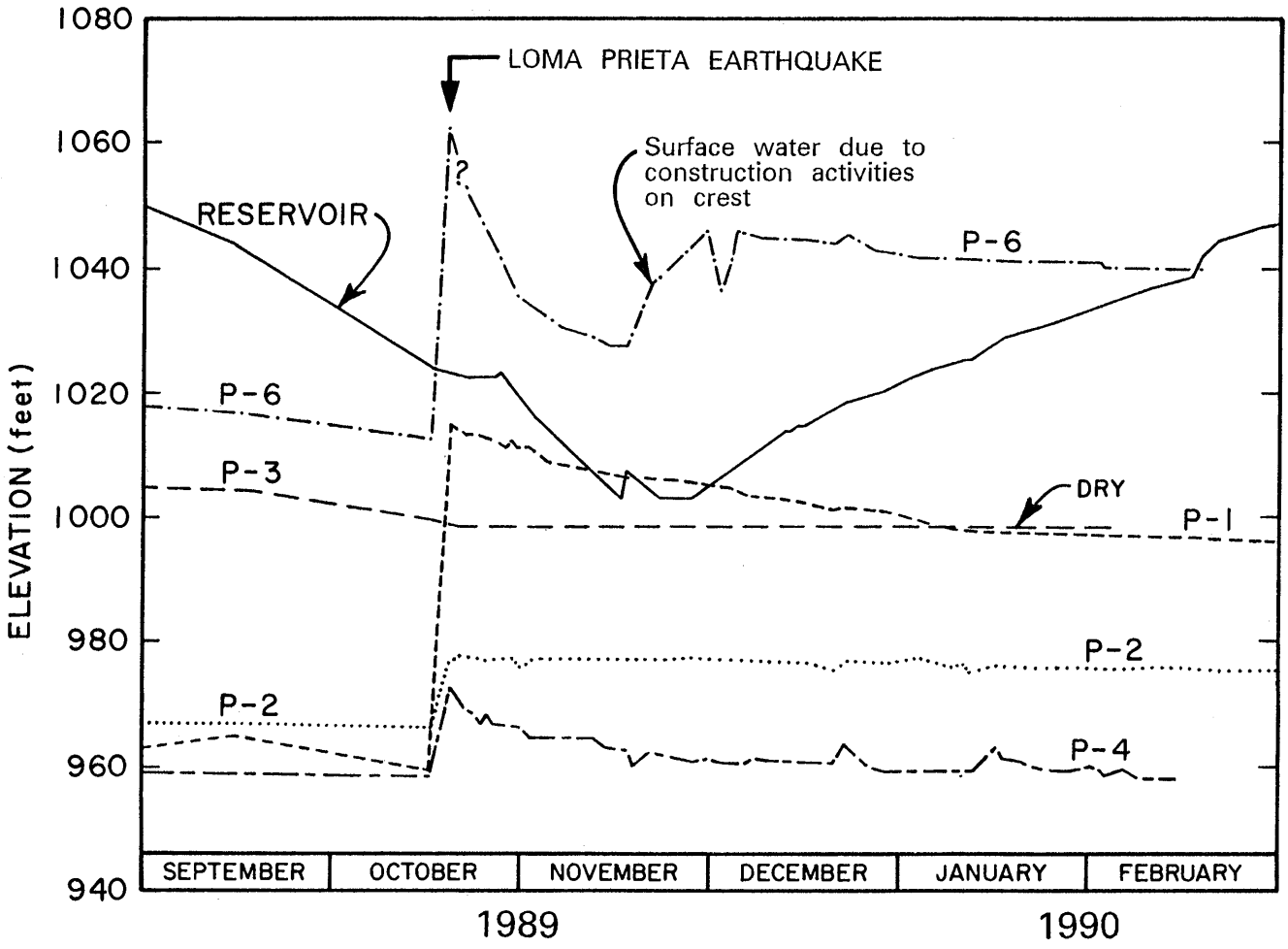

Figure 6.—Piezometer measurements for preearthquake piezometers at Austrian Dam (from Wahler Associates, 1990).

LEXINGTON DAM

Lexington Dam is a 205-foot-high dam located about 6 miles downstream of Austrian Dam and about 2 miles from the fault rupture associated with the earthquake (fig. 2). The dam was completed in 1953 as a zoned earth structure having a relatively thick sandy and gravelly clay core that is supported by upstream and downstream random shell zones of clayey sands and gravels. The dam also has relatively flat upstream (5.5:1) and downstream (3:1) slopes. A plan view and cross section are shown in figure 7. The embankment material properties are summarized in table 7. At the time of the earthquake, the reservoir was about 100 feet below the crest of the dam. Previous summaries of damage were presented by Bureau and others (1989), Seed and others (1990), and in the studies by R. L. Volpe & Associates (1990a).

Lexington Dam was instrumented with strong-motion instruments on the left abutment, left crest, and right crest. These accelerographs recorded transverse peak accelerations of 0.45, 0.39, and 0.45 *g*, respectively. This shaking was composed of about 6 to 7 s of relatively strong long- period motion. The left abutment or "bedrock" peak acceleration is within the range predicted by appropriate strong-motion attenuation relationships for a site approximately 2 miles from the nearest point on the fault rupture surface for a $M_s = 7.1$ event, but is a bit lower than the mean or expected value based on such relationships. In addition, there appears to be some spectral acceleration amplification at lower frequencies (0.9 to 1.2 Hz). This low frequency amplification may indicate that the recorded "bedrock" motion may have been affected by local topographic or geologic conditions.

The strong ground shaking produced transverse cracking on both the upstream and downstream sides of both abutments, oblique cracking on the crest about 150 feet in from the left abutment, longitudinal cracking on both the upstream and downstream slopes of the dam, and cracking of an access road on the right abutment upstream of the dam. The cracks, which were fairly isolated, were commonly less than 3/4 of an inch wide, and trenching indicated that they only extended to depths generally between 2 and 7 feet (R. L. Volpe & Associates, 1990a). The maximum earthquake-induced crest deformations were approximately 0.85 feet of vertical settlement, and 0.25 feet of lateral displacement in the downstream direction (R. L. Volpe & Associates, 1990a). An old slope indicator casing was found to have raised from beneath the crest to over 3 inches above the crest due to the embankment settling around it. The earthquake shaking and ground movements produced extensive cracking in the bridge abutment at the left abutment and ruptured a buried water line near the crest of the dam.

About 6 weeks after the earthquake, a relatively large seepage area developed high up on the downstream face of the dam. The seepage area was about 170 feet long and 35 feet wide and oriented at an oblique angle with the axis of the dam. This seepage area was really more of a wet or damp area and never really flowed water. Although the cause of the seepage area is not definitively known, one explanation that has been offered is the fact that old exploration holes extending into the rock foundation lie within the area and that these old borings could have been acting as relief wells for earthquake-induced pore pressures within the lower portions of the embankment and bedrock (R. L. Volpe & Associates, 1990a). Another possible explanation is that the fill is relatively impervious at this elevation and that any surface water that infiltrates the dam becomes perched at this level.

The repairs made to the dam consisted of trenching the cracked areas to depths ranging between 3 and 7 feet and compacting the excavated soil back into the trenches (R. L. Volpe & Associates, 1990b).

GUADALUPE DAM

Guadalupe Dam is a 142-foot-high dam located about 6 miles from the Loma Prieta fault-rupture zone, and it probably experienced peak ground accelerations between 0.4 and 0.45 *g* (fig. 2). The dam was completed in 1935 as a rolled earth structure with an upstream facing of concrete panels for erosion protection. In a manner similar to that described for Austrian Dam, the embankment is apparently nearly homogeneous, as the selective borrowing to create upstream "impervious" and downstream "pervious" zones did not appear to be completely successful in creating distinctly different zones. In 1972, an upstream buttress was added to the dam to improve drawdown stability. A plan view and cross section are shown in figure 8. At the time of the earthquake, the reservoir was about 78 feet below the crest of the dam; however, the reservoir had been full up to about 3 months before the earthquake, and it is assumed that the upstream shell materials were nearly saturated at the time of the earthquake. Previous summaries of damage were presented by Bureau and others (1989), Seed and others (1990), and in the studies by R. L. Volpe & Associates (1990a).

The earthquake induced up to 0.64 feet of settlement and 0.15 feet of lateral displacement in the upstream direction as measured on the crest. Minor transverse cracking developed at the crest at both abutment contacts along with minor longitudinal cracking on the crest. The principal damage was to the upstream slope, where the upper portion of the buttress fill developed longitudinal cracking. Shortly after the earthquake, these cracks were observed to have a maximum width of less than 1 inch and extended across the entire face of the dam. About 5 weeks later, the cracks had widened to about 4 inches and extended to a depth of about 5 feet (R. L. Volpe & Associates, 1990a).

These cracks may have been caused by concentrations of dynamic stresses induced by the change in slope geometry. Alternatively, they may have resulted from possible past settlements caused by the placement of the berm. These past settlements may have created preexisting cracks which surfaced only after the development of strong ground motion.

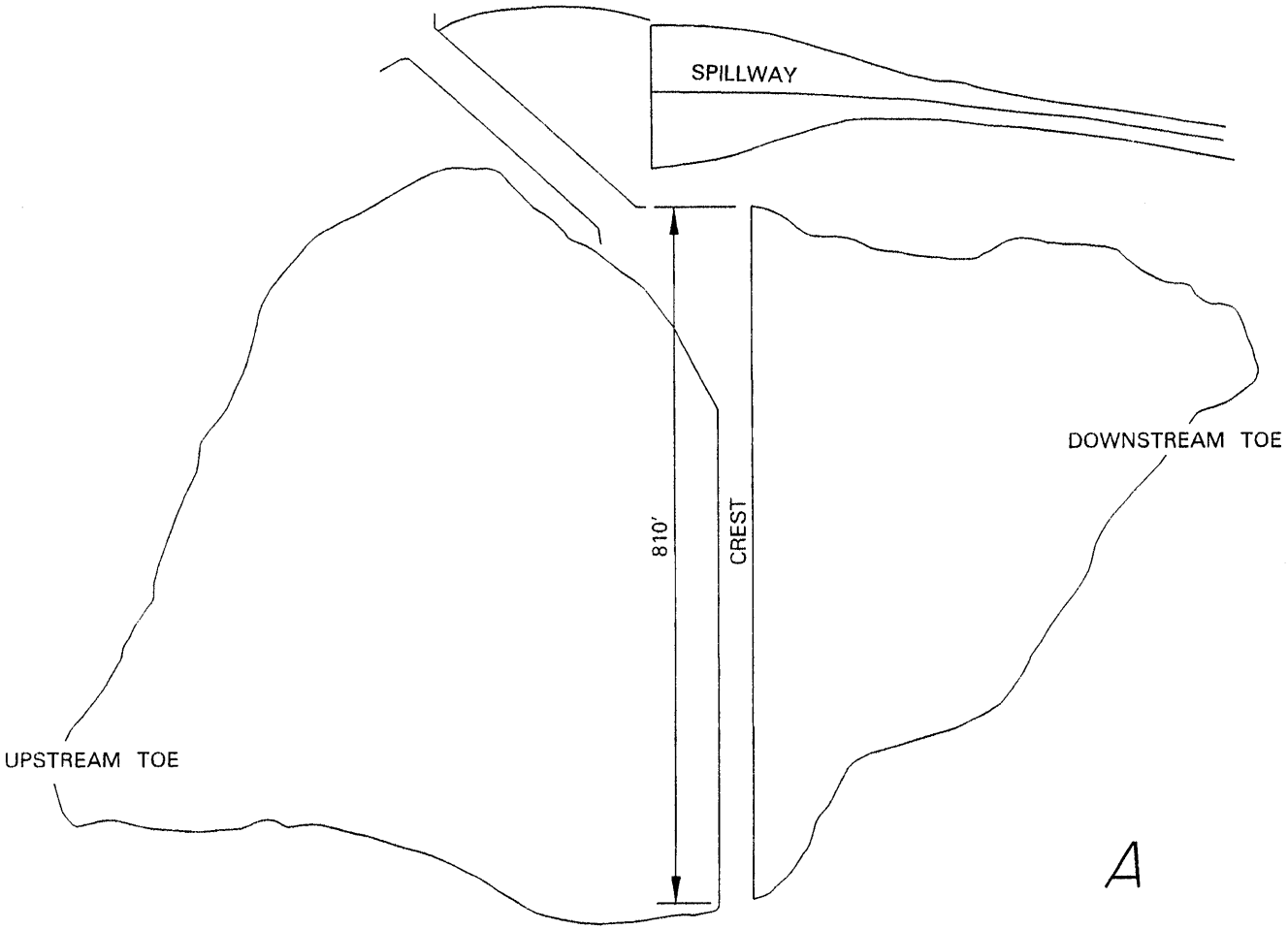

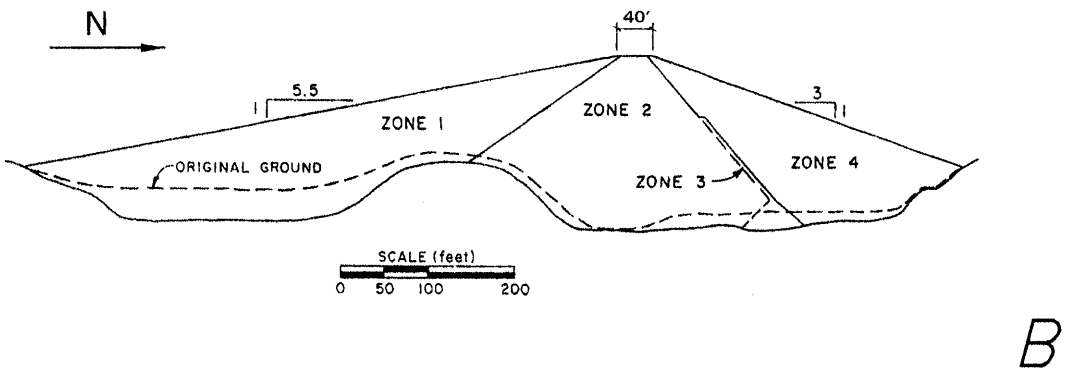

Figure 7.—Plan view (*A*) and cross section (*B*) of Lexington Dam.

Table 7.—*Characterization of Lexington Dam fill materials*

Engineering Property	CORE (Zone 2)		SHELL (Zones 1 & 4)
Depth (ft)	0-80	>80	
Classification	SC, CL-CH		SC, GC, CL
Gradation: > No. 4 (%)	13-30	0-2	[1]0-50
Gradation: < No. 200 (%)	29-52	86-97	[2]18-97
Specific Gravity, *Gs*	2.67 -	2.73	2.73
Liquid Limit	31 -	37	33 - 39
Plasticity Index	14 -	18	14 - 24
Wc (in situ range and avg., %)	11.2-17.7 (14.4)	21.5-30.6 (25.6)	9.4-26.5 (15.3)
γ_d (in situ range and avg., pcf)	117.5-131.5 (120.9)	92.5-102.2 (96.6)	[3]95.2-134.8 (119.8)
γ_{dmax}, W_{copt} (20,000 ft-lb/ft3)			131.7 pcf 8 %
C' (psf)	400	0	0
ϕ' (degrees)	36	25	36
C (psf)	1200	0	0
ϕ (degrees)	18	17	22
K_{2max}	100-150	~50	~100
V_{smax} (ft/sec)	1200-1600	1400-1600	1400-2200

Notes: [1] Only one sample had less than 13 percent gravel.
[2] For 70 percent of the samples, <35 percent finer than No. 200.
[3] Average dry unit weight was about 6 pcf lower at depths of 0-40', and 4 pcf higher at depths >40'.

The earthquake also caused the concrete panels on the upstream face above the berm to pound against each other, resulting in cracking and spalling in about 10 percent of the panels (R. L. Volpe & Associates, 1990a).

The repairs made to the dam consisted principally of excavating a 70-foot band of material (as measured along the slope, parallel to the crest) at the top of the upstream buttress to a depth of about 6 feet. The excavated material was temporarily stored in order to allow the material to dry to an acceptable water content and then recompacted into place. The cracks in the crest at the abutment contact were excavated to about 3 to 4 feet and the excavated material was recompacted back into place (R. L. Volpe & Associates, 1990b).

NEWELL DAM

Newell Dam is a 182-foot-high dam located about 6 miles from the Loma Prieta fault-rupture zone, and it probably experienced peak ground accelerations between 0.4 and 0.45 *g* (fig. 2). The dam was completed in 1960 as a zoned earth and rockfill dam generally composed of clayey zones except for an upstream zone of dirty rockfill. At the time of the earthquake, the reservoir was about 49 feet below the crest of the dam. Previous summaries of damage were presented by Bureau and others (1989), Seed and others (1990), and Creegan (1990).

Although the earthquake did not induce significant crest movements, a longitudinal crack was found on the 3:1 upstream slope running the entire width of the dam face at about the spillway elevation. This crack was generally between 1 and 9 inches in width. Trenching explorations of the crack indicated that it was formed by tension within the zone 2 rockfill. The trenches, however, only extended to a maximum depth of 10 feet, and the crack, which was about 1 inch in width at the bottom of the trenches, extended farther to greater depths. There were also other minor cracks at various locations. Seepage through the dam and abutments, measured at the downstream toe, was also found to have increased from a normal 8 gpm to 41 gpm, but remained clear (Creegan, 1990). By early December 1989, the seepage had decreased back down to about 17 gpm.

The development of the longitudinal cracking was theorized to have resulted from settlement of the dirty rockfill upstream shell relative to the rest of the dam. This material consisted of quarried sandstone and shale and was placed in 5-foot lifts and compacted by sluicing. The other clayey zones were placed in thin lifts and compacted to about the maximum Standard Proctor dry density. Consequently, the upstream rockfill zone was relatively loose in comparison with the other zones in the embankment. There were indications that some of the cracking ran along the interface of the zone 2 rockfill and the clayey core. Further evidence of settlement of the zone 2 material was found at the bell toggle joints along the sloping intake tower where the embankment seemed to have pulled away from the structure by about 1 to 3 inches in a downstream direction (Creegan, 1990).

The repair of the longitudinal cracks consisted of using a large backhoe to excavate to a depth of about 6 feet along the alignment of the crack. The trench was then backfilled in 18-inch lifts with each lift being compacted with a vibrating shoe on the backhoe. The upstream slope was then rolled with a vibratory roller (Creegan, 1990).

ELMER J. CHESBRO DAM

The Elmer J. Chesbro Dam is a 95-foot-high embankment located about 8 miles from the Loma Prieta fault-rupture zone, and it probably experienced peak ground accelerations between 0.4 and 0.45 *g* (fig. 2). As for many of the embankment dams in this area, the embankment is a nearly homogeneous compacted fill, as selective borrowing to create upstream "impervious" and downstream "pervious" zones do not appear to be entirely successful in creating distinctly different materials. The upstream slope varies between 2:1 and 3:1. The downstream slope is about 2:1, but is fitted with a 45-foot-wide berm at about half the height of the dam. At the time of the earthquake, the reservoir was about 69 feet below the crest of the dam. Previous summaries of damage were presented by Bureau and others (1989), Seed and others (1990), and in the studies by R. L. Volpe & Associates (1990a).

Surveys of crest monuments showed that the earthquake induced up to 0.37 feet of settlement and 0.05 feet of lateral displacement in the upstream direction. The main area of cracking that developed at this dam occurred as longitudinal cracking near the upstream edge of the crest. This cracking extended about 240 feet and had a 4-inch width together with

a 4-inch vertical offset, with the upstream side of the crack being on the down side. There was also minor transverse cracking on the right abutment at both the crest area and near the spillway entrance (R. L. Volpe & Associates, 1990a).

Trenching explorations indicated that the longitudinal cracking on the upstream edge of the dam extended to a maximum depth of about 8 feet and was related to settlement of an upstream slope-protection zone. The transverse cracking on the crest at the right abutment was estimated to have a maximum depth of 4.5 feet (R. L. Volpe & Associates, 1990a).

The repairs to Chesbro Dam consisted of excavating the upper 10 to 12 feet of the upstream slope and replacing this material with compacted, imported materials. The cracking on the right abutment was repaired by trenching to a depth of about 5 feet and recompacting the excavated material back into place (R. L. Volpe & Associates, 1990b).

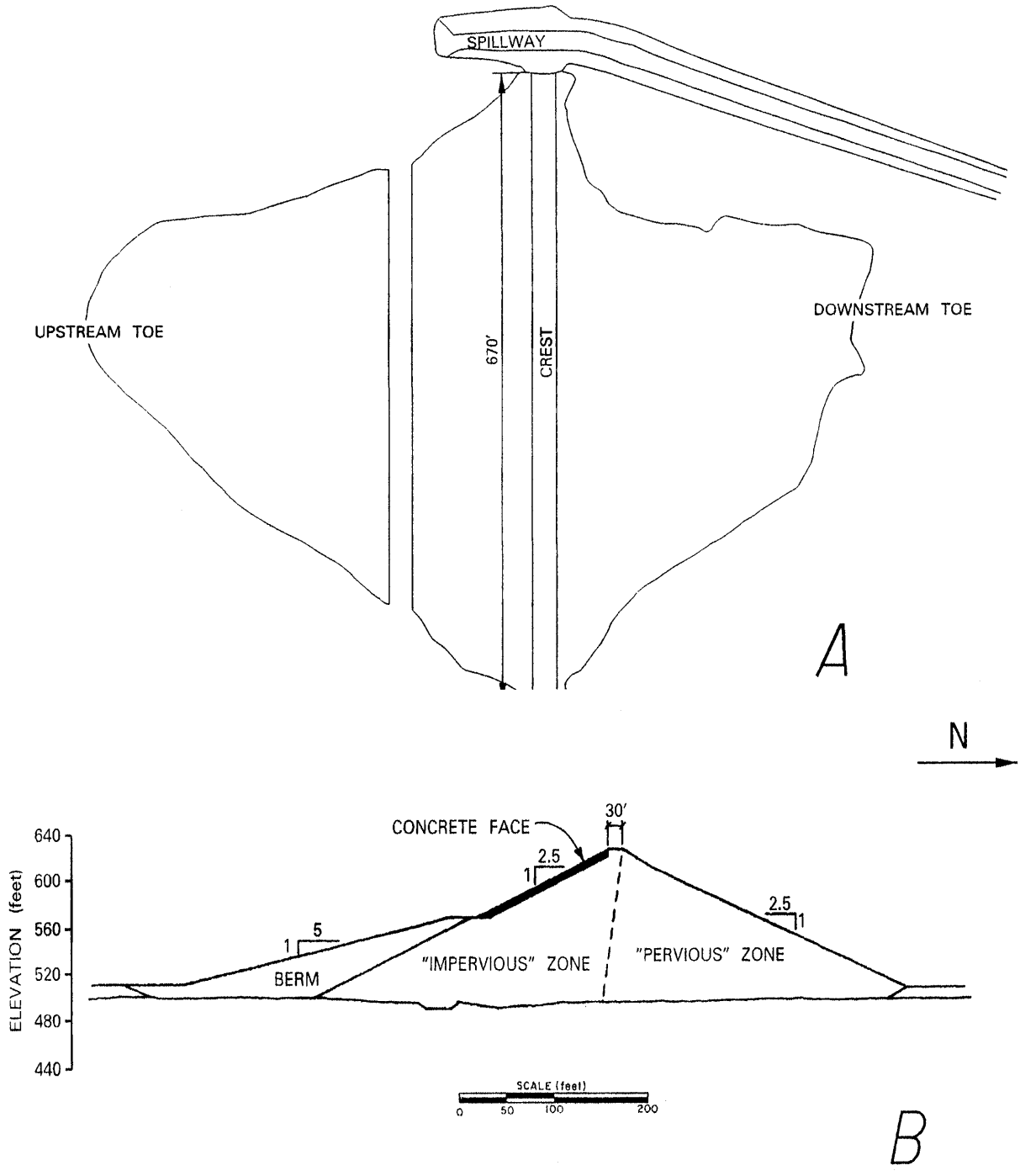

Figure 8.—Plan view (*A*) and cross section (*B*) of Guadalupe Dam.

VASONA PERCOLATION DAM

The Vasona Percolation Dam is a 34-foot-high embankment located about 5.5 miles north of the Loma Prieta fault-rupture zone, and it probably experienced peak ground accelerations between 0.35 and 0.4 *g* (fig. 2). The dam is composed of two embankments flanking a central concrete spillway. The two embankments were completed in 1935 and contain an upstream zone of rolled "fine" material together with downstream zones of coarse and random materials. Beneath the upstream "fine" material there is a puddled clay cutoff trench which extends 25 feet to an impervious foundation material. At the time of the earthquake, the reservoir was about 12 feet below the dam crest (R. L. Volpe & Associates, 1990a).

The dam developed maximum settlements of about 0.16 feet and about 0.09 feet of lateral movement in the downstream direction (R. L. Volpe & Associates, 1990a). The major damage consisted of longitudinal cracking along the crest of the right embankment. This cracking was intermittent, but extended along the entire length of the embankment. These cracks were up to 3/4 of an inch in width, and trenching indicated a maximum depth of about 5.5 feet. There was also limited longitudinal cracking on the crest of the left crest embankment, generally between 1/8 to 1/2 inches in width. Minor transverse cracking, generally less than 1/8 of an inch in width, was found along the spillway contact from the crest centerline to the downstream toe. Cracking was also noted along the spillway wingwall at the downstream toe of the dam and along the parapet wall along the crest of the dam.

Longitudinal cracking of the crest had previously been noted following the August 8, 1989 earthquake (M=5.1), now considered a possible foreshock of the Loma Prieta earthquake. In some locations, the longitudinal cracks observed following the Loma Prieta earthquake were in the same locations as those from the earlier earthquake.

The repair principally consisted of removing the upper 4.2 feet of the right embankment and recompacting the material back into place (R. L. Volpe & Associates, 1990b).

SODA LAKE DAM

Soda Lake Dam consists of four embankments that are used to retain granite tailings from a nearby quarrying operation. The dam had been enlarged in 1978 to give a maximum height of 35 feet for the main or south embankment. The dam is located approximately 5.5 miles from the Loma Prieta fault-rupture zone, and it probably experienced peak ground accelerations between 0.3 and 0.35 *g* (fig. 2). Although the reservoir was nominally empty at the time of the earthquake, most of the reservoir volume had been filled with granite tailings.

Although the reservoir may have been considered empty, portions of the granite tailings were evidently saturated, as they appeared to have liquefied in several places. Evidence of liquefaction was in the form of numerous sand boils developed within the reservoir deposits and the fact that the reservoir sediments settled about 2 to 3 feet relative to the embankments and reservoir rim. One reconnaissance team found the sand boils still ejecting water and sand 72 hours following the main shock (J. Egan, oral commun., 1993).

No damage was found at the north, south, or east embankments. However, the 10-foot-high West Saddle Dam was found to have an extensive pattern of cracking at and below the crest. As shown in figure 9, the cracking was in the pattern of an arc and seemed to identify a wedge of material that had developed into a minor slump towards the reser-

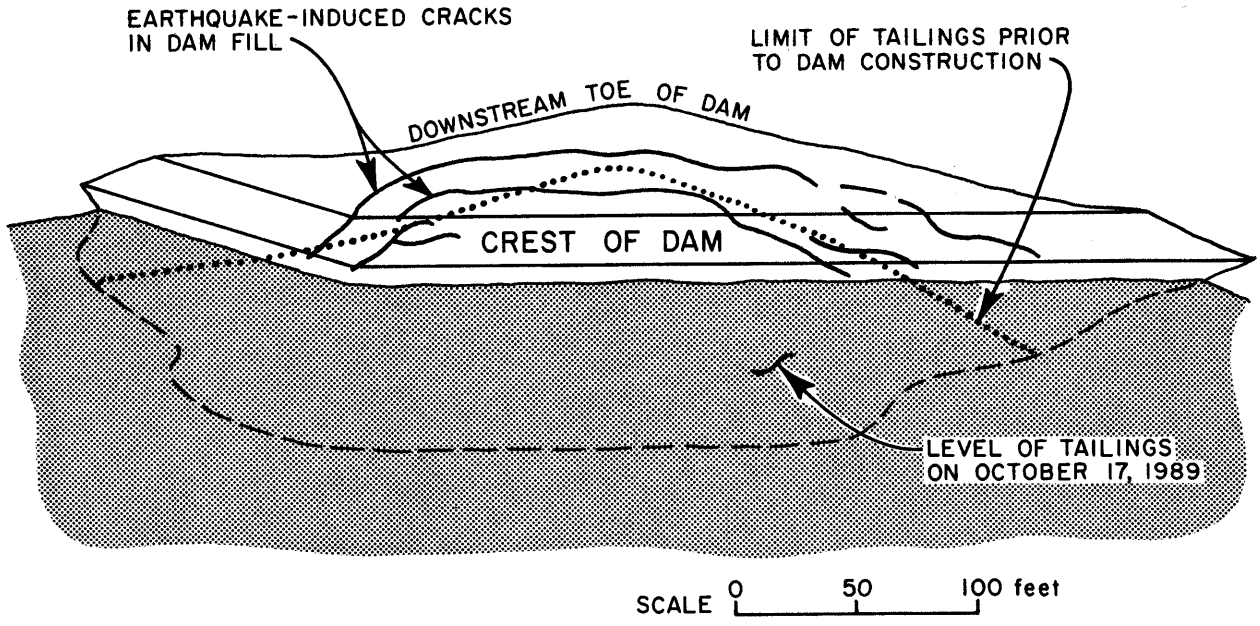

Figure 9.—Plan view of the Soda Lake west saddle dam showing earthquake-induced cracking.

voir. These cracks had typical widths of about 1 to 4 inches and could be probed to depths of at least 6 feet. The cracks also had vertical offsets of about 1 inch with the reservoir side of the crack being lower than the downstream side.

The cause of the cracking and/or slumping of the West Saddle Dam was theorized by engineers within the California Division of Safety of Dams to be a result of having left potentially liquefiable tailings deposits in the foundation beneath this embankment during its construction in 1978. As shown in figure 10, prior to construction of the West Saddle Dam, preexisting tailings extended from the reservoir to about the centerline of the dam to be built. These tailings were supposed to have been removed. However, if they were not completely removed, then liquefaction of tailings remnants within the foundation might explain the cracking and movements observed following the earthquake. Supporting this theory is the fact that the shape and location of the cracked wedge appears to match the contour of the limits of preexisting tailings in the foundation (figure 9).

As a result of the cracking/slumping in the West Saddle Dam, the dam was not considered safe to store water, and the owner was required to take the dam and reservoir out of service.

MILL CREEK DAM

Mill Creek Dam is a 76-foot-high dam with a complicated history. It was originally built in 1889 as a timber crib dam, with a substantial hydraulic fill zone placed upstream of the timber crib portion. There is apparently no information available concerning its status and performance following the 1906 earthquake. In 1932, additional fill was placed upstream to give the upstream face a 3:1 slope. In 1947, part of the timber crib dam burned. Part of the burned timber crib zone was removed, leaving a downstream slope of about 1.5:1. In 1957, a large sinkhole formed in the upstream face above corroded sections of the original 14-inch outlet pipe. The repair for the sinkhole consisted of excavating a large triangular trench to remove portions of the corroded pipe and then recompacting the excavated materials back into the trench. A new outlet consisting of a 12-inch pipe was also installed at this time. Figures 11 and 12 present sections illustrating the different materials present in the dam.

Mill Creek Dam is located approximately 12 miles from the Loma Prieta fault-rupture zone, and about 17 miles from the epicenter. The dam may have experienced peak ground accelerations of up to about 0.3 *g* (fig. 2). At the time of the earthquake, the reservoir was about 16 feet below the crest. Despite the questionable materials left within it, the dam performed well during the earthquake. The only damage observed was minor cracking at the crest, which became obscured during the rains that followed a few days after the earthquake.

The good performance is particularly surprising due to the presence of the sandy and silty hydraulic fill left in place beneath the 1957 repair trench. Piezometers indicated that these soils were saturated prior to the earthquake. Penetration tests made during investigations conducted in 1987 and 1992 indicated that these soils are very loose [Standard Penetration Test $(N1)_{60,cs}$ of the hydraulic fill is equal to about 10 blows per foot].

A Standard Penetration Test-based analysis of the dam was performed by Wahler Associates (1992) for the Loma Prieta earthquake using an estimated peak acceleration in bedrock of 0.17 *g*. The results indicated that liquefaction would be triggered in the hydraulic fill, resulting in a flow slide of the upstream slope during the Loma Prieta earthquake. A back-analysis was also performed to determine the value of residual strength of the hydraulic fill which would have been needed to prevent the calculated onset of a flow slide and result in computed deformations in agreement with the actual observed seismic displacements. It was determined that a residual strength of about 600 psf would have been needed. However, based on the Standard Penetration Test results, the estimated actual in-situ residual strength would only have been about 300 psf.

A possible explanation for the discrepancies between observed and back-calculated performances is that the site acceleration could have been significantly less than the estimated 0.17 *g* peak value. Low cyclic loadings might not have caused liquefaction of the hydraulic fill and would explain the lack of damage to the dam. There were no seismic instruments at the site, and there were no physical indications that liquefaction had occurred.

Although the dam performed well during the 1989 Loma Prieta earthquake, design modifications to the existing spillway were developed to restrict the reservoir surface to an operating level which would reduce the risk of sudden release of the reservoir during a future large earthquake.

LEROY ANDERSON DAM

Leroy Anderson Dam is a 235-foot dam located about 13 miles from the Loma Prieta fault-rupture zone. The dam was completed in 1950 and is composed of central core zones of compacted sandy clay and clayey sand that are flanked by shell zones of rockfill. The rockfill was placed by end-dumping from trucks into 10 to 25-foot-high lifts that were compacted by sluicing with water (fig. 13).

The dam is well instrumented with seismographs, which indicated a peak horizontal ground acceleration of about 0.26 *g* at the base together with a crest horizontal peak acceleration of about 0.43 *g*. There were several other instruments placed on the crest and downstream face which recorded peak horizontal accelerations of between 0.1 and 0.4 *g*.

This dam also experienced strong shaking during the nearby 1984 Morgan Hill earthquake (M_L=6.2), with a peak

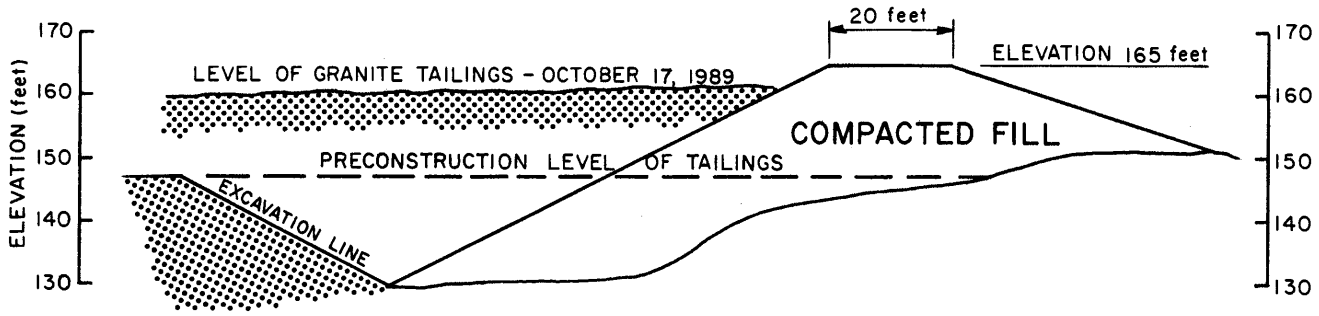

Figure 10.—Cross section of the Soda Lake west saddle dam.

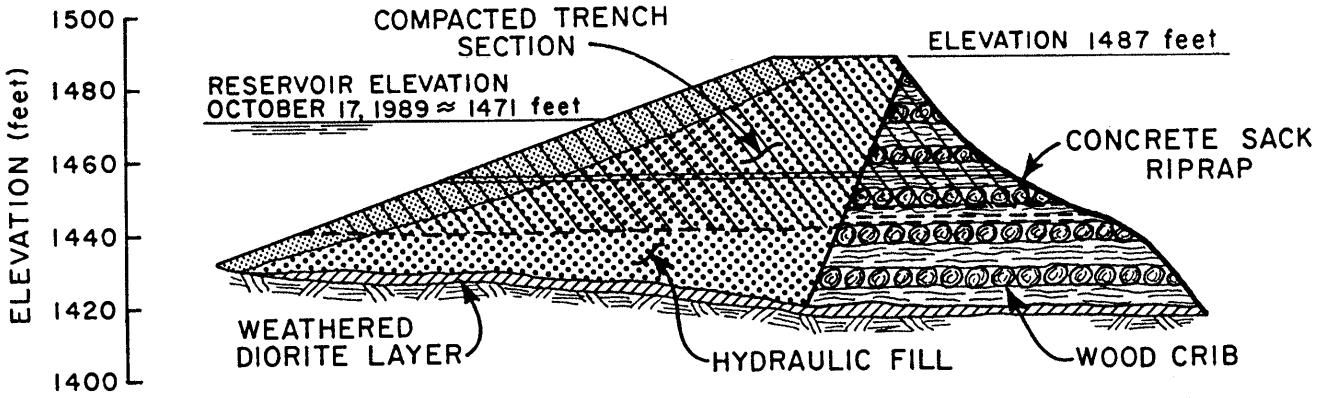

Figure 11.—Cross section of Mill Creek Dam .

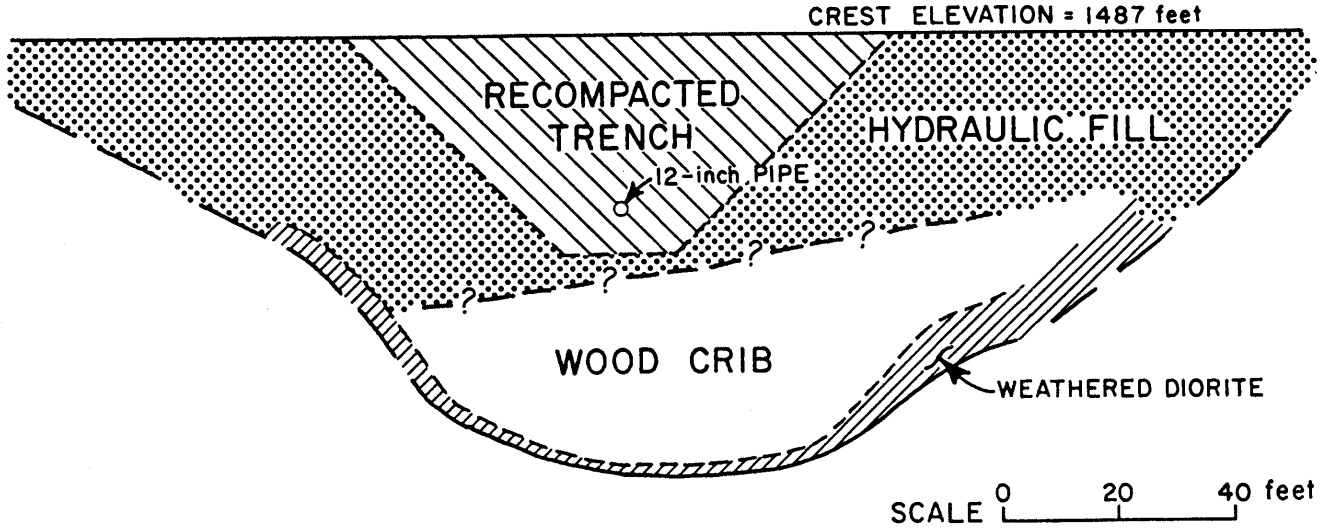

Figure 12.—Longitudinal section of Mill Creek Dam.

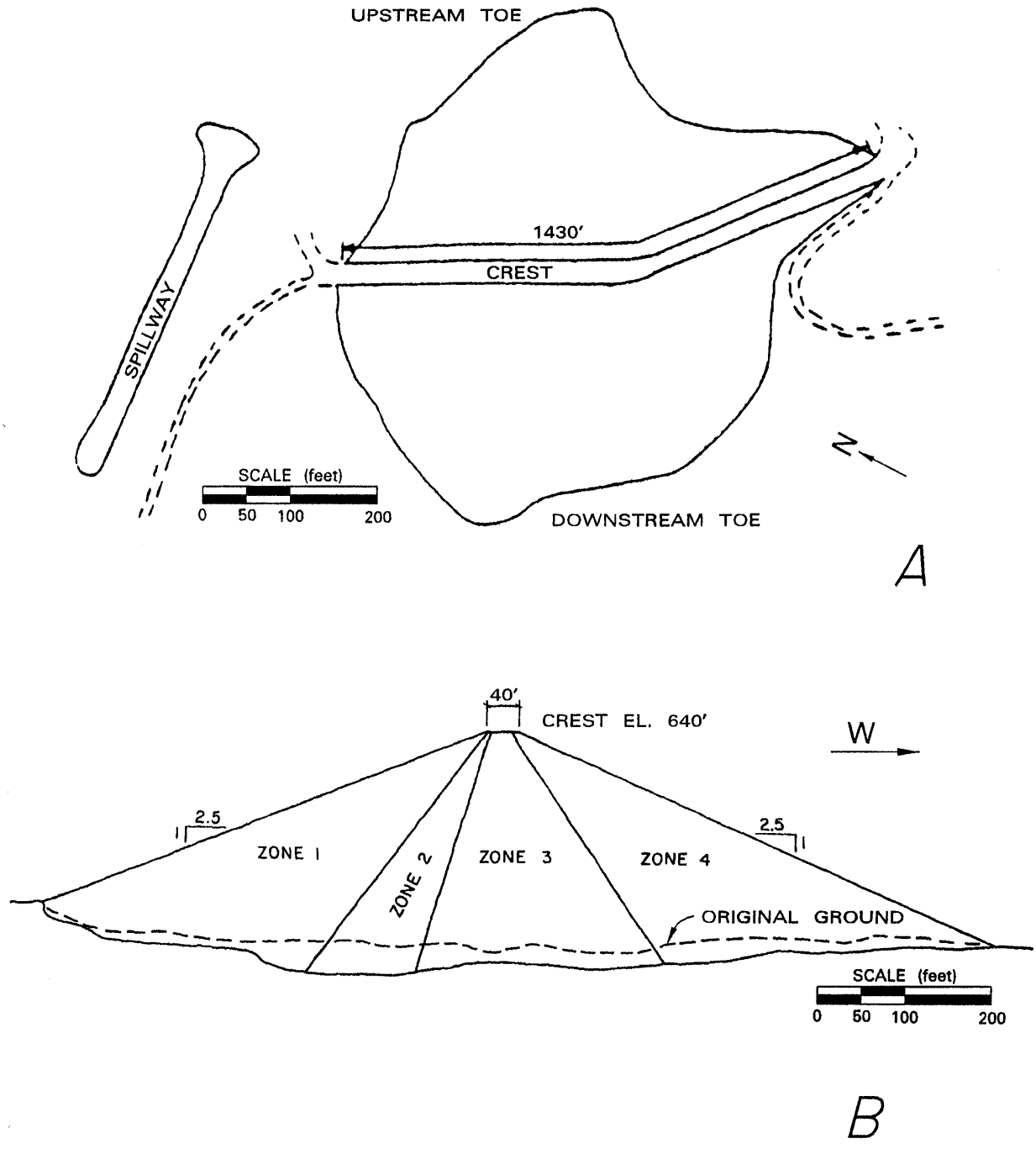

Figure 13.—Plan view (*A*) and cross section (*B*) of Leroy Anderson Dam.

acceleration at the downstream toe of about 0.41 g and a corresponding horizontal peak acceleration of 0.63 *g* at the crest. Although of larger peak amplitude, the duration of strong shaking was less during the 1984 earthquake than during the 1989 event.

Both the 1984 and 1989 earthquakes produced similar patterns of distress in the embankment. In 1984, two parallel, and relatively shallow, longitudinal cracks formed in the compacted fill along the crest approximately overlying the buried contacts between the central clayey core and the upstream and downstream rockfill shell zones. These cracks were generally less than an inch in width and are thought to have been the result of settlement of the shell zones relative to the core zones. Between 1984 and 1989, the embankment crest was raised about 5 feet and a small sliver fill was placed in a localized area on the downstream edge of the crest. The

5-foot crest raise was placed to provide additional head for a modified spillway, and the sliver fill was placed to provide space for an instrumentation vault.

The main damage following Loma Prieta was a longitudinal crack on the downstream half of the crest approximately above the contact between the shell and core zones. In addition, the longitudinal cracking extended to and around the base of the vault on top of the sliver fill. These cracks were generally less than 3/4 of an inch in width. A second set of longitudinal cracks was also observed at both edges of the paved crest road along the bases of guard rail posts. This latter set of cracks were as much as 1.5 inches in width.

The maximum settlements of crest monuments following Loma Prieta were less than 0.04 feet on the upstream edge and about 0.13 feet on the downstream edge. Only minor repairs were considered necessary for the crest cracking (R. L. Volpe & Associates, 1990a).

SAN JUSTO DAM

San Justo Dam is a 135-foot dam located about 17 miles from the Loma Prieta fault rupture zone (fig. 2). The dam is relatively new and was completed in 1986 as a zoned earth and rockfill embankment (figs. 14 and 15). Although no significant damage was observed following the earthquake, this dam provides an outstanding opportunity to investigate the dynamic response characteristics of earth dams. This is because the dam is heavily instrumented with strong-motion sensors. Furthermore, one of the sensors was embedded in a borehole approximately 62 feet below the crest of the dam, providing one of the few opportunities to calibrate response analyses with the internal motions of an embankment dam.

Figures 14 and 15 illustrate the peak accelerations recorded at different locations at San Justo Dam. The transverse horizontal peak acceleration recorded at the downstream toe was about 0.26 *g*; whereas the transverse horizontal peak acceleration recorded at the crest was about 0.40 *g*, an amplification of about a factor of 2. However, the interior sensor at about the mid-height of the dam indicated a transverse peak acceleration of only about 0.26 *g*. This would suggest that most of the transverse amplification took place within the upper half of the dam.

The strong-motion sensors also suggest that longitudinal peak horizontal accelerations were amplified by about a factor of 3, but that the longitudinal amplification took place in the lower half of the embankment.

HAWKINS DAM

Hawkins Dam is a 72-foot-high hydraulic fill that was built slowly between 1912 and 1931. It is located about 21 miles from the Loma Prieta fault-rupture zone, and it probably experienced peak horizontal ground accelerations of about 0.2 to 0.25 *g* (fig. 2). Although the reservoir was empty at the time of the earthquake, the dam experienced minor longitudinal cracking on the crest and on the upstream slope.

The dam was investigated by Lee and Roth (1977) during the performance of a seismic stability evaluation. This study found that the dam was generally composed of a fairly homogeneous and impervious gravel-sand-clay fill, together with a small zone of homogeneous clay in the central portion of the embankment (fig. 16). Because it was built slowly, with only about 2 to 3 feet of material added each year, there was time for consolidation and desiccation of the fill to take place. The study by Lee and Roth (1977) concluded that the dam would have adequate stability for even a magnitude 8+ earthquake on the San Andreas fault. Unfortunately, because the reservoir was empty at the time of the earthquake, an opportunity to verify this evaluation was lost.]

PERFORMANCE OF EARTH DAMS AT GREATER DISTANCES

In addition to the dams located in relatively close proximity to the earthquake, the performance of a few dams located at greater distances is also of interest.

CALAVERAS DAM

Calaveras Dam is a 210-foot-high hydraulic fill dam that was completed in 1925. During construction, it developed a large slide due to static liquefaction. Although the larger portion of the embankment is composed of hydraulic fill, the upper portion was built with a rolled clayey core flanked by rockfill shell zones. In 1974, a rockfill buttress was added to the upstream slope to increase freeboard and to provide increased stability.

The dam is located approximately 24 miles from the Loma Prieta fault-rupture zone, and it probably experienced peak ground accelerations between 0.1 and 0.15 *g* (fig. 1). At the time of the earthquake, the reservoir was about 70 feet below the crest of the dam.

The dam experienced no significant damage. Reported incidents consisted of minor changes in piezometers, a temporary 25 to 30 percent increase in seepage, and the muddying up of seepage water attributed to a stirring up of silt by the shaking of the earthquake.

SAN LUIS DAM

San Luis Dam is a 313-foot-high dam that was completed in 1967. It is composed of a homogeneous section of compacted clayey material with internal drains and is flanked with slope protection zones. In 1981, a portion of the upstream slope developed a large slide following a severe draw-

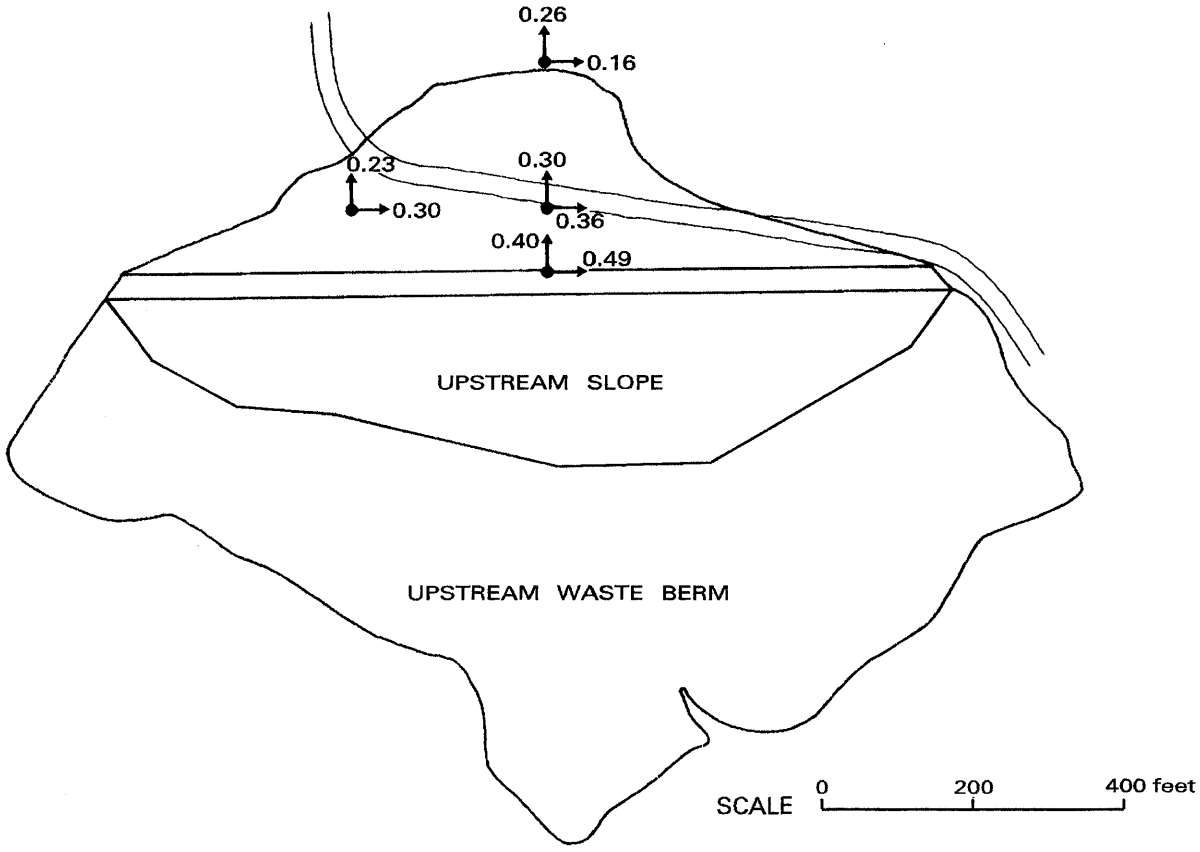

Figure 14.—Plan view of San Justo Dam.

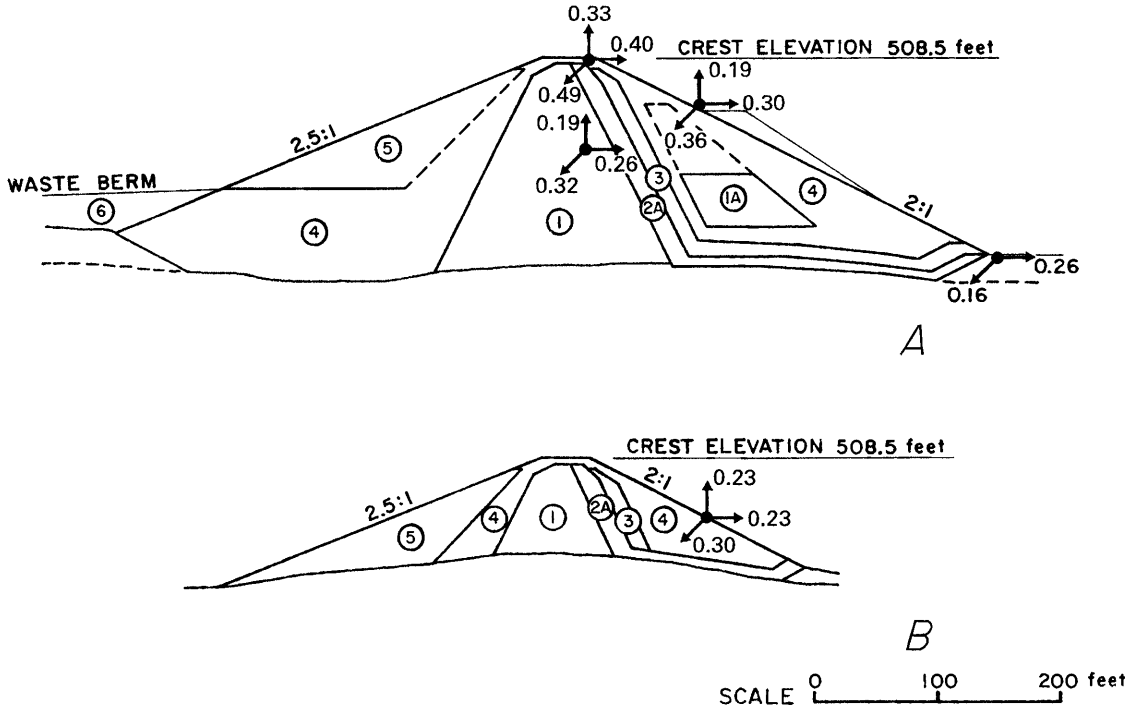

Figure 15.—Maximum (*A*) and Left Quarter (*B*) sections of San Justo Dam.

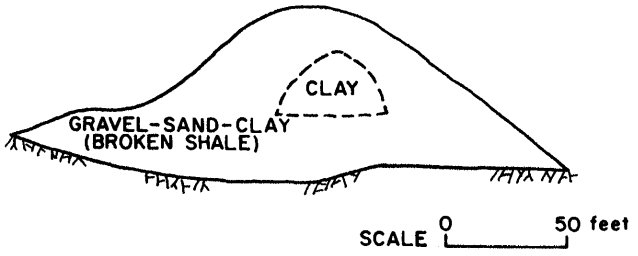

Figure 16.—Cross section of Hawkins Dam (from Lee and Roth, 1977).

down of the reservoir. Although the slide began below the crest, the slide propagated far enough back to take out a portion of the crest. The slide was found to involve slopewash material left in place in the foundation. The dam was repaired by leaving the slide material largely in place, buttressing the slide with a large upstream berm, and rebuilding the crest section.

San Luis Dam is located about 34 miles from the Loma Prieta fault-rupture zone (fig. 1). At the time of the earthquake, the reservoir was less than half full. Strong motion sensors at two locations along the downstream toe recorded peak horizontal accelerations of 0.06 and 0.10 *g*. The corresponding locations on the crest recorded peak horizontal accelerations of 0.25 and 0.17 *g*. Despite experiencing moderate levels of ground motion, the dam experienced no significant damage. Two days after the earthquake, small longitudinal hairline cracks were found on the crest in the vicinity of the slide. These cracks appeared to be largely preexisting cracks which may have widened slightly following the earthquake. Longitudinal hairline cracks were also found on the crest at other locations. The largest crack was longitudinal and had a width of less than 1/4 of an inch. It was located near the right abutment, where the height of fill was only about 5 feet. No repairs were needed at this dam as a result of the earthquake.

O'NEILL DAM

O'Neill Dam stores a reservoir that serves as the forebay to San Luis Dam. It was also completed in 1967 and is a homogeneous earth dam with an internal downstream blanket drain and exterior slope protection zones. It has a maximum height of about 70 feet (fig. 17).

Recent studies have indicated that the alluvial foundation contains in some locations a layer of potentially liquefiable sand lying immediately beneath a surface clay cap. Corrected Standard Penetration Test (SPT) blowcounts in this sand layer have been found to be as low as three in some areas. Because the dam may someday experience a peak acceleration as high as 0.55 *g* from a nearby *M*=6.5 earthquake, it had been concluded that these shallow layers could liquefy and result in a failure of the dam. As a result of these evaluations, suspect areas were treated in 1991 by removing and replacing the shallow liquefiable sands downstream of the dam with compacted, imported material. Large downstream buttresses were also constructed.

O'Neill Dam is located about 37 miles from the Loma Prieta fault-rupture zone (fig. 1). At the time of the earthquake, the reservoir was about 13 feet below the crest of the dam. Strong-motion sensors recorded a peak horizontal acceleration of 0.10 *g* at the downstream toe and values of 0.11 *g* and 0.14 g at two locations on the crest. No damage was reported.

Because of the planned repair to improve seismic stability, it was of interest to compare the predicted versus actual performance of the liquefiable sand layers during Loma Prieta. To this end the downstream areas of two sites having the lowest SPT blowcounts, the station 100 and station 133 areas, were analyzed to determine the predicted factors of safety against the development of liquefaction. The resulting calculated factors of safety against triggering liquefaction during Loma Prieta were between 1.2 and 1.5. These "predicted" factors of safety correspond well with the observation of no damage at this dam.

COSTS OF MAJOR REPAIRS FOR EARTHQUAKE DAMAGE

Although most dams performed reasonably well during the earthquake, some required minor to major repairs. The approximate repair costs for some of the dams discussed in this report are summarized in table 8.

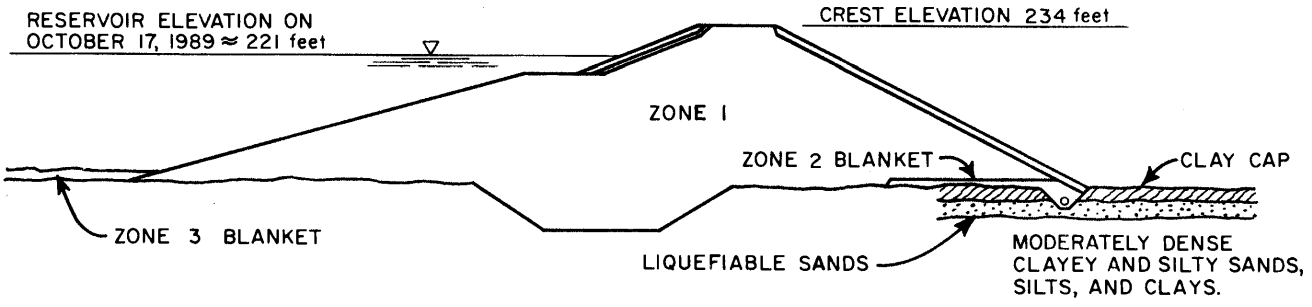

Figure 17.—Maximum cross section of O'Neill Dam.

Table 8.—*Approximate repair costs for earthquake damage*

Dam	Approximate Repair Cost
Austrian	[1] $ 2,500,000
Lexington	$ 150,000
Guadalupe	$ 100,000
Chesbro	$ 75,000
Vasona	$ 20,000

[1] Another $ 8 million was expended for the design and construction of a new spillway as a result of the earthquake.

Table 9.—*Peak accelerations measured at earth dams during the Loma Prieta earthquake*

[T, transverse direction; L, longitudinal direction; V denotes vertical direction]

Dam	Maximum height (feet)	Peak accelerations (*g*) Base			Abutment			Crest		
		T	L	V	T	L	V	T	L	V
Lexington	205				.45	.41	.15	.39	.40	.22
								.45	.34	.20
San Justo[1]	135	.26	.16					.40	.49	.33
Leroy Anderson[1]	235	.26	.25	.17	.07	.08	.05	.39	.26	.19
		.23	.18	.16				.43	.32	.16
								.38	.32	.23
San Luis	313	.04	.06	.02				.19	.25	.07
		.07	.10	.03				.17	.14	.05
O'Neill	70	.08	.10	.05				.11	.11	.06
								.14	.10	.06
Martinez	54	.09	.08	.02				.14	.15	.04
Del Valle	222	.04	.06	.03				.08	.08	.07
Contra Loma	88							.07	.05	.03

Note: [1] denotes that other records are available from other instruments at this dam

STRONG MOTIONS RECORDED ON EMBANKMENT DAMS

The Loma Prieta earthquake provided an excellent opportunity to calibrate dynamic response techniques. As illustrated in table 9, strong-motion records were recorded at eight embankment dams. This information was summarized from the studies by Maley and others (1989), Shakal and others (1989), and Wood and others (1991).

Presented in figure 18 is a plot comparing the peak transverse accelerations measured at both the base and crest of several earth and rockfill dams. These measurements include those made during the Loma Prieta earthquake as well as those made during previous events. As may be observed, the

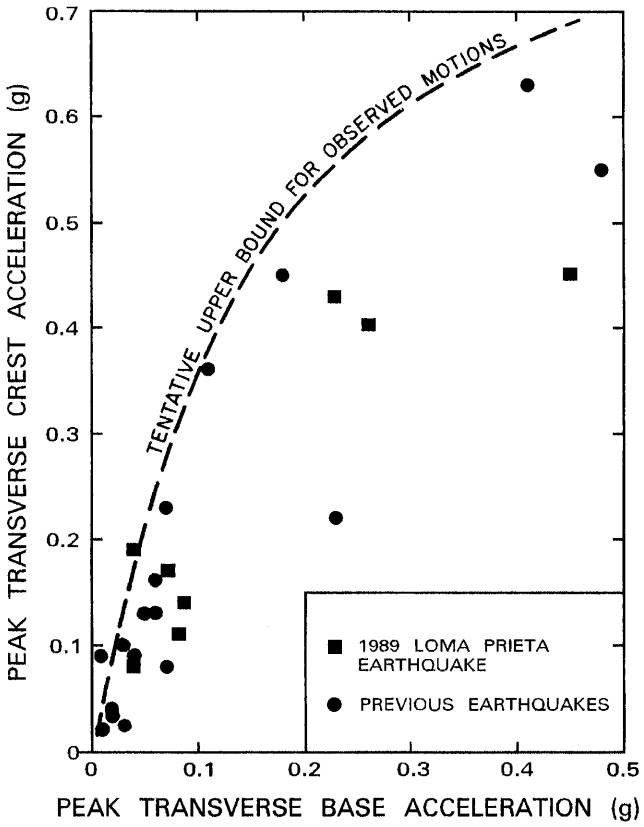

Figure 18.—Comparison of peak base and crest transverse accelerations measured at earth dams.

points indicate that at low accelerations, the amplification through embankment dams is relatively large. However, as the peak base accelerations become larger, the amount of amplification is relatively low, possibly a result of increased damping or yielding of embankment materials. Also shown in figure 18 is a tentative upper bound curve. This curve should not necessarily be used for design purposes, but it may be useful as a verification tool in the performance of dynamic response analyses.

CONCLUSIONS

Several earth dams were subjected to relatively strong shaking during the Loma Prieta earthquake and, in general, performed satisfactory. One major dam (Austrian) and one minor dam (Soda Lake) developed moderate damage. A small number of other dams developed minor to moderate cracking which required repair.

A major factor in the good performance of some dams was the fact that the reservoirs were commonly at less than half their maximum height. Consequently, major portions of the embankments were not as saturated as they would have been during full reservoir condition. Thus, the earthquake was not the most critical test of these structures. Nevertheless, the performance and strong-motion data will provide researchers with invaluable opportunities to learn more about how earth and rockfill dams behave during earthquakes.

ACKNOWLEDGMENTS

The purpose of this paper was to present an overview of the performance of earth dams during the Loma Prieta earthquake. To this end, the detailed inspection reports prepared by the California Division of Safety of Dams following the earthquake were invaluable. Providing other details were the generally excellent reports prepared by consulting engineers that are presented in the list of references. The authors also acknowledge Professor Raymond B. Seed and several staff members of the California Division of Safety of Dams for providing many useful pieces of information. The assistance of Thomas Holzer in the publication of this paper is also gratefully acknowledged.

REFERENCES

Aydin, Atilla, Johnson, Arvid M., and Fleming, Robert W., 1992, Right-lateral-reverse surface rupture along the San Andreas and Sargent faults associated with the October 17, 1989, Loma Prieta, California, Earthquake: Geology, v. 20, p. 1063-1067.

Bureau, Gilles, Babbitt, Donald H., Bischoff, John A., Volpe, Richard L., and Tepel, Robert E., 1989, Effects on dams of the Loma Prieta Earthquake of October 17, 1989: United States Committee on Large Dams, Newsletter no. 90, p. 1-4.

Creegan, Patrick, 1990, Newell Dam and the Loma Prieta earthquake: United States Committee on Large Dams, Newsletter no. 91, p. 9-11.

Lee, Kenneth L., and Roth, Wolfgang, 1977, Seismic stability analysis of Hawkins hydraulic fill: Journal of the Geotechnical Engineering Division, American Society of Civil Engineers, v. 103, no. GT6, p. 627-644.

Maley, R., Acosta, A., Ellis, F., Etheredge, E., Foote, L., Johnson, D., Porcella, R., Salsman, M., and Switzer, J., 1989, U. S. Geological Survey Strong-Motion Records from the Northern California (Loma Prieta) earthquake of October 17, 1989: U. S. Geological Survey Open-File Report 89-568.

Rodda, K. V., Harlan, R. D., and Pardini, R. J., 1990, Performance of Austrian Dam during the October 17, 1989 Loma Prieta earthquake: United States Committee on Large Dams, Newsletter no. 91, p. 7-9.

Seed, H. Bolton, Makdisi, Faiz I., and De Alba, Pedro, 1978, The performance of earth dams during earthquakes: Journal of the Geotechnical Engineering Division, American Society of Civil Engineers, v. 104, no. GT7, p. 967-994.

Seed, R. B., Dickenson, S. E., Riemer, M. F., Bray, J. D., Sitar, N., Mitchell, J. K., Idriss, I. M., Kayen, R. E., Kropp, A., Harder, L. F., and Power, M. S., 1990, Preliminary report on the principal geotechnical aspects of the October 17, 1989 Loma Prieta earthquake: Earthquake Engineering Research Center, Report No. UCB/EERC-90/05, University of California, Berkeley.

Shakal, A., Huang, M., Reichle, M., Ventura, C., Cao, T., Sherburne, R., Savage, M., Darragh, R., and Peterson, C., 1989, CSMIP strong-motion records from the Santa Cruz Mountains (Loma Prieta), California earthquake of 17 October 1989: California Division of Mines and Geology, Report No. OSMS 89-06.

Spudich, Paul, 1996, Synopsis, *in* The Loma Prieta, California, earthquake of October 17, 1989—Main-shock Characteristics: U. S. Geological Survey Professional Paper 1550-A.

Volpe, R. L. & Associates, 1990a, Investigation of SCVWD Dams affected by the Loma Prieta earthquake of October 17, 1989: Report prepared for the Santa Clara Valley Water District.

Volpe, R. L. & Associates, 1990b, Repair of SCVWD dams affected by the Loma Prieta earthquake of October 17, 1989: Report prepared for the Santa Clara Valley Water District.

Wahler Associates, 1990, Austrian Dam—Investigation and remedial construction following the October 17, 1989 Loma Prieta earthquake: Report prepared for the San Jose Water Company.

Wahler Associates (1992), Seismic Safety Evaluation of Mill Creek Dam: Report prepared for Lockheed Missiles and Space Company.

Wood, Chris, Copeland, David, and Viksne, Andy, 1991, Strong-motion data—Loma Prieta Earthquake of October 17, 1989, San Justo dam and dike, San Luis dam, O'Neill dam, Martinez dam: U. S. Bureau of Reclamation.

EARTH STRUCTURES AND ENGINEERING CHARACTERIZATION OF GROUND MOTION

ANALYSIS OF SOIL-NAILED EXCAVATIONS STABILITY DURING THE 1989 LOMA PRIETA EARTHQUAKE

By Mladen Vucetic, University of California, Los Angeles;
Mark R. Tufenkjian, California State University, Los Angeles;
Guy Y. Felio, National Research Council, Ottawa, Canada;
Pirooz Barar, Pirooz Barar & Associates, Oakland, California; and
K. Ronald Chapman, Schnabel Foundation Co., Walnut Creek, Calif.

CONTENTS

ABSTRACT

The performance of nine different grouted soil-nailed excavations in the San Francisco Bay area during the Loma Prieta earthquake is analyzed on the basis of postearthquake visual inspections, subsequent stability analyses, and dynamic centrifuge model tests. None of the excavations showed any signs of movements or similar distress, even though one of them was located in the vicinity of the earthquake epicenter where there was strong shaking and important seismic-related damage to other structures. The design and construction practices of grouted soil-nailed excavations in California are discussed. It is concluded that a combination of conservative design and construction is the primary reason for excellent seismic stability. It is also confirmed that the method developed and used by Caltrans for calculating the factor of safety is suitable for the stability analysis of the grouted soil-nailed excavations encompassed by the study. This method is based on a bilinear failure surface and the so-called German mode of failure that considers two sliding blocks.

INTRODUCTION

Soil nailing is an in-situ technique of mechanically stabilizing soil masses which has been used in Europe for more than two decades (Stocker and others, 1979; Chapman and Ludwig, 1993; Federal Highway Administration, 1993). In North America, as well as in Japan (Japan Highway Public Corporation, 1987; Ochiai and others, 1992), soil nailing is steadily gaining popularity because it can be used with conventional shoring equipment, it reduces excavation time, it allows construction-related activities to proceed in restricted space, and it can produce significant savings over conventional shoring techniques in the proper ground conditions.

The main feature of soil nailing is that it is an in-situ method where the existing natural soil is reinforced, as opposed to a backfill reinforcement. As shown in figure 1, the inclusions, commonly called nails, are installed during the excavation using a "top-down" construction procedure, unlike reinforced earth walls which are constructed from the bottom up. This allows soil retention in areas where little space is available for the excavation. The soil-nailing concept is to reinforce the soil with passive inclusions, so that the nailed soil mass behaves as a composite unit, similar to a gravity retaining wall supporting a soil backfill (Juran and Elias, 1991; Mitchell and Villet, 1987). In that sense, soil nailing also differs from the conventional tie-back excavation support since the soil nails are not prestressed; that is, their resistance can be mobilized only by the movement of soil mass or the face of the excavation to which the nails are fixed. Figures 2 to 4 show several soil-nailed retaining structures treated in this paper.

At present, there are three major concerns about soil-nailed excavations: (1) the adequacy of the analysis or design meth-

ods, (2) the long-term behavior, and (3) the performance during seismic loading. Items (1) and (2) have been addressed by many researchers, including recently by Gassler (1992), Juran and others (1990), Plumelle and others (1990), and Stocker and Riedinger (1990). With respect to soil-nailing performance during earthquakes, no full-scale field observations were available until the Loma Prieta earthquake. During the earthquake, nine soil-nailed structures were subjected to different levels of shaking, including horizontal ground-surface accelerations probably as high as 0.4 g. In spite of such relatively high horizontal accelerations, these structures did not show any visible movements or other signs of distress (Felio and others, 1990; Hudson, 1990). A systematic description of these structures and a discussion of possible reasons why they performed so well are the main purposes of this paper. More details about the corresponding investigation can be found in Tufenkjian and Vucetic (1993).

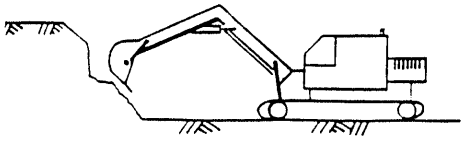

1. Excavation

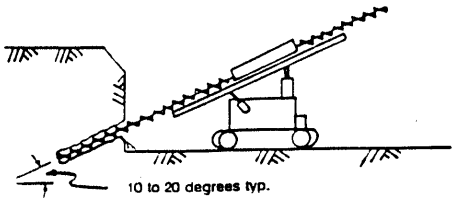

2. Drilling of nail holes

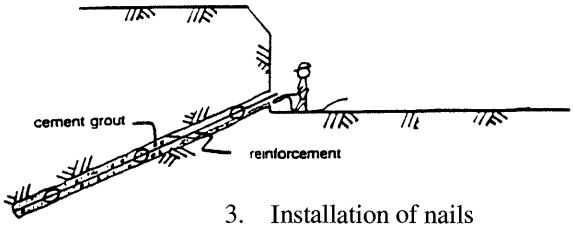

3. Installation of nails

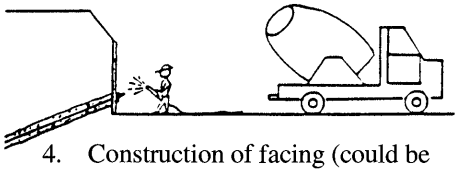

4. Construction of facing (could be also done before the nails are installed)

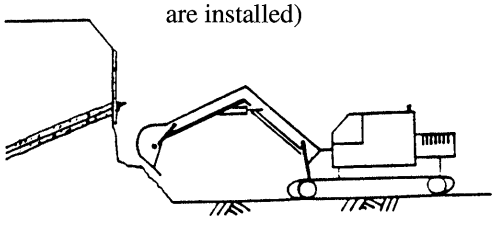

5. Repeat excavation and steps 2 to 4

Figure 1.—Steps in the construction of a grouted soil-nailed excavation.

SOIL NAILING PRACTICE IN CALIFORNIA

There are three major steps in the construction of a soil-nailed wall, as illustrated in figure 1. They are (1) excavation, (2) installation of nails, and (3) construction of facing. The excavation generally proceeds in stages ranging from 1.2 to 1.8 m in depth. One of the major requirements for successful soil-nailed systems is that the excavation be capable of self-support for at least a few hours prior to nailing and construction of facing. For the most economical construction, however, the self-support should be able to last 1 to 2 days. As the excavation of each level proceeds, the nails are installed at predetermined locations. These reinforcing elements may be one of several types: driven, grouted, jet-grouted, or even pneumatically propelled into the ground (Myles and Bridle, 1991). However, the vast majority of installations are of the open drilled and grouted type (Chapman and Ludwig, 1993; Federal Highway Administration, 1993).

In California, and North America in general, the most popular type of nails are the grouted nails, such as those shown in figures 2, 3 and 4, since in many locations the soil conditions allow the excavation to stand open long enough. Grouted nails generally consist of Grade 60 mild steel bars (15 to 45 mm in diameter) placed in boreholes of 100 to 250 mm diameter. Plastic centralizers are often used to ensure proper grout cover of the nail. A cement grout is then placed into the boreholes by gravity flow or low pressure. Typical horizontal and vertical spacings range from 1 to 3 m, depending upon the designer's experience and soil conditions. The nails are generally inclined at 10° to 20° from the horizontal.

Either before or after the nails are in place, a facing structure is built. The facing is required to control soil erosion at the excavation face and reduce changes in the moisture content of the soil. The most common type of facing is shotcrete layer, 100 to 250 mm thick, which is usually placed by the shotcrete method and which is reinforced with welded wire mesh. A typical detail of the nail connection to such facing is presented in figure 5. If necessary, a blanket of nonwoven geotexile is placed between the natural soil and the shotcrete to control the drainage. The grouted nail is attached to the facing by bolting the steel bar to a square plate usually 300 to 400 mm wide. For additional reinforcement and strengthening of the facing, horizontal waler bars may be installed to connect the plates. Other methods of attachment are used for driven nails. For permanent walls, the shotcrete facing

may not provide for the aesthetic requirements of the project. In such cases, either cast-in-place reinforced concrete facing or prefabricated panels can be used. Figure 6 shows photos of large soil-nailed excavation structures recently completed in California.

THE LOMA PRIETA EARTHQUAKE

The Loma Prieta earthquake (M_s=7.1) was one of the most costly single natural disasters in U.S. history. It caused extensive damage, such as landslides in the epicentral region, liquefaction in various areas of the San Francisco Bay region, structural distress to commercial, industrial, and residential buildings, widespread disruption or total destruction of utility systems, and damage to critical transportation systems. The earthquake has been the subject of a wide range of studies, many of them on geotechnical-related failures, as summarized by Seed and others (1991).

Figure 7 presents an overview of the regional geology and the recorded peak horizontal ground-surface accelerations during the earthquake. The locations of the nine soil-nailed walls considered in this paper are identified on the figure by stars, and the location of the epicenter by a circle. The figure shows that in the epicentral area the measured maximum horizontal ground-surface accelerations, a_{max}, were as high as 0.64 g and the vertical up to 0.60 g. It can be seen that the soil-nailed walls in the northern region (in Richmond, San Francisco, Walnut Creek, and San Ramon) were subjected to seismic forces corresponding to a_{max} of about 0.10 g. In the vicinity of the two walls in Mountain View, an a_{max} of around 0.2 g was measured. In the vicinity of the wall in San Jose, a_{max} was between 0.11 and 0.18 g. The largest a_{max} (0.47 g) recorded near a soil-nailed wall was in Santa Cruz, some 16 km due west of the epicenter.

Most of these locations were visited and inspected 2 days after the earthquake by a team from the University of California, Los Angeles (Felio and others, 1990), and some walls were inspected subsequently by design and construction companies. As stated earlier, no signs of distress or corresponding deformation were found on the walls, indicating excellent performance of such structures during moderate and strong shaking.

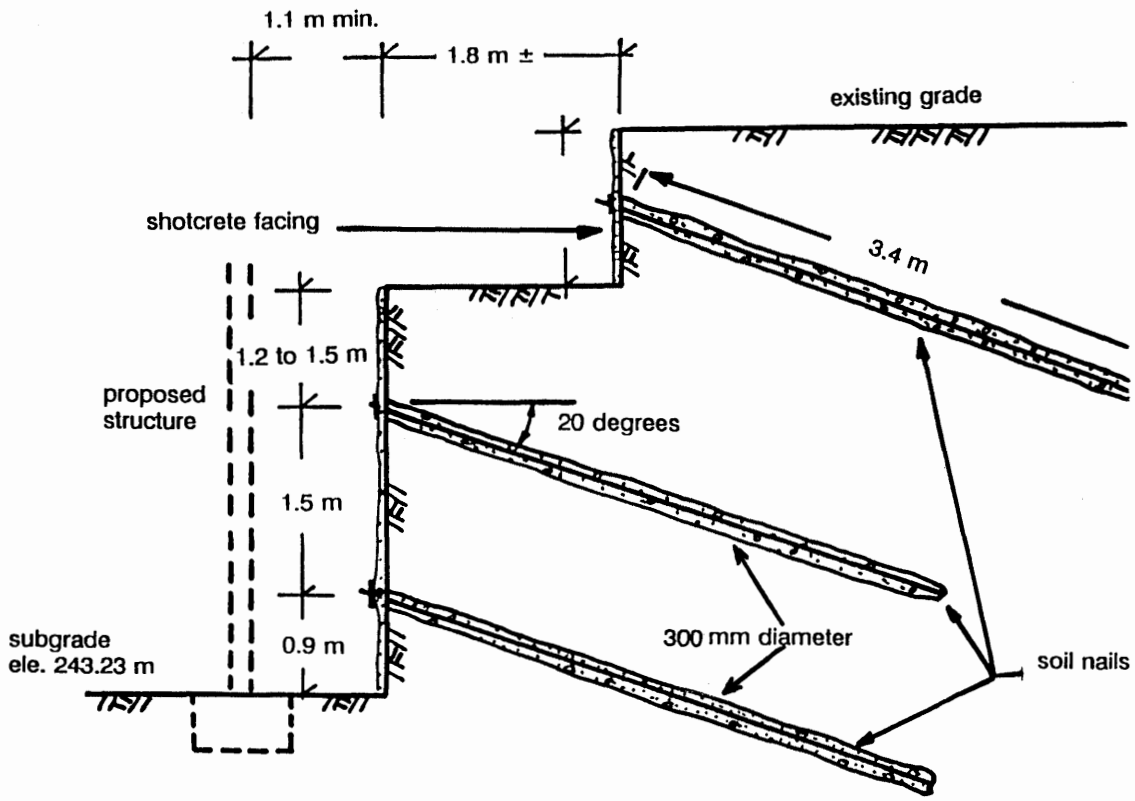

Figure 2.—Cross section of a soil-nailed excavation for a building constructed in Santa Cruz (UCSC wall), Calif. (Felio and others, 1990).

CHARACTERISTICS AND DESCRIPTION OF THE WALLS

The main characteristics of the nine walls inspected after the earthquake are summarized in table 1. In figure 8 the dimensions of the walls are presented in a uniform scale. The variation of the geometry, characteristics of the walls, soil conditions, and estimated ground-surface accelerations are evident. The walls are further characterized in table 2 in terms of the following three dimensionless ratios commonly used as design criteria (Bruce and Jewell, 1987):

$$\text{Length ratio} = \frac{\text{maximum nail length}}{\text{excavation height}} \quad (1)$$

$$\text{Bond ratio} = \frac{\text{hole diameter} \times \text{nail length}}{\text{horizontal spacing} \times \text{vertical spacing}} \quad (2)$$

$$\text{Strength ratio} = \frac{(\text{nail diameter})^2}{\text{horizontal spacing} \times \text{vertical spacing}} \quad (3)$$

Table 3 further compares the three dimensionless ratios computed for the nine San Francisco walls, with the values computed by Bruce and Jewell (1986, 1987) for soil-nailed structures with drilled and grouted nails constructed all over the world. The bond and strength ratios generally fall within the range of other soil-nailed retaining structures. However, the length ratios for the San Francisco walls are generally much higher than those calculated from other sites, suggesting that the San Francisco walls are more conservatively designed. Note from table 2 that the length ratio for the UC Santa Cruz wall is the smallest. This wall is apparently the least conservatively designed of all of the walls, yet it is located in the vicinity of the highest estimated peak horizontal ground-surface acceleration. In spite of these facts, no ob-

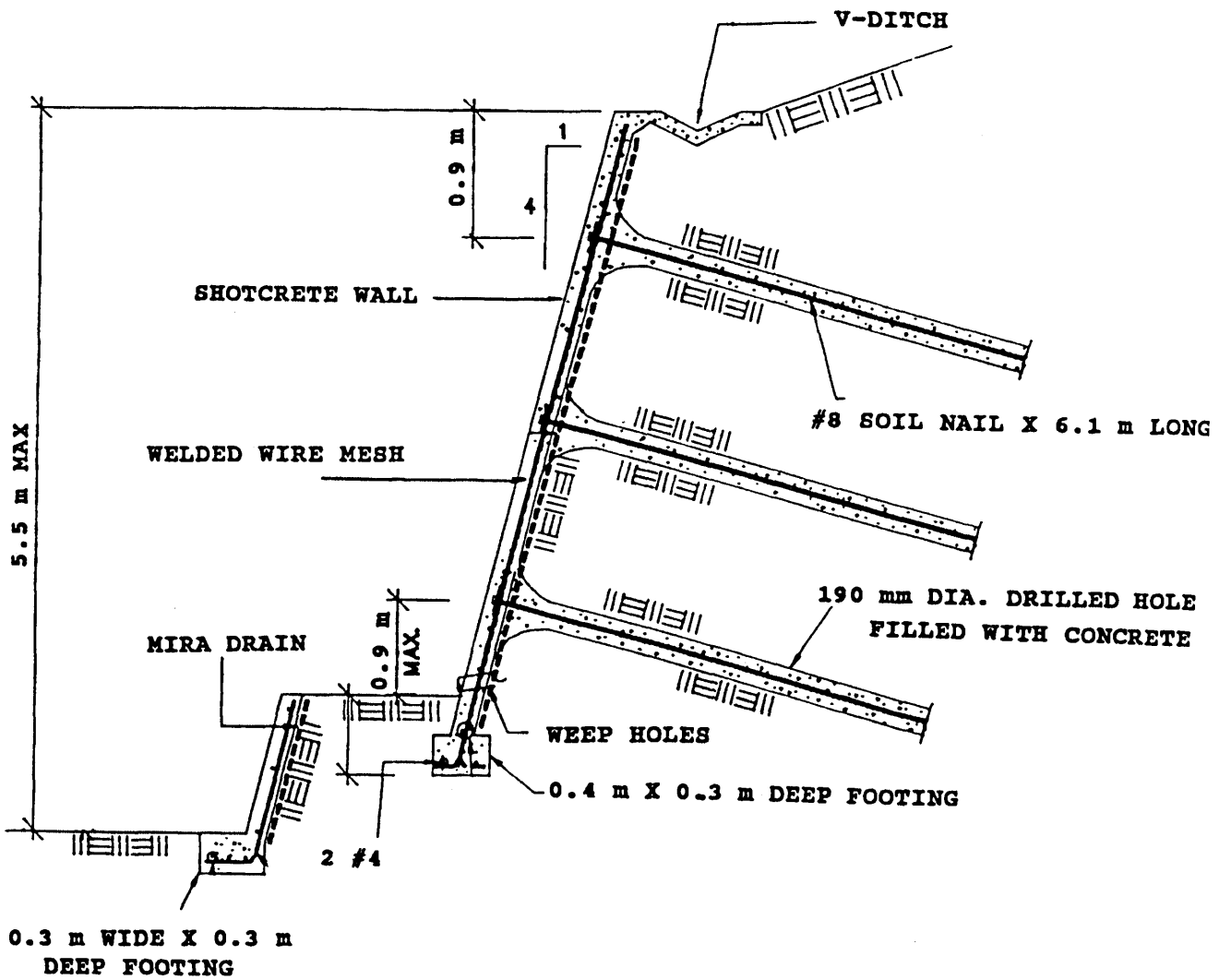

Figure 3.—Cross section of a permanent soil-nailed retaining structure located in San Ramon (NME wall), Calif. (Barar, 1990).

servable damage was noted on the Santa Cruz structure after the earthquake. The walls are described in greater detail below.

MOUNTAIN VIEW, 2350 EL CAMINO REAL (ECR WALL)

Nearly 280 m^2 of soil-nailing construction was used to provide temporary shoring of an excavation for an office building. The concrete wall for the new structure was to be poured in front of the soil-nailed concrete facing. The subsurface soil consisted of gravelly and clayey sand. The shear-strength parameters used in design were $c = 9.6$ kN/m^2 and f = 30°, while the soil unit weight was assumed to be 17.3 kN/m^3. The soil-nailed wall was completed by May of 1989 and the excavation was still open when the earthquake struck. Postearthquake observations revealed only a few shallow hairline cracks in the concrete facing, typical of flexural cracking if the facing is considered as a vertical slab with the nails acting as reaction points. Note in table 1 that the facing of this wall was relatively thin (100 mm), while the estimated horizontal acceleration was considerable (0.21 to 0.27 *g*).

MOUNTAIN VIEW, KAISER PERMANENTE PARKING GARAGE (KPG WALL)

Approximately 380 m^2 of shoring was provided for the construction of a parking garage. Soil nailing was used only on one side of the excavation, while a combination of other shoring techniques were used on the remaining sides. The soil conditions at the site consisted of stiff sandy to clayey

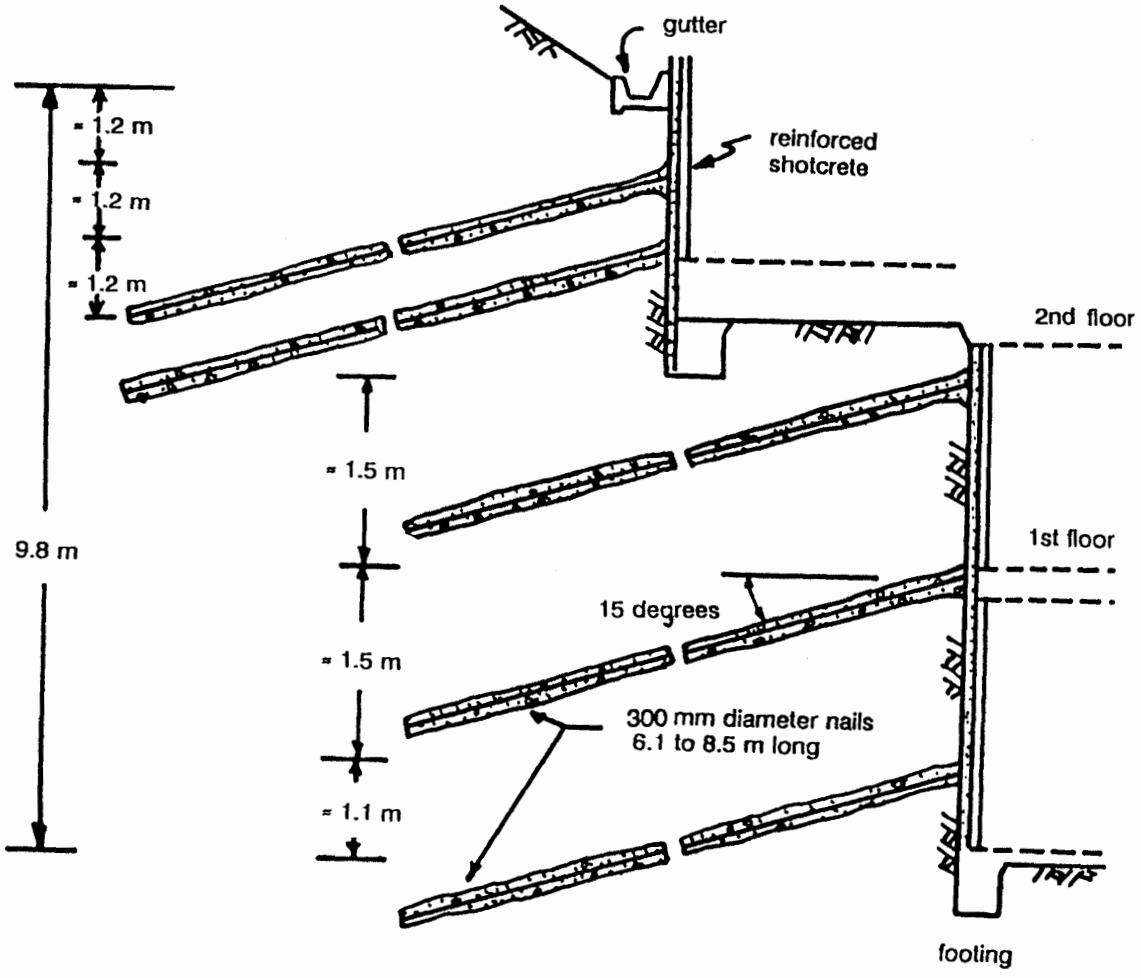

Figure 4.—Cross section of a soil-nailed retaining wall constructed on a steep hill in San Francisco (CVA wall), Calif., to provide adequate space for an apartment complex (Felio and others, 1990).

silt overlying silty to sandy clay. The shear strength parameters used in design were $c = 23.9$ kN/m^2 and f = 14°, while the soil unit weight was assumed to be 18.8 kN/m^3. The construction of the shoring was completed just 8 days before the earthquake. The postearthquake observations revealed no visible distress to the soil-nailed wall, while the opposite side

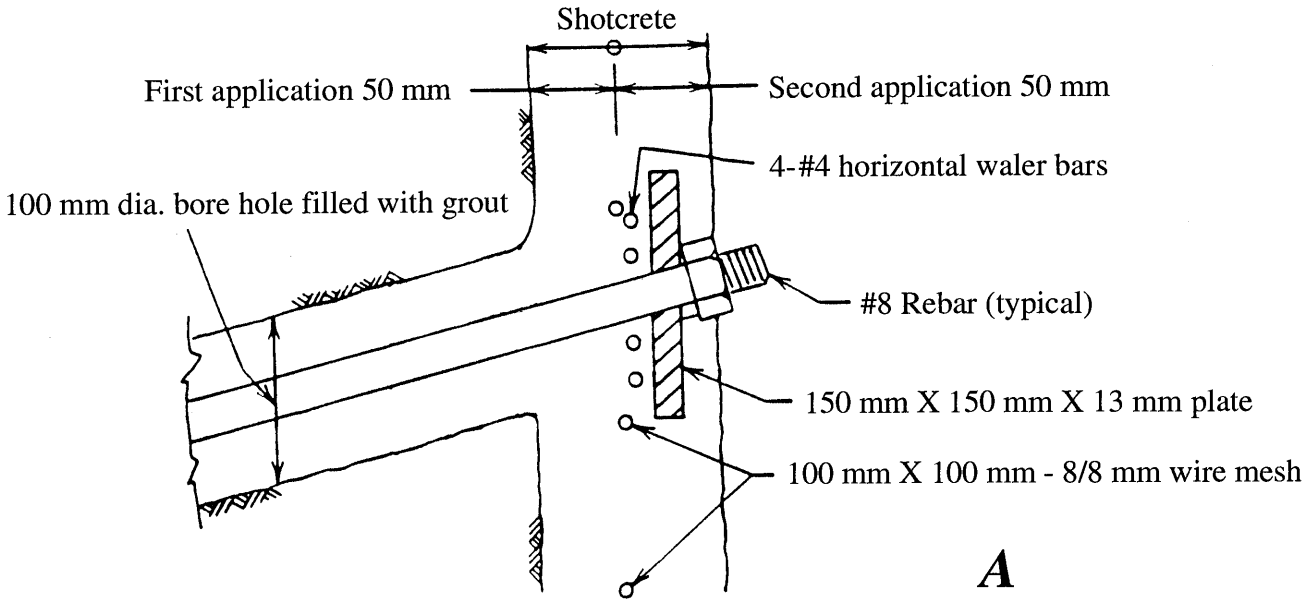

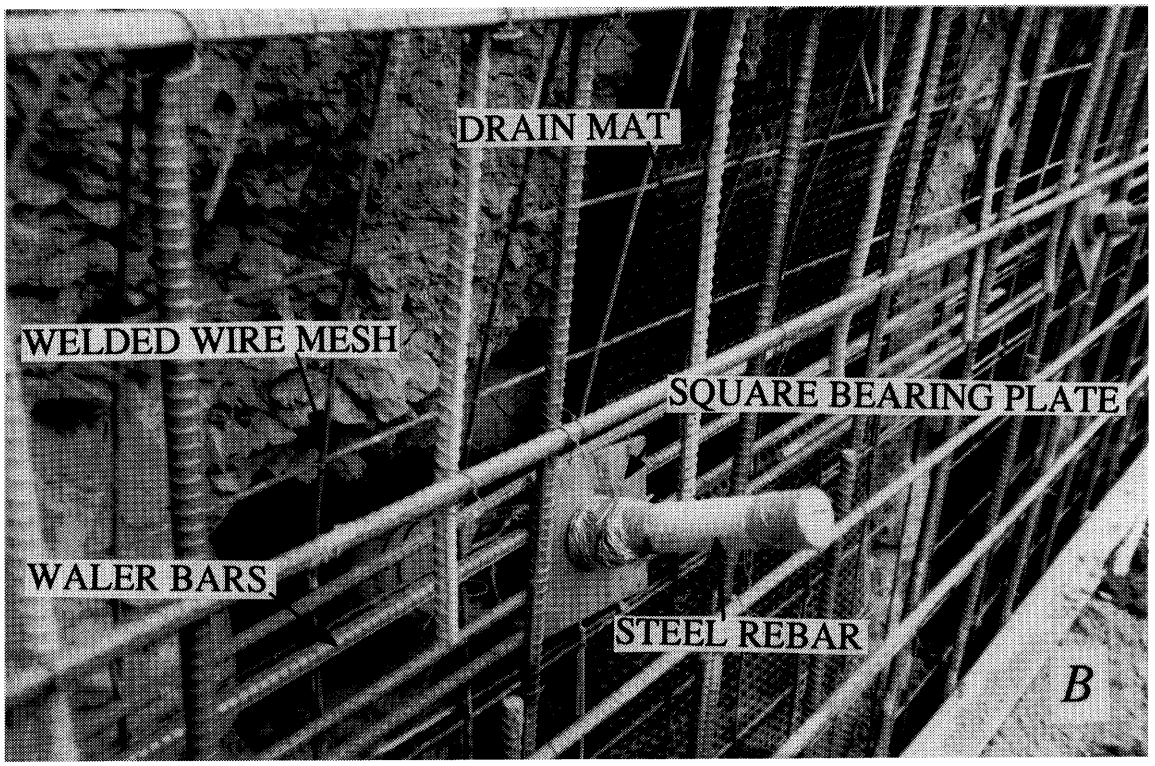

Figure 5.—Connection between grouted nail and facing. *A*, Cross section of a typical connection (from Koerner, 1984). *B*, Strong reinforcement around the nail tip.

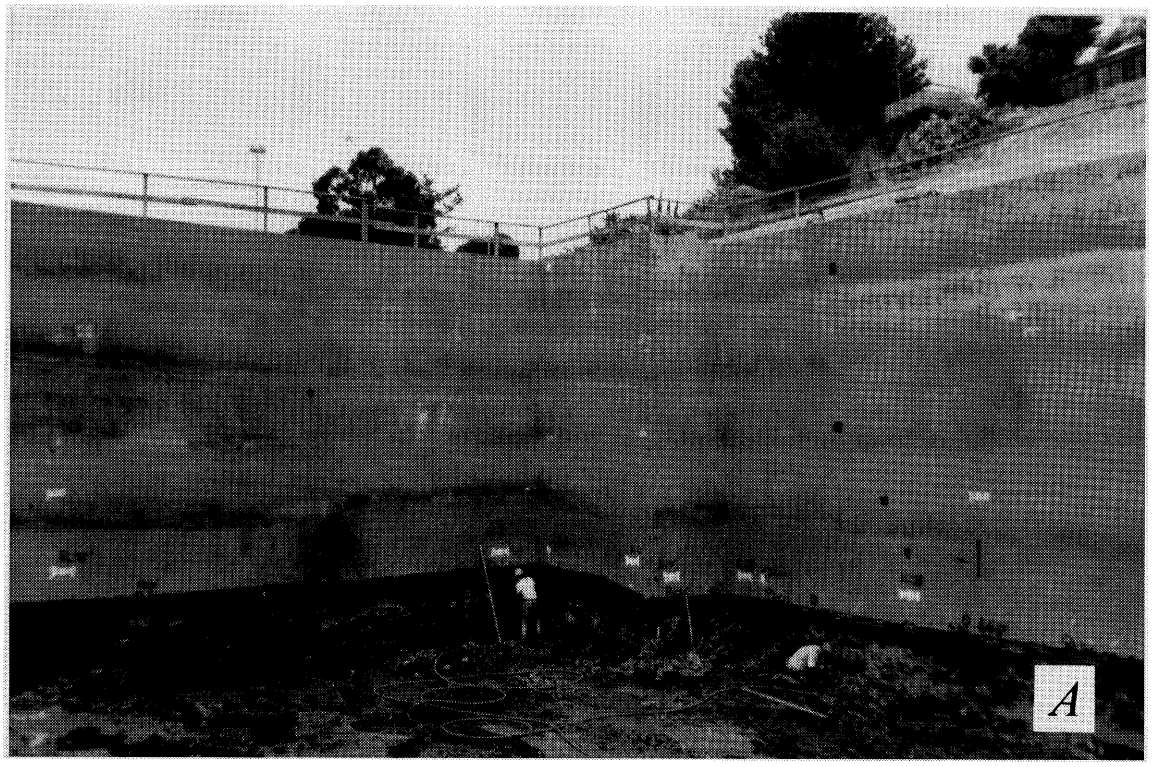

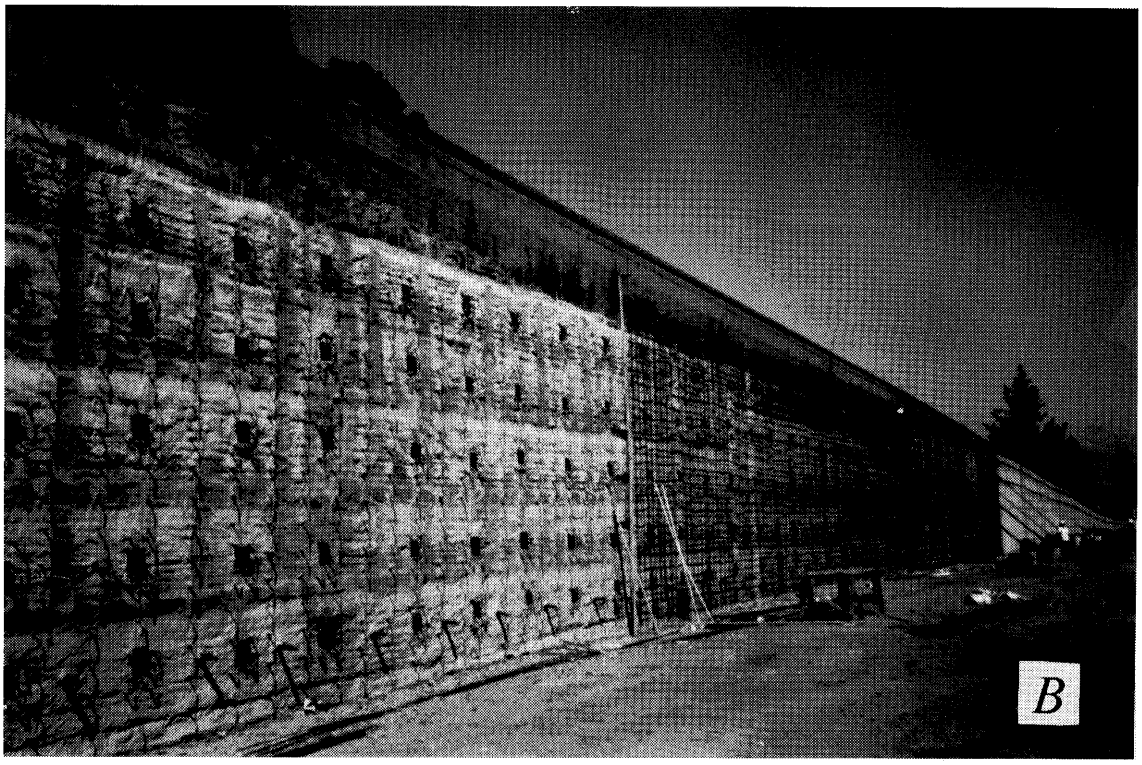

Figure 6.—Soil-nailed structures recently completed in California. *A*, Soil-nailed excavation for an underground structure of a building. *B*, A highway retaining soil-nailed wall showing different stages of the construction of permanent facing.

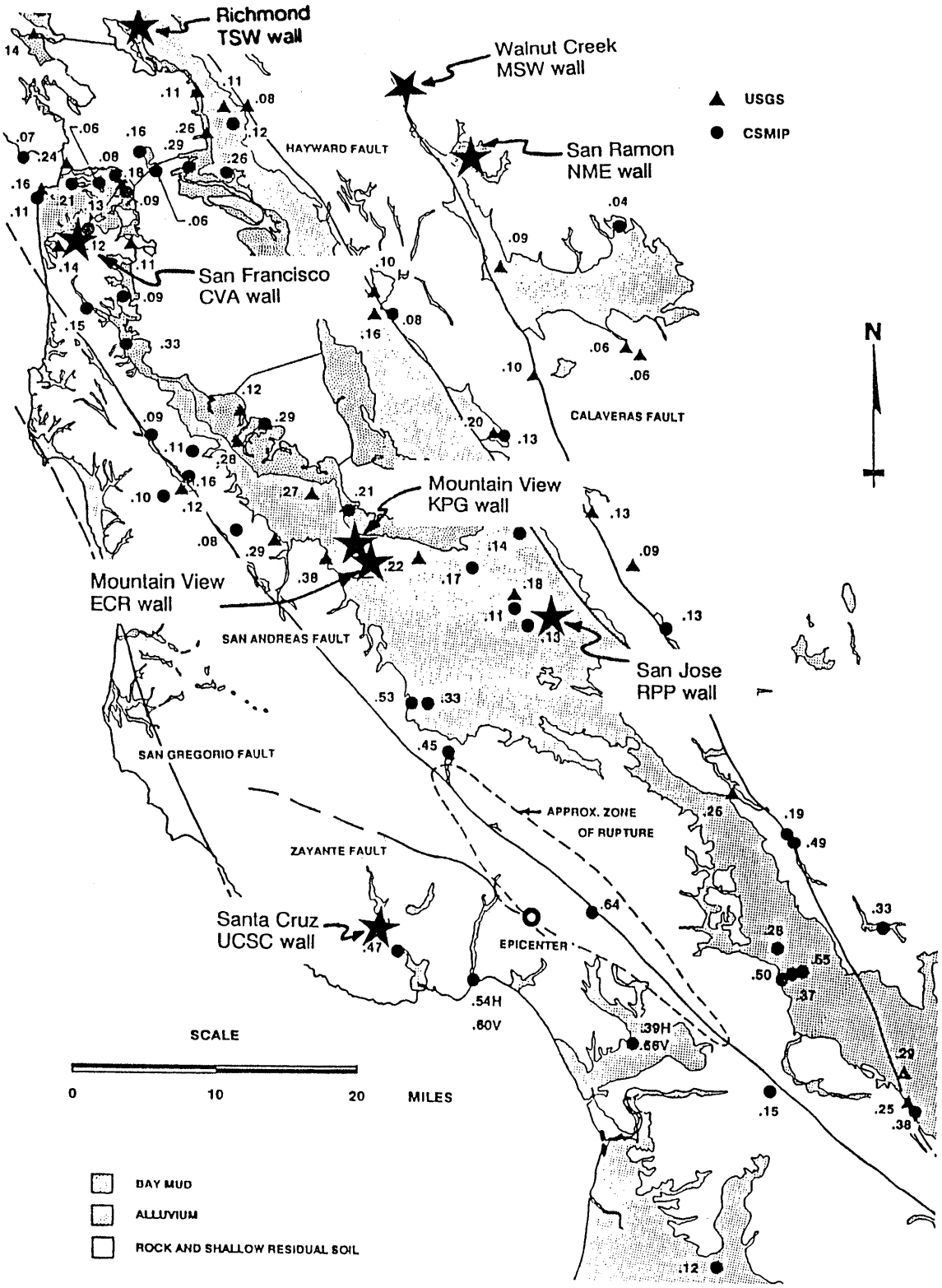

Figure 7.—Overview of regional geology and recorded peak horizontal ground-surface accelerations during the Loma Prieta earthquake (from Seed and others, 1991).

of the excavation, which used cantilevered soldier beams with a concrete facing between the beams, revealed some vertical hairline cracks in the facing.

SANTA CRUZ, UNIVERSITY OF CALIFORNIA AT SANTA CRUZ (UCSC WALL)

Approximately 350 m^2 of shoring was required to construct a new science library on the UCSC campus. The soil conditions at the site consisted of sandy silt to sandy clayey silt extending from the ground surface to a depth of approximately 6.4 m. The soil has an average dry unit weight of 13.8 kN/m^3 and a moisture content ranging from 26.2 percent in the clayey silt near the surface to 13.9 percent in the sandy silt at 6.4 m. Shear strength properties used in design were c = 23.9 kN/m^2 and f = 25°. The cross section at the highest location of the wall is shown in figure 2. Construction of the wall was completed on September 28, 1989, less than 3 weeks before the earthquake. Since three sides of the excavation were soil nailed, at least one side may have been subjected to the full strength of the earthquake, which produced in the vicinity of the excavation peak horizontal ground-surface accelerations of about 0.47 g. It should be noted that this wall was located closest to the epicenter and presumably was subjected to the strongest shaking, while at the same time it had the smallest length ratio and thinnest facing among the nine walls examined (see tables 1 and 2). Prior to the earthquake, some wall and column spread footings had been poured (see fig. 2). A postearthquake inspection revealed significant cracking in the concrete of the footings. This cracking was not attributed to shrinkage since foundations constructed after October 17 showed fewer cracks. As opposed to that, the inspection of the soil-nailed wall after the earthquake revealed no cracking. A week after the earthquake, nine nails were tested to 150 percent of their design pull-out load. The tests showed no loss in the carrying capacity of the nails due to the seismic activity.

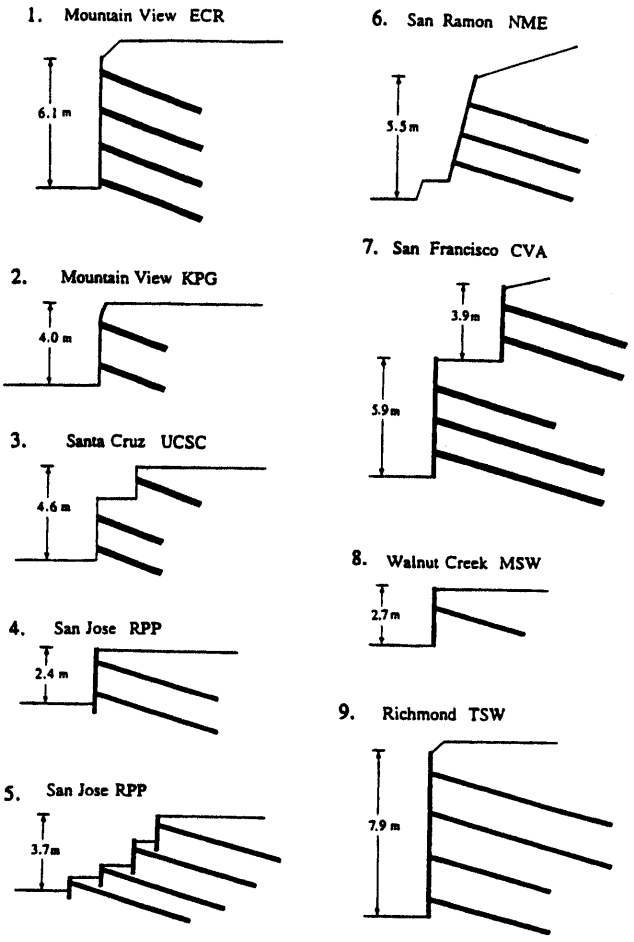

Figure 8.—Dimensions of the investigated soil-nailed walls.

SAN JOSE, RIVERPARK PROJECT (2 RPP WALLS)

These two retaining walls were designed and built as permanent structures along the Guadalupe River in San Jose, approximately 40 km north of the epicenter. The subsurface soil consists of silty and sandy clays to a depth of about 4.5 to 6 m. According to the geotechnical report, these clays have an intermediate to high plasticity with an approximate average dry unit weight and moisture content of 14.1 kN/m^3 and 22 perecent, respectively, and an undrained shear strength ranging from 72 to 240 kN/m^2, as interpolated from static cone penetration tests. The clays are underlain by a 3 m zone of dense, clayey, silty, gravelly sand with an average dry unit weight and moisture content of about 17.3 kN/m^3 and 15 percent, respectively. The shear strength parameters used in design were c = 23.9 kN/m^2 and f = 0°, while the total unit weight was assumed to be 19.6 kN/m^3. Since these are permanent walls, the concrete surface was finished off with architectural concrete and in some places clad with granite. The postearthquake observations revealed no signs of distress.

SAN RAMON, NATIONAL MEDICAL ENTERPRISES COMMUNITY HOSPITAL (NME WALL)

This soil-nailed retaining structure forms a part of a permanent retaining wall used for the roads and landscape that surround the medical center. The wall cross section is shown in figure 3. According to the geotechnical report, the soil conditions consist mainly of engineered fill up to a maximum depth of 24 m, generated from cut-and-fill operations performed previously. Therefore, the soil-nailed retaining structure was built in fill material. The fill consists of sandy and silty clay of moderate to high plasticity, with an average dry unit weight and moisture content of approximately 17.1 kN/m^3 and 18 percent, respectively. The shear strength prop-

Table 1.—*Summary of soil-nailed walls investigated*

Project No.	Location (see fig. 7)	Height of wall (m)	Nail details: Spacing (m)	Length (m)	Diameter: Grout (mm)	Diameter: Rebar (mm)	Inclination (degrees)	Facing thickness (mm)	General soil Type	Soil unit weight (KN/m³)	Shear strength design parameters: c (KN/m²)	Shear strength design parameters: ϕ (degrees)	Estimated horizontal ground surface acceleration (g)
1	Mountain View ECR	6.1	1.7V 1.5H	5.2	300	32	20	100	clayey sand	17.3	9.6	30	0.21 to 0.27
2	Mountain View KPG	4.0	2.0V 1.5H	3.4	300	25	20	100	sandy to clayey silt	18.8	23.9	14	0.21 to 0.27
3	Santa Cruz UCSC	4.6 2-levels	1.5V 1.8H	3.4	300	32	20	75	sandy to clayey silt	18.1	23.9	25	0.47
4	San Jose RPP1	3.7 4-levels	1.8V 1.8H	6.1	180	25	15	200	alluvial clay, silt and sand	19.6	23.9	0	0.10 to 0.15
5	San Jose RPP2	2.4	1.8V 1.8H	6.1	180	25	15	200	alluvial clay, silt and sand	19.6	23.9	0	0.10 to 0.15
6	San Ramon NME	5.5	1.8V 1.8H	6.1	190	25	15	150	engineered fill	18.8	47.9	0	0.05 to 0.10
7	San Francisco CVA	9.8 2-levels	1.8V 1.5H	6.1 to 8.5	300	25	15	200	fill over silty clay and highly weathered siltstone	19.6	9.6	35	0.10 to 0.15
8	Walnut Creek MSW	2.7	(one row) 1.8H	4.6	190	25	15	200	fill over medium stiff to stiff clay	18.8	14.4	28	0.01 to 0.10
9	Richmond TSW	7.9	1.8V 1.8H	6.1 to 9.1	190	25	15	200	alluvium deposits	18.8	19.1	28	0.05 to 0.15

erties used in design were $c = 47.9$ kN/m² and $f = 0°$. Since this is a permanent structure, the facing of the soil-nailed wall was finished with a colored architectural concrete finish. The postearthquake walk-through revealed that the surface of the concrete remained smooth and free of cracks.

SAN FRANCISCO, CRESTA VISTA APARTMENTS (CVA WALL)

This wall demonstrates the unique concept of using soil nailing on a permanent basis to retain the slope and cut on a

Table 2.—*Dimensionless ratios for San Francisco area soil-nailed walls*

Project No.	Location	Length ratio $\left(\frac{\text{max. nail length}}{\text{excav. height}}\right)$	Bond ratio $\left(\frac{\text{hole dia. x nail length}}{\text{H. spacing x V. spacing}}\right)$	Strength ratio (10^{-3}) $\left(\frac{(\text{nail dia.})^2}{\text{H. spacing x V. spacing}}\right)$
1	Mountain View ECR	0.85	0.61	0.40
2	Mountain View KPG	0.85	0.34	0.21
3	Santa Cruz UCSC	0.74	0.38	0.38
4	San Jose RPP	1.6	0.34	0.19
5	San Jose RPP	2.5	0.34	0.19
6	San Ramon NME	1.1	0.36	0.19
7	San Francisco CVA	1.5 to 1.7	0.68 to 0.94	0.28
8	Walnut Creek MSW	1.7	not applicable	not applicable
9	Richmond TSW	1.2	0.36 to 0.53	0.19

Table 3.—*Dimensionless ratios for soil-nailed walls*

	Drilled and grouted in granular soils (Bruce and Jewell, 1986, 1987)	Drilled and grouted in morraine and marl (Bruce and Jewell, 1986, 1987)	San Francisco walls
Length ratio	0.5 to 0.8	0.5 to 1.0	0.7 to 0.25
Bond ratio	0.3 to 0.8	0.15 to 0.20	0.34 to 0.94
Strength ratio (10^{-3})	0.4 to 0.8	0.1 to 0.25	0.19 to 0.40

steep hill to make room for the development of a housing project. The wall cross section is shown in figure 4. The 9.8-m-high soil-nailed structure was constructed at the toe of a 45.7-m-high slope to allow for the construction of apartment units. The wall is about 90 m long and consists of two levels. Due to the permanent nature of the structure, a 200 mm reinforced concrete facing and a small footing at the base were used. The soil conditions at the site can be described as colluvium and residual soil deposits. The design parameters used were cohesion c = 9.6 kN/m^2 and an angle of internal friction of f = 35°. The inspection that took place 3 days after the earthquake showed no signs of distress to the wall and no indications of lateral movements or tension cracks in the hill behind the wall.

WALNUT CREEK, MINI STORAGE FACILITY (MSW WALL)

The project consisted of a three-story building with two levels above grade and one level of basement below. The soil-nailed wall was integrated into the final basement wall. The soil at the site consists mainly of fill material up to 3 m depth, including a nonuniform mixture of gravel, sand, and clay. The underlying soil consists of stiff silty clay. The average dry unit weight and moisture content of the fill is 16.5 kN/m^3 and 20 percent, respectively. The shear strength parameters assumed in design were c = 14.4 kN/m^2 and f = 28°, while the total unit weight of the soil was assumed to be 18.8 kN/m^3. The postearthquake observations revealed no signs of distress on the surface of the wall or at grade behind the wall.

RICHMOND, TEMPORARY SHORING WALL (TSW WALL)

Soil nailing was used here to construct a temporary shoring wall which has the tallest single-level vertical face of any of the walls examined in this paper. A permanent retaining wall was eventually built in front of the soil-nailed wall. Unfortunately, soil stratigraphy data is not available for this site. However, the shear strength parameters used in design were c = 19.1 kN/m^2 and f = 28°, while the unit weight of the soil was assumed to be 18.8 kN/m^3. A walk-through of the site following the earthquake did not reveal any signs of distress attributable to seismic activity.

METHODS OF ANALYSIS

Most of the current design methods for soil-nailed retaining structures under static loads are derived from classical slope-stability analyses, which incorporate a limit equilibrium approach. Accordingly, they evaluate global factors of safety along assumed failure surfaces such as those shown in figure 9. They are usually referred to as the German method (Stocker and others, 1979; Gassler and Gudehus, 1981; Lambe and Jayaratne, 1987), Davis method (Shen and others, 1981; Bang and others, 1992), French method (Schlosser and others, 1983), and Caltrans method (computer program SNAIL: Caltrans, 1993). The differences in the methods result from the definition of the factor of safety, assumed failure surface shape, and the assumed contribution of the soil nails to the stability. In that respect, the methods are contradictory, and because of the lack of full-scale observations of actual failure mechanisms, different points of view about their applicability have emerged.

The German method (fig. 9*A*) assumes a bilinear failure surface passing through the toe of the excavation. The failing soil mass is broken into two parts. The first part contains most of the nailed soil mass, while the second part forms the active earth pressure wedge behind it—behind the "soil-nailed gravity wall." The analysis considers the tensile and pull-out resistance of the nails crossing the failure surface and, of course, the forces of interaction between the nailed mass and active wedge behind it. The assumed failure surfaces are consistent with the concept of soil nailing, that is, the nailed soil mass behaves like a reinforced block.

The Davis method incorporates a parabolic failure surface that also passes through the toe, as shown in figure 9*B*. The sliding surface either passes entirely through the nails or intersects the ground surface somewhere beyond the reinforced zone. In the analysis, the tensile and pull-out resistance of the nails crossing the failure surface are considered the governing stabilizing forces. Because of its successful track

record and easy implementation, it has been a popular design method in the United States. This has been the case in spite of the fact that the assumption of a parabolic slip surface (which does not change slope when crossing from the nonreinforced to the reinforced zone) has not been adequately verified by laboratory or field tests.

The French method follows procedures similar to the Davis method, but assumes a circular failure surface passing entirely through the nails, as shown in figure 9*C*. But, unlike the previous two methods, this method considers the shear and bending of the nails, which adds to the complexity of the analysis.

The Caltrans method also assumes a bilinear failure surface, just like the German method. However, unlike in the German method, the bilinear failure surface may pass entirely through the nails (see fig. 9*D*).

More recently, a kinematical limit analysis approach has been proposed for the design of soil-nailed retaining structures (Juran and others, 1990). It differs from the other analysis procedures in that it suggests a method for estimating nail forces. In this way, it may provide a check on local stability at each level of nail reinforcement. The method assumes that the failure surface is defined by a log-spiral passing partially through the nails and that the failure occurs by rotation of a quasi-rigid body along this surface.

All of the San Francisco walls examined in this study were designed using a modified version of the Davis method (Barar, 1990; Felio and others, 1990). Seismic forces were accounted for by using an equivalent static horizontal force $H = W \times k_h$, applied at the center of gravity of the potentially unstable soil nailed mass, where W is the weight of the moving soil mass and k_h is the horizontal seismic coefficient.

It should be mentioned at this point that the Davis method, as well as the German and Caltrans methods, has a certain degree of the inherent conservatism in that the potential stabilizing effects of the shear and bending resistances of the nails are ignored. New studies (Jewell and Pedley, 1992; Federal Highway Administration, 1993) show, however, that the effects of bending stiffness are small. Also, the contribution of the steel reinforced facing to the strength of the system is unaccounted for. The lack of full understanding of the role of facing in the global and local stability apparently led to the difference by a factor of 3 (75 mm vs. 200 mm) in the thicknesses of the facing among the nine walls under consideration. Some designers and construction companies feel comfortable with thinner facing, while some prefer more conservative thicker facing. Figure 5, for example, illustrates a rather heavily reinforced facing with a sturdy nail contact. The role of the facing in soil reinforcing stability is just beginning to be studied as a separate issue (Tatsuoka, 1992), and it should definitely be given more attention in the future.

The factors of safety for the CVA and TSW soil-nailed walls obtained by the Davis method, modified to account for earthquake forces by the pseudostatic technique, are presented in table 4. The location of the assumed failure surfaces that yield minimum factors of safety for the TSW wall are shown in figure 10. In general, the factors of safety are relatively low, especially for the range of estimated peak horizontal ground accelerations during the Loma Prieta earthquake. According to such low factors of safety, and given the fact that some soil-nailed structures were probably subjected to much larger horizontal forces, some visible damage should have occurred during the earthquake. This should have been expected in particular for the UCSC Wall in Santa Cruz, which had the smallest length ratio and facing thickness, and yet is likely to have undergone horizontal seismic forces as large as 0.4 g. The lack of visible damage on any of the walls, except very thin cracks on the ECR wall, suggests that either the design, analysis, or construction, or most likely their combination, may have been more conservative than necessary. The lack of damage also indicates that the assumed failure surface and mechanism of failure of the Davis method may not be fully appropriate for the nine walls treated here. In the following section, the components of the analysis, design, and construction that appear to be on the conservative side, and therefore could be responsible for such excellent seismic performance, are discussed.

POSSIBLE REASONS FOR THE OBSERVED BEHAVIOR

Since soil nailing is a relatively new soil-stabilization technique, with very little practical experience of full-scale static failures and practically no experience of seismic failures, the design and construction are usually quite conservative. The preliminary design of a soil-nailed retaining structure proceeds much like that of retaining walls, by trial and error. Based mainly on the expected excavation height and the soil strength properties, tentative characteristics of nails and facing (length, diameter, horizontal, and vertical spacings of nails, and the thickness and reinforcement of facing, etc.) can be assumed and some sort of stability analysis performed. The assumed values and characteristics depend primarily on the designer's experience with other satisfactorily constructed soil-nailed walls, which may lead to an overly conservative design, and to a lesser extent on charts and dimensionless parameters derived by others, such as those by Bruce and Jewell (1986, 1987) and Guilloux and Schlosser (1982). Table 3 shows, for example, that the length ratios and bond ratios for the nine walls considered here are on the conservative side in comparison with the values suggested by Bruce and Jewell (1986, 1987).

The main components of the conservative design and construction for seismic loads include (1) conservative and most probably unrealistic assumption of the failure mechanism, (2) no consideration of the contribution of the facing in the stability analysis, and (3) conservative construction due to the lack of field experience and understanding of the various

aspects of soil-nailed excavation seismic response. The first two components are discussed below.

FAILURE-MECHANISM ASSUMPTION

Due to a lack of full-scale observations of failures and corresponding failure mechanisms under both static and seismic loads, there is currently no consensus among designers on which failure mode is the most realistic among the four basic modes presented in figure 9. To cast more light on possible modes of failures under dynamic loads, two series of dynamic centrifuge tests were conducted, one in 1991 (Tufenkjian and others, 1991; Tufenkjian and Vucetic, 1992; Vucetic and others, 1993) and the other in 1996 (Vucetic and others, 1996). Figures 11 and 12 show the main features of the models tested and results obtained in 1991.

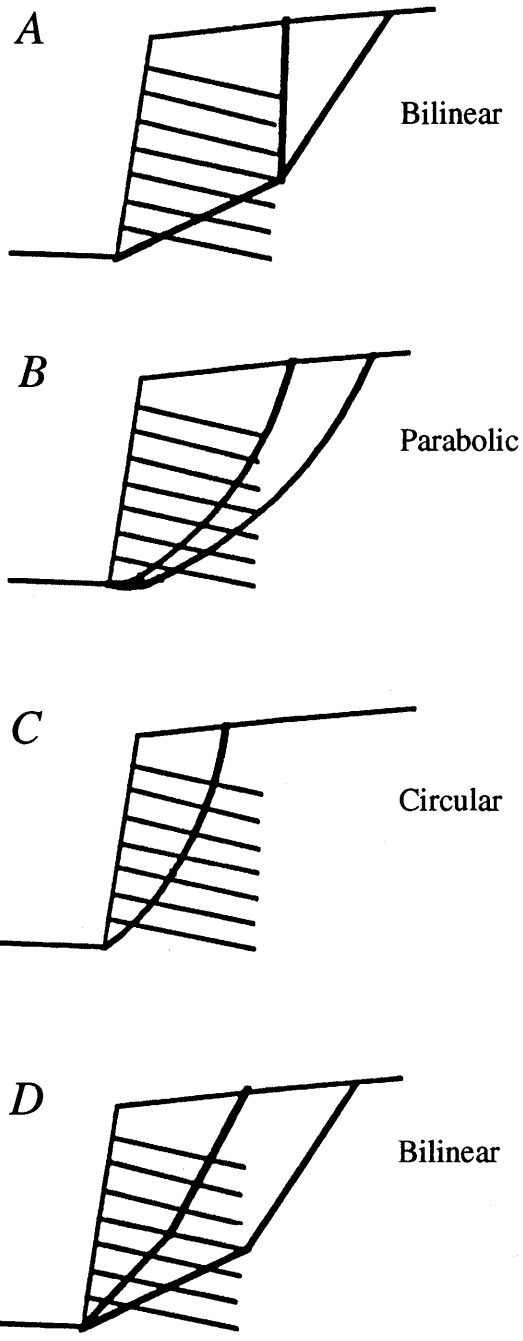

Figure 9.—Assumed failure surfaces used in analyses. *A*, German Method. *B*, Davis Method. *C*, French Method. *D*, Caltrans Method.

The centrifuge tests were performed at the Rensselaer Polytechnic Institute (RPI) Geotechnical Centrifuge Research Center on a 3-m radius Accutronic 665-1 centrifuge (Elgamal and others, 1991). The scale factor was 50 in all of the tests. Accordingly, to simulate prototype geostatic stresses, the models had to undergo a centrifugal acceleration of 50 *g*. For dynamic testing, a servo-hydraulic earthquake simulation shaker mounted on the centrifuge platform was used. Four models were tested in 1991.

They represented 7.6-m-high soil-nailed excavations with grouted nails, corresponding roughly to an excavation height of a two- to three-story underground garage. The effects of two important characteristics of soil-nailed structures were tested: the length of nails (expressed in terms of the length ratio), and the axial and flexural rigidities of the nails.

Three length ratios were tested, 0.33, 0.67, and 1.0, which could be characterized as the ratios corresponding to short, medium, and long nails (see table 3). These ratios cover approximately five out of the nine walls listed in table 2. The four other walls have very large length ratios between 1.5 and 2.5. Two axial and flexural rigidities of the nails were used, one that can be considered regular and the other than can be considered small. By varying the axial and flexural rigidities of the soil nails, their effect on the failure surface geometry and stability could be assessed. As shown in figures 11*A* and 11*C*, three displacement transducers (LVDT's) were used to record the lateral movements of the facing and the vertical soil settlement behind the facing. During dynamic loading, four accelerometers were utilized to measure the accelerations of the model box and in various locations within the model box. The soil used in the experiments was fine sand. The sand was partially saturated to generate an apparent cohesion, necessary for a rough simulation of in-situ cohesion and cementation. Other details of the 1991 testing are described by Vucetic and others (1993).

Figures 11*B* and 12 show a typical failure mechanism obtained in the tests under horizontal dynamic loads. In all four tests the failure surface never started at the ground surface above the nails. Instead, it started at the ground surface behind the ends of the nails. Figure 11*B* reveals that the failure mechanism involves three soil "zones" and two soil "blocks," with two failure surfaces, one of which consists of two parts. The primary failure surface extends from behind the nails at the ground surface down to the end of the second row of nails, at which point it changes curvature and continues down to the bottom of the excavation through the toe. The secondary failure surface develops within the sliding soil mass and divides zones 1 and 3. Such deformation patterns after the tests point to the following failure mechanism. The soil above the second row of nails in zone 1 moves horizontally under

Table 4.—*Calculated factors of safety using the Davis method (see also Hudson, 1990)*

Horizontal acceleration coefficient, k_h	Cresta Vista apartments CVA	Temporary shoring wall TSW
0	1.31	1.19
0.1	1.14	1.06
0.2	1.00	0.94

Indicates the factors of safety corresponding to the range of estimated horizontal peak ground-surface accelerations near the site.

large inertial forces as a relatively rigid block held together by the nails. Consequently, the soil in zone 2 is pushed outward by the horizontal friction along the interface between the upper zone 1 and the lower zone 2. Accordingly, the failure surface passes through the bottom row of nails. In such a mechanism, the bottom nails obviously act as anchors between the back soil and the facing, while the top nails hold the soil together in the upper part of the excavation. As zones 1 and 2 move horizontally outward during seismic shaking, the lateral stresses in zone 3 are greatly reduced. Consequently, zone 3 represents a typical failure wedge behind a retaining wall, the retaining wall being zone 1. This mechanism and kinematics of the soil movement resemble the geometry of German method for static stability evaluation, shown in figure 9*A* (Gassler and Gudehus, 1981), while they contradict the assumption that rotation of one monolith occurs along a continuous circular or parabolic failure surface.

To examine the factors governing the failure corresponding to the above mechanism, the forces and factors of safety for the TSW Wall in Richmond (see fig. 10 and table 4) are reevaluated. Figure 13 shows the assumed failure surfaces and governing forces, while figure 14 shows the corresponding polygons of forces. To account for the effects of dynamic horizontal forces the pseudostatic method of analysis is used again, where the dynamic action is represented by the static horizontal force $H = W \times k_h$. Two definitions of the factor of safety, *FS*, based on the German type of failure mechanism are considered below. First is the definition for static stability proposed by Stocker, Korber, Gassler and Gudehus (1979), which is adapted here for the dynamic stability by adding to the poligon of forces a horizontal force $H = W \times k_h$. The second is the definition proposed and used by Caltrans (1993). Accordingly, the two methods for the calculation of *FS* are called here the SKGG method and the Caltrans method.

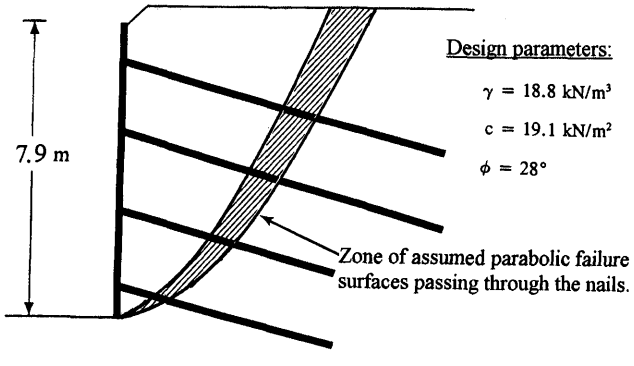

Figure 10.—Assumed failure surfaces passing through the nails for the factor of safety evaluation of the TSW wall in Richmond using Davis method and its modifications.

According to the SKGG method, the factor of safety is calculated as

$$FS = \frac{Z_a}{Z_e}, \qquad (4)$$

where Z_a = cumulative axial pull-out force of the nails beyond the failure surface and Z_e = mobilized cumulative axial force of the nails beyond the failure surface. Therefore, the entire factor of safety is based on the pullout of the nails. For the TSW wall, *FS* for different seismic coefficients, k_h, was calculated. The results of this calculation are presented in terms of the *FS* vs. k_h relationship in figure 15. On the same figure the equivalent relationship between *FS* and k_h obtained by the Caltrans method is presented as well.

The bilinear failure surface assumed in the Caltrans method is similar to the failure surfaces assumed in the SKGG method and thus to the deformation patterns and failure surfaces observed in the centrifuge tests. In fact, as indicated in figure 13, the forces and their positions relative to the free bodies for the TSW wall are the same for the SKGG and Caltrans methods. However, the methods differ fundamentally in their definitions of the factor of safety. The Caltrans method applies a unique factor of safety to the soil cohesion, c, soil friction angle, ϕ, and the cumulative nail pullout force, Z_a :

$c' = c/FS$ = mobilized cohesion,
$\phi' = \tan^{-1}[(\tan\phi)/FS]$ = mobilized friction angle, and
$Z_e = Z_a/FS$ = mobilized pullout force.

The method then utilizes these "mobilized" parameters in the force equilibrium equations to solve for the interwedge forces, *F* (see figs. 13 and 14). Since these forces must be equal in magnitude and opposite in direction, assumed value of *FS* is systematically varied until this condition is fulfilled, which then yields the corresponding *FS* used in design. The Caltrans method has been coded into a computer program-

ming language and can be run on personal computers. The computer program is called SNAIL (Caltrans, 1993). By inputting the geometry of the slope and details of the soil strength and nail properties, the program can systematically vary the location of the bilinear failure surfaces, until the one producing the lowest factor of safety is found. The program also has an option to calculate the *FS* for a specified surface, as well as for considering seismic forces by the pseudostatic technique.

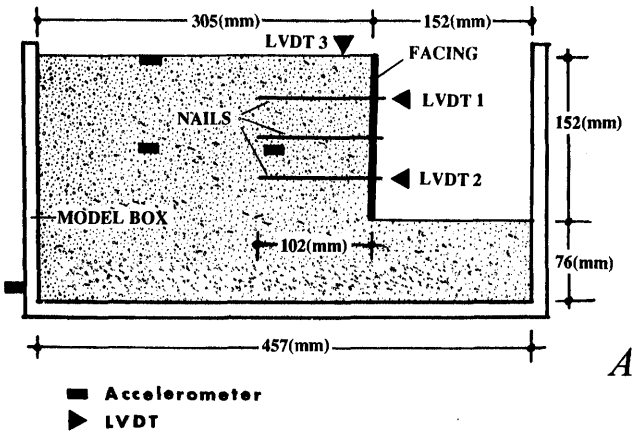

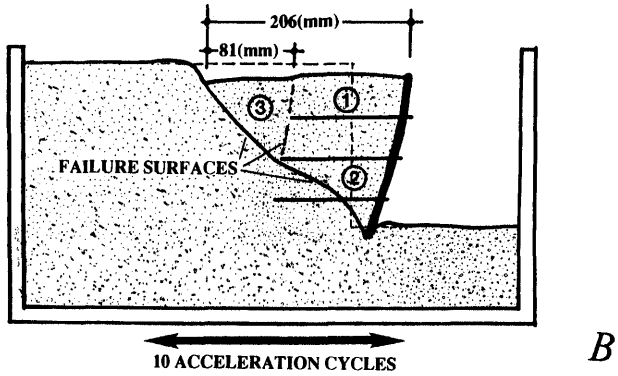

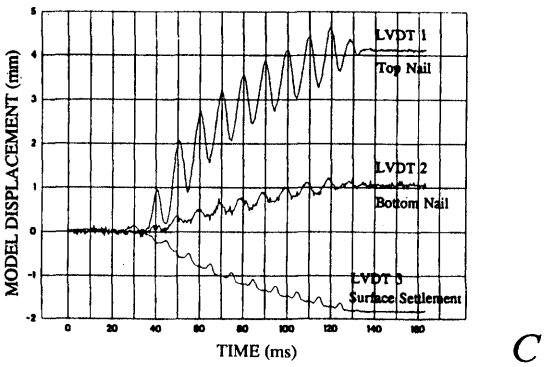

Figure 11.—Features of the typical centrifuge model test with length ratio of 0.67 (Tufenkjian and others, 1991; Vucetic and others, 1993). *A*, Longitudinal cross section of the soil-nailed excavation centrifuge model box. *B*, Failure mechanism obtained in the centrifuge due to strong horizontal shaking. *C*, Typical records of soil mass movements during shaking with 10 cycles of 0.27 *g* cyclic acceleration amplitude.

Several interesting conclusions can be derived from figure 15. First is that for $FS = 1$ (the conditions of the failure of the wall), $k_h \approx 0.37$ is obtained by both methods. Second, this k_h value is much larger than $k_h \approx 0.1$ to 0.20 corresponding to $FS = 1$ calculated according to the Davis method (see table 4). Third, $k_h \approx 0.37$ is in relatively good agreement with the amplitude of the cyclic acceleration of 0.45 g that was required in the centrifuge testing for the failure of the soil-nailed excavation model of similar length ratio (see Vucetic and others, 1993). And fourth, the *FS* versus k_h relationship for the SKGG method has a singularity point, while the same relationship for the Caltrans method does not.

Based on these observations it can be concluded that the failure mechanism according to the German method seems to be more appropriate than that of the Davis method. However, figure 15 also shows that using the SKGG method to calculate the factor of safety may not be suitable for the calculation of stability involving the horizontal forces ($W \times k_h$), because it is too sensitive to the variation of k_h. By varying k_h from 0.3 to 0.4, *FS* varies from -1 to $-\infty$ and then from $+\infty$ to 0.7—that is, as noted above, the function $FS = f(k_h)$ has a singularity point. The reason for such sensitivity of *FS* with respect to k_h can be easily understood from the polygon of forces in figure 14*B*. For example, if the force $H_1 = W_1 \times k_h$ is increased by only 15 percent, the Z_e force will double—that is, change by 100 percent. Consequently, the $FS = Z_a / Z_e$ will change dramatically too. Such sensitivity of *FS* comes from the fact that *FS* is defined on the basis of forces which are of secondary importance for the stability of the structure. In other words, force Z_e is relatively small compared to the other forces in the polygon. More dominant forces are apparently the reaction force Q_1 and cohesion force C_1 mobilized along the failure surface.

In the configuration of forces such as shown in the polygon in figure 14*B*, corresponding to the German method type of failure mechanism, the role of the nails is predominantly to interact with the soil and form the nailed block. Such a large soil block is evidently seismically very stable, and its stability is governed by the large forces of friction and cohesion at the interfaces with the surrounding soil, not by the small forces such as Z_e. This, of course, would change if Z_e is relatively large, that is, corresponding to very long nails installed deep beyond the failure surface. In such a case the kinematics of the failure would be different too. Instead of predominantly sliding along the failure surfaces, the facing and thus the soil mass would be forced to rotate around the bottom row of nails which are anchored beyond the failure surface.

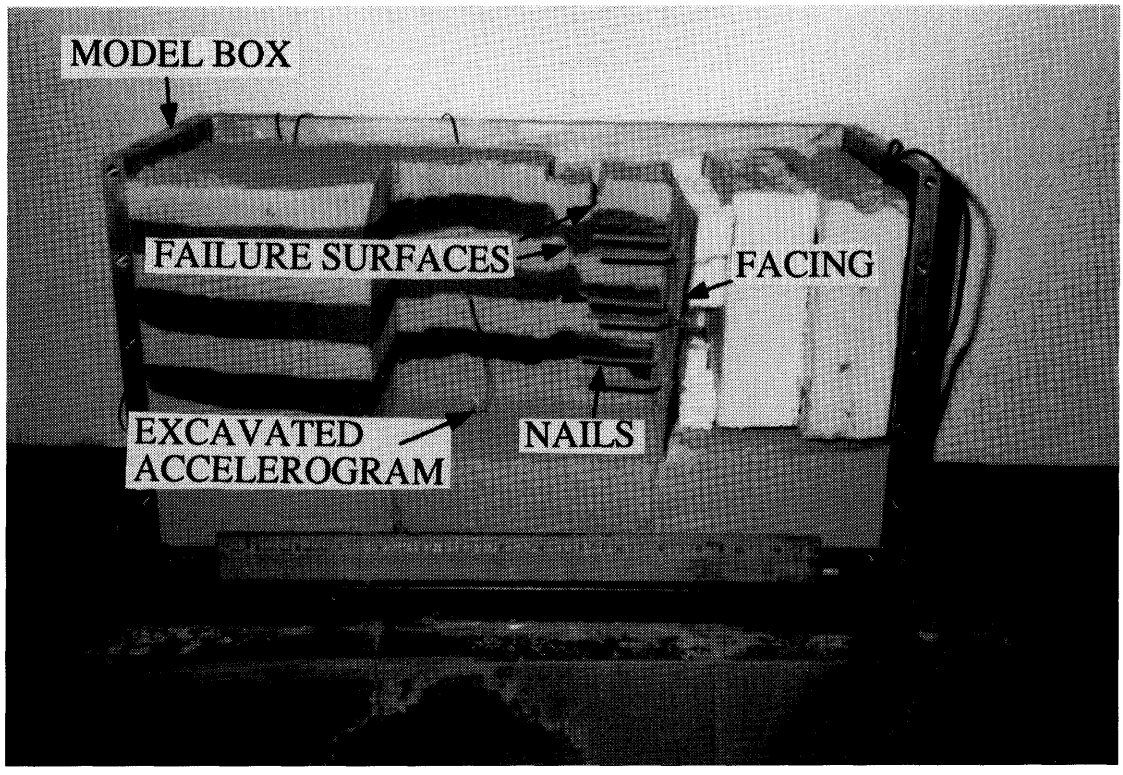

Figure 12.—Excavated model of a test with the length ratio of 0.33 (short nails) shaken by 10 cycles of the uniform acceleration amplitude of 0.10 *g*.

As opposed to the SKGG method of stability evaluation, the Caltrans method does incorporate all significant forces in the definition of *FS* and consequently yields a more meaningful relationship between *FS* and k_h. This, along with the above discussion, leads to the following conclusions: (1) the German-method type of failure mechanism seems to be appropriate, (2) the Caltrans method for calculating *FS* seems to yield appropriate and meaningful results, and (3) the Davis method used in the design of the San Francisco Bay area soil-nailed walls seems to be overly conservative, apparently because it employs an unlikely failure mechanism.

To confirm the above conclusions, the factors of safety of the eight soil-nailed walls subjected to the Loma Prieta earthquake were calculated by the Caltrans method. The four-level RPP wall located in San Jose could not be accurately reproduced using the SNAIL program. The wall geometries were scaled from figure 8 and the soil design parameters were taken from table 1. The calculated factors of safety are shown in table 5, where those corresponding to the range of estimated horizontal ground-surface accelerations near each soil-nailed wall are indicated by double-headed arrows. Note that the factors of safety are generally much greater than unity for the range of estimated ground-surface accelerations, even for the UCSC wall which was subjected to horizontal accelerations in the range of 0.4 to 0.5 *g*. Recall from Table 4, for example, that the Davis method predicted failure ($FS = 1.0$) for the TSW wall for the acceleration coefficient between

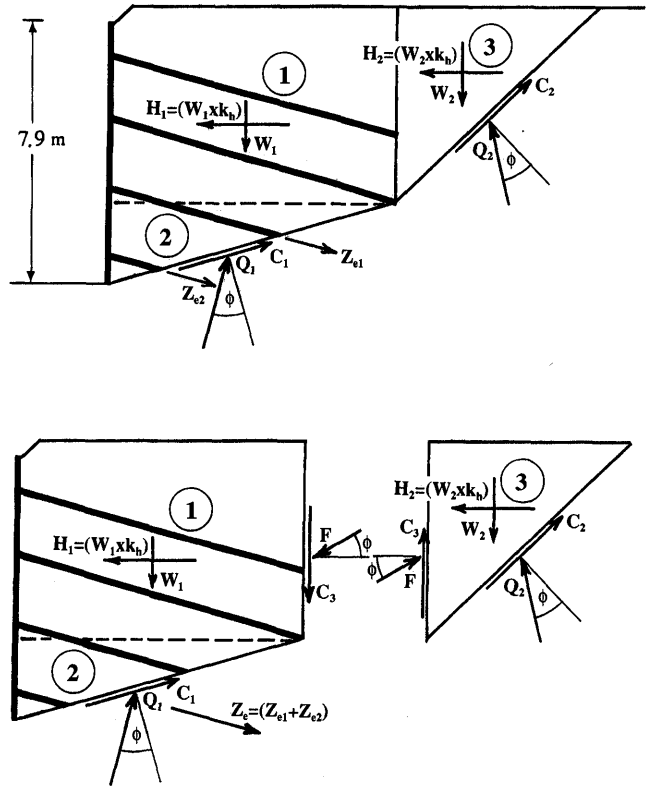

Figure 13.—Failure surfaces and forces for the TSW wall employed in both SKGG and CALTRANS methods for the calculation of the factor of safety according to the German type of failure.

0.10 and 0.20, while the Caltrans method required an acceleration coefficient between 0.4 and 0.5. Such large values of *FS* obtained by Caltrans method are in agreement with the excellent performance of the walls during the earthquake.

ROLE OF FACING

None of the methods discussed above account explicitly for the contribution of the facing in the evaluation of the global factor of safety, although they do incorporate the evaluation of punching shear around the nail connection. In other words, the factor of safety is calculated without considering axial and flexural rigidities of the facing. In that respect, there is no consensus on what the contribution of the facing to the global stability of soil nailed structure really is. However, it is obvious that stronger facing and stronger contact between the facing and the nails will make the nailed soil mass more coherent. The failure mechanism of such a coherent soil mass is likely to be of the German type—that is, behaving as a large seismically stable block. In addition, the inability of the nails (which are firmly fixed to the facing) to move freely decreases the likelihood of local failures, especially in the zones most critically stressed during construction and seismic loading. As suggested earlier, the lack of full understanding of the role of facing in the global and local stability apparently led to the difference by a factor of 3 (75 mm vs. 200 mm) in the thicknesses of the facing between the nine walls considered here.

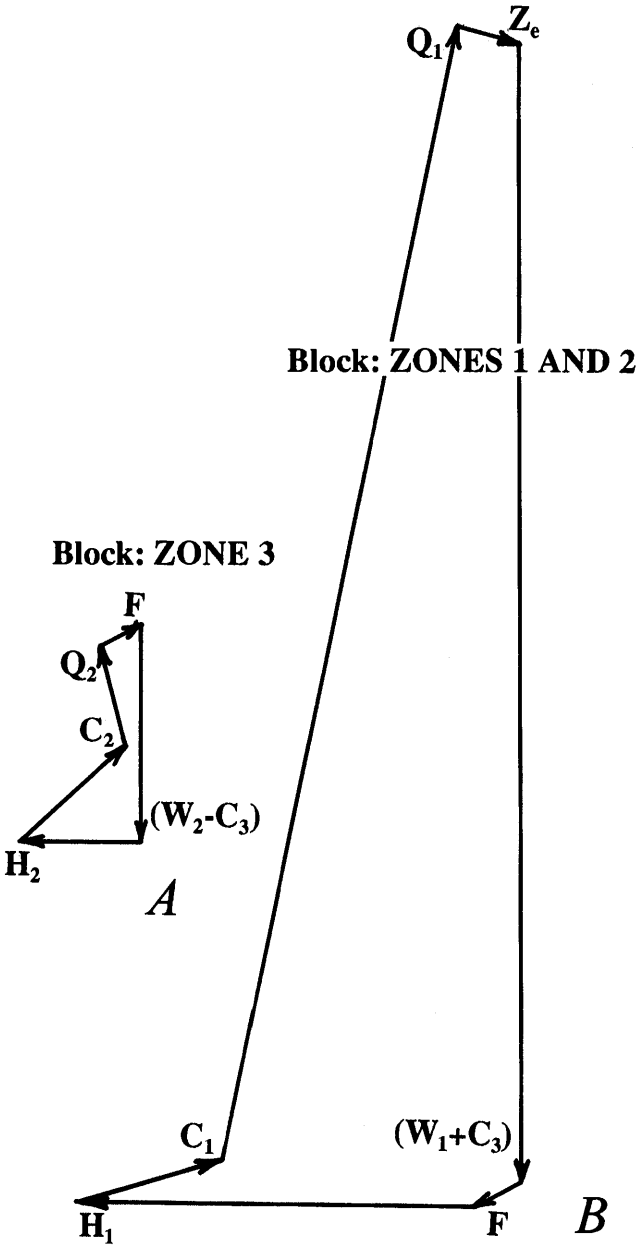

Figure 14.—Polygons of forces identified in figure 13. *A*, Polygon for block comprising zone 3. *B*, Polygon for block comprising zones 1 and 2.

CONCLUSIONS

Postearthquake inspections of nine soil-nailed walls following the Loma Prieta earthquake indicated superior performance and no signs of distress, even though one of the walls was subjected to horizontal accelerations probably as high as 0.4 *g*. It was shown that the excellent performance may be attributed to a conservative design, generally conservative stability analysis which is mainly the result of an

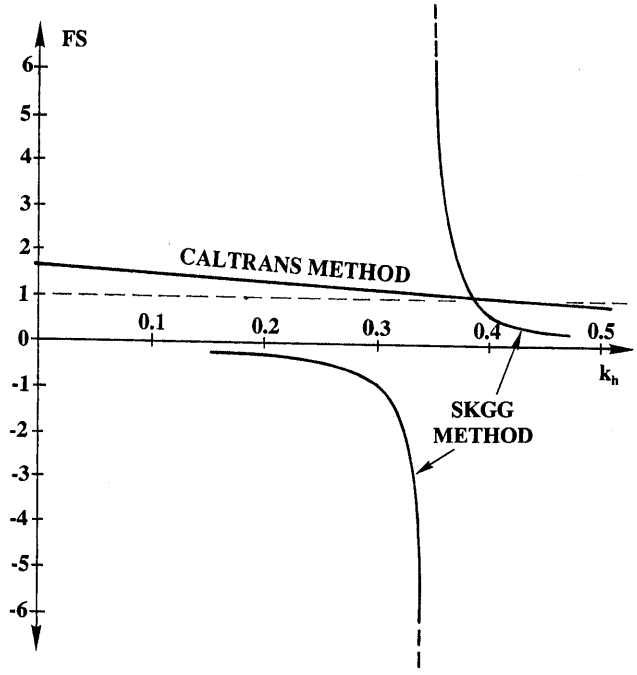

Figure 15.—Variation of the factors of safety, *FS*, with the seismic coefficient, k_h, for the TSW wall.

Table 5.—Calculated factors of safety using the Caltrans method for San Francisco area soil-nailed walls

Horizontal acceleration coefficient, k_h	Soil-nailed wall							
	ECR	KPG	UCSC	RPP (single-level)	NME	CVA	MSW	TSW
0.0	2.28	2.53	3.30	5.15	1.88	1.59	3.07	1.64
0.1	2.00	2.26	2.75	4.44	1.52	1.35	2.68	1.51
0.2	1.74	1.96	2.32	2.80	1.27	1.17	2.35	1.39
0.3	1.51	1.71	2.01	1.99	1.10	1.02	1.97	1.19
0.4	1.31	1.43	1.76	1.54	0.97	0.89	1.64	1.03
0.5	1.16	1.18	1.53	1.26	0.86	0.78	1.39	0.91

Indicates the factors of safety corresponding to the range of estimated horizontal peak ground-surface accelerations near the site.

unlikely mechanism and geometry of failure, and conservative construction.

Because seismic failures of soil-nailed excavations have not occurred in the past and are therefore absent from the literature, dynamic centrifuge testing was performed to provide evidence of the most probable failure mechanism. The centrifuge testing revealed that the most likely failure mechanism is the German type of failure mechanism. Furthermore, a simple analysis of the dynamic centrifuge test results and field observations showed that the Caltrans method for calculating the factor of safety, which also incorporates the German type of failure mechanism, yields very consistent and logical results. Accordingly, the Caltrans method implemented by the computer program SNAIL seems to be an appropriate method for calculating the static and dynamic stability of grouted soil-nailed excavations of the type discussed in this paper.

ACKNOWLEDGMENTS

The investigations described in this paper were supported by the National Science Foundation through the grants BCS-9001610, BCS-9011819 and BCS-9224479. This support is gratefully acknowledged. We would also like to thank professors R. Dobry, A.-W. Elgamal, and T.F. Zimmie, Dr. P. Van Laak, and Dr. L. Liu, all from the RPI Geotechnical Centrifuge Research Center, for their excellent service and continued assistance. Special thanks go to Dr. Macan Doroudian, former student at UCLA, for his help in performing the centrifuge tests. We would also like to recognize Mr. Ken Jackura from Caltrans who supplied the computer program SNAIL and provided valuable suggestions.

REFERENCES CITED

Bang, S., Kroetch, P.P., and Shen, C.K., 1992, Analysis of soil nailing system, *in* Proceedings of the International Symposium on Earth Reinforcement Practice, Fukuoka, Kyushu, Japan: Balkema, Rotterdam, v. 1, p. 457-462.

Barar, P., 1990, The behavior of five soil nailed earth retaining structures during the Loma Prieta earthquake of October 17, 1989: Report prepared for the Department of Civil Engineering, University of California, Los Angeles, 101 p.

Bruce, D.A., and Jewell, R.A., 1986, Soil nailing—Application and practice, part 1: Ground Engineering, November, p. 10-15.

———1987, Soil nailing—Application and practice, part 2: Ground Engineering, January, p. 21-33.

Caltrans, 1993, California Department of Transportation—SNAIL Computer Program, Version 2.06: California Department of Transportation, Office of Geotechnical Engineering, Sacramento, California.

Chapman, K.R., and Ludwig, C., 1993, ADSC participates in FHWA international geotechnology tour: Drilling Foundation, December/January, p. 17-19.

Elgamal, A.-W., Dobry, R., and Van Laak, P., 1991, Design construction and operation of 100 g-ton centrifuge at RPI, in Proceedings of the International Conference Centrifuge 1991, Boulder: Balkema, Rotterdam, p. 27-34.

Felio, G.Y., Vucetic, M., Hudson, M. Barar, P., and Chapman, R., 1990, Performance of soil nailed walls during the October 17, 1989 Loma Prieta Earthquake, *in* Proceedings of the Forty-Third Canadian Geotechnical Conference, Quebec: Canadian Geotechnical Society, p. 165-173.

Federal Highway Administration, 1993, FHWA Tour for Geotechnology—Soil Nailing: Federal Highway Administration Report No. FHWA-PL-93-020, 84 p.

Gassler, G., 1992, Full scale test on a nailed wall in consolidated clay, in Proceedings of the International Symposium on Earth Reinforcement Practice, Fukuoka, Kyushu, Japan: Balkema, Rotterdam, v. 1, p. 475-480.

Gassler, G., and Gudehus, G., 1981, Soil nailing—some aspects of a new technique, in Proceedings of the 10th International Conference Soil Mechanics and Foundation Engineering: Balkema, Rotterdam, v. 3, p. 665-670.

Guilloux, A., and Schlosser, F., 1982, Soil nailing practical applications, in Proceedings of the Symposium on Soil/Rock Improvement Technique: A.I.T.

Hudson, M.B., 1990, The effects of the Loma Prieta earthquake on soil-nailed earth retaining structures in the San Francisco Bay area: Civil Engineering Department, University of California, Los Angeles, M.S. thesis, 108 p.

Japan Highway Public Corporation, 1987, Guide for design and construction on reinforced slope with steel bars: September, 33 p.

Jewell, R.A., and Pedley, M.J., 1992,Analysis for soil reinforcement with bending stiffness: Journal of Geotechnical Engineering, v. 118, no. 10, p. 1505-1528.

Juran, I., Baudrand, G., Farrag, K., and Elias,V., 1990, Kinematical limit analysis for soil nailed structures: Journal of Geotechnical Engineering, v. 116, no. 1, p. 54-72.

Juran, I., and Elias, V., 1991, Ground anchors and soil nails retaining structures, in Foundation Engineering Handbook (2d ed.): Van Nostrand Reinhold, New York, p. 868-905.

Koerner, R.M., 1984, Construction and geotechnical methods in foundation engineering: McGraw-Hill, Inc.

Lambe, P.C., and Jayaratne, N.N., 1987, Construction of retaining walls from the top down: Center forTransportation Engineering Studies, Department of Civil Engineering, North Carolina State University at Raleigh, Research Report No. 23241-86-6, 183 p.

Mitchell, J.K., and Villet, W.C.B., 1987, Reinforcement of Earth Slopes and Embankments,Appendix C, Soil Nailing: National Cooperative Highway Research Program, Report 290,Washington, D.C., June, p. 258-323.

Myles, B., and Bridle, R.J., 1991, Fired soil nails—the machine: Ground Engineering, v. 24, no. 6, p. 38-39.

Ochiai, H., Hayashi, S., and Otani, J., eds, 1992, Proceedings of the International Symposium on Earth Reinforcement Practice, IS Kyusha '92, v. 1 and 2. Fukuoka, Japan: Balkema, Rotterdam.

Plumelle, C., Schlosser, F., Delage, P., and Knochenmus, G., 1990, French national research project on soil nailing Clouterre: American Society of Civil Engineers SpecialTechnical Publication No. 25, p. 660-675.

Schlosser, F., Jacobsen, H.M., and Juran, I., 1983, Soil reinforcement—general report, *in* Proceedings of the Eighth European Conference on Soil Mechanics and Foundation Engineering: Balkema, Rotterdam, v. 3, p. 1159-1180.

Seed, R.B., Dickenson, S.E., and Idriss, I.M., 1991, Principal geotechnical aspects of the 1989 Loma Prieta earthquake: Soils and Foundation, v. 31, no. 1, p. 1-26.

Shen, C.K., Herrmann, L.R., Romstad, K.M., Bang, S., Kim,Y.S., and DeNatale, J.S., 1981, An in situ earth reinforcement lateral support system: Department of Civil Engineering, University of California, Davis, Report No. 81-03, 188 p.

Stocker, M.F., Korber, G.W., Gassler, G., and Gudehus, G., 1979, Soil nailing, in Proceedings of the International Conference on Soil Reinforcement, Paris, v. 2, p. 469-474.

Stocker, M.F., and Riedinger, G., 1990, The bearing behavior of nailed retaining structures: American Society of Civil Engineers Special Technical Publication No. 25, p. 612-628.

Tatsuoka, F., 1992, Keynote lecture—roles of facing rigidity in soil reinforcing, *in* Preprints of Special and Keynote Lectures of the International Symposium on Earth Reinforcement Practice Kyusha '92, Fukuoka, Japan: Institute of Industrial Science, Tokyo, p. 77-115.

Tufenkjian, M.R., and Vucetic, M., 1992, Seismic stability of soil nailed excavations, *in* Proceedings of the International Symposium on Earth Reinforcement Practice, Fukuoka, Kyushu, Japan: Balkema, Rotterdam, p. 573-578.

———1993, Seismic stability of soil nailed excavations: Civil and Environmental Engineering Department, University of California, Los Angeles, Research Report ENG-97-169, June, 298 p.

Tufenkjian, M.R., Vucetic, M., and Doroudian, M., 1991, Stability of soil nailed excavations, in Proceedings of the International Workshop on Technology for Hong Kong's Infrastructure Development: Commercial Press Ltd., Hong Kong, p. 751-762.

Vucetic, M., Iskandar, V.E., Doroudian, M., and Luccioni, L., 1996, Dynamic failure of soil-nailed excavations in centrifuge,*in* Proceedings of the International Symposium on Earth Reinforcement Practice, Fukuoka, Kyushu, Japan: Balkema, Rotterdam, v. 1, p. 829-834.

Vucetic, M., Tufenkjian, M.R., and Doroudian, M., 1993, Dynamic centrifuge testing of soil nailed excavations: Geotechnical Testing Journal, v. 16, no. 2, p. 172-187.

EARTH STRUCTURES AND ENGINEERING CHARACTERIZATION OF GROUND MOTION

EMPIRICAL ANALYSIS OF PEAK HORIZONTAL ACCELERATION, PEAK HORIZONTAL VELOCITY, AND MODIFIED MERCALLI INTENSITY

By Kenneth W. Campbell,
EQE International, Inc., Evergreen, Colo.

CONTENTS

ABSTRACT

A total of 137 ground-level accelerograms recorded during the earthquake were used to develop empirical models for predicting the dependence of peak horizontal acceleration (PHA), peak horizontal velocity (PHV), and modified Mercalli intensity (MMI) on distance from the fault, source-to-site azimuth, and surficial geology. These models indicate that (1) PHA recorded on alluvium at distances farther than 50 km from the seismogenic rupture zone were significantly higher than those predicted from attenuation relationships available at the time of the earthquake; (2) both the amplitude and rate of attenuation of PHA, PHV, and MMI exhibited a strong dependence on azimuth with ground motions recorded at azimuths corresponding to Santa Cruz, San Francisco, and Oakland (west and northwest direction) having significantly higher amplitudes and lower rates of attenuation than those recorded in the east and northeast direction; and (3) PHA recorded at intermediate and far distances at all azimuths exhibited a strong dependence on site geology, with PHA on bay mud (SC-IV, S_E), alluvium (SC-III, S_D), and soft rock (SC-II, S_C) being on average 2.76, 1.47, and 1.25 times higher than on hard, or predominantly Franciscan, rock (SC-Ib, S_B). The azimuthal dependence of PHA and PHV is consistent with the observed geographic distribution of MMI. The observed azimuthal dependence of PHA, PHV, and MMI is consistent with the combined effects of source directivity, shear-wave radiation pattern, and propagation effects (that is, critical reflections from layers within and at the base of the crust). The observed dependence of PHA on surficial geology is consistent with low-strain site amplification factors recommended for use in building-code and engineering applications. However, these recommended factors are generally not consistent with the amplitude-dependent factors predicted from empirical attenuation relationships. A comparison of the model predictions with published data indicates that the models accurately predict the observed dependence of PHA, PHV, and MMI on azimuth and distance throughout central California to distances as far as 250 km from the earthquake rupture zone.

INTRODUCTION

The earthquake caused considerable damage to man-made structures in the San Francisco Bay area. The amount of damage observed in San Francisco and Oakland during this earthquake is superseded only by that sustained during the great 1906 San Francisco earthquake (Housner, 1990; U.S. Geological Survey Staff, 1990). The amount of damage was unusually large compared to other California earthquakes of similar magnitude, especially when one considers the relatively short duration of the ground motions and the relatively large epicentral distance to San Francisco and Oakland. This damage is, however, consistent with the unusually high ground motions that were recorded in San Francisco and Oakland.

A compilation of peak accelerations published by Boore and others (1989) and Brady and Shakal (1994) indicates that peak horizontal accelerations as large as 0.20 to 0.25 *g* were routinely recorded on alluvium and soft soil in the San

Francisco and Oakland areas—the largest being 0.41 *g* on Holocene bay deposits (Bay mud) in a hanger at the Alameda Naval Air Station approximately 93 km from the epicenter. Campbell (1991) demonstrated that these accelerations are 1.5 to 3 times larger, on average, than those predicted from strong-motion attenuation relationships that were available at the time of the earthquake, but they are consistent with the unusually large amount of damage (Housner, 1990) and unusually high intensities (Stover and others, 1990) observed in these areas.

In an attempt to understand this phenomenon, values of peak horizontal acceleration (PHA), peak horizontal velocity (PHV), and Modified Mercalli intensity (MMI) recorded and observed during this earthquake were analyzed to determine their dependence on distance, azimuth, and surficial geology. The dependence on distance, or what is simply referred to as "attenuation" throughout this paper, includes the effects of geometrical spreading, material damping, and scattering. The analysis was intended to be an engineering rather than a seismological study, emphasizing those aspects of ground motion which have the greatest influence on the empirical prediction of ground motion for seismic design. As demonstrated later, these results clearly show why damage in San Francisco and Oakland was more severe than at other locations of comparable distance throughout the region, an observation consistent with the geographic distribution of MMI in the Bay area (Stover and others, 1990).

The seismological aspects of the earthquake have been discussed extensively in several special volumes dedicated to this earthquake, including Geophysical Research Letters, v. 17, no. 9, August, 1990; the Bulletin of the Seismological Society of America, v. 81, no. 5, October 1991; and companion volumes of this Professional Paper 1550 on "Earthquake Occurrence" and Professional Paper 1551 on "Strong Ground Motion and Ground Failure". This information will not be presented in this paper; rather, the reader is referred to these publications for a complete discussion of the seismological aspects of the earthquake

STRONG-MOTION DATA

The strong-motion database used in this study consisted of 137 ground-level accelerograms compiled by Campbell (1991). These recordings were taken from reports published by Maley and others (1989), Shakal and others (1989), Brady and Mork (1990), and California Strong Motion Instrumentation Program (1991a, b, c). MMI observations were taken from compilations by Stover and others (1990) and C. Stover (written commun., 1991).

The source-to-site distance measure used in this study is the closest distance to the zone of seismogenic rupture, a measure first proposed by Campbell (1987) and later adopted by Campbell and Bozorgnia (1994b) and Campbell (1997). It is defined as that portion of the rupture zone responsible for most, if not all, of the seismically radiated energy observed at the ground surface. This zone was interpreted to be approximately 40 km long, extend between depths of 4.5 to 19 km, and dip approximately 70° to the southwest as defined by the location of aftershocks that occurred within several weeks after the earthquake (see cross sections in Plafker and Galloway, 1989) and by seismological, geological, and geodetic studies conducted within several years after the earthquake (for example, Bulletin of the Seismological Society of America, v. 81, no. 5; Professional Paper 1551).

A description of surficial geology for each of the recording sites was obtained from Campbell (1989, 1990), Shakal and others (1989), and Fumal (1991). These descriptions were independently verified and supplemented with data derived from 30 geology maps of the region. Based on these descriptions, each site was assigned to one of four surficial geologic classifications defined by Campbell (1981): soft soil (artificial fill; Holocene fluvial, bay, and estuarine deposits; and other soft soils), alluvium (Quaternary deposits >10 m deep), soft rock (primarily Tertiary and Cretaceous sedimentary rock), and hard rock (primarily crystalline, metamorphic, and pre-Cretaceous sedimentary rock). The approximate correspondence between this site-classification criteria and those proposed for building-code and engineering applications by Borcherdt (1994), Borcherdt and Glassmoyer (1994), and the International Conference of Building Officials (1996) is given in table 1.

GROUND-MOTION MODELS

Boore and others (1989), Plafker and Galloway (1989), Housner (1990), and Borcherdt and Glassmoyer (1992, 1994) found that surficial geology had a profound effect on peak accelerations recorded during the earthquake. In order to minimize this effect on the determination of attenuation, the regression analyses presented below were restricted to the 71 alluvial recordings compiled by Campbell (1991). These data are summarized in tables 2 and 3. Model coefficients were estimated from a nonlinear least-squares regression algorithm developed by More and others (1980).

PEAK GROUND ACCELERATION

A preliminary analysis of PHA using an attenuation relationship whose functional form predicted a monotonically decreasing amplitude with distance resulted in a set of residuals that were strongly biased with respect to distance. A similar bias was noted by several other investigators (see fig. 6 of Boore and others, 1989). For distances less than 50

Table 1.—*Summary of site classification criteria*

[$V_{S,30}$, average shear-wave velocity in the upper 30 m of the deposit]

This study (Campbell, 1981, 1997)		Borcherdt (1994b), Borcherdt and Glassmoyer (1994)			Proposed 1997 UBC (International Conference of Building Officials)		
Class	Description	Class	Description	$V_{S,30}$ (m/s)	Class	Description	$V_{S,30}$ (m/s)
Hard rock	Crystalline, metamorphic, and pre-Cretaceous sedimentary rock	SC-Ib	Firm to hard rock	700–1,400	S_B	Rock	750–1,500
Soft rock	Tertiary and Cretaceous sedimentary rock, soft volcanics	SC-II	Gravelly soils and soft to firm rock	375–700	S_C	Very dense soil and soft rock	360–760
Alluvium	Unconsolidated Quaternary deposits >10m deep	SC-III	Stiff clays and sandy soils	200–375	S_D	Stiff soil	180–360
Soft soil	Artificial fill and Holocene fluvial, bay, and estuarine deposits (for example, Bay mud[1])	SC-IV	Soft soil	100–200	S_E	Soft soil	<180

[1]Refers to Holocene bay mud deposits along the margin of San Francisco Bay.

Table 2.—*Strong-motion data on alluvium (SC-III, S_D)[1] used for regression analyses of PHA*

[PHA, mean peak horizontal acceleration; R_s, closest distance to seismogenic rupture zone; g, acceleration of gravity]

Station No.	R_s (km)	PHA (g)	Station No.	R_s (km)	PHA (g)
1103	78.3	0.098	57355	18.6	0.100
1116	72.0	0.125	57356	18.9	0.113
1226	51.9	0.005	57357	19.6	0.102
1227	26.4	0.360	57382	15.0	0.320
1230	33.4	0.195	57425	23.2	0.280
1239	75.3	0.110	57458	81.0	0.060
1265	51.5	0.050	57476	11.4	0.265
1439	80.6	0.095	57502	27.6	0.130
1446	74.6	0.095	57504	20.7	0.180
1474	54.1	0.070	57528	64.8	0.040
1479	68.0	0.115	57562	13.4	0.190
1481	51.5	0.165	57563	13.2	0.275
1575	28.1	0.240	58000	77.8	0.100
1601	30.9	0.240	58065	8.2	0.435
1652A	19.3	0.255	58224	71.5	0.228
1652C	19.7	0.205	58233	48.9	0.075
1656	25.4	0.280	58235	8.4	0.295
1675	68.0	0.090	58261	64.4	0.145
1678	79.3	0.180	58393	51.6	0.155
1686	38.1	0.175	58394	60.7	0.115
1687	33.1	0.105	58462	49.5	0.105
1689	57.1	0.085	58483	70.4	0.160
1695	23.2	0.205	58490	60.8	0.130
46173	88.8	0.065	58492	86.6	0.058
47125	15.8	0.505	58496	76.3	0.115
47179	32.8	0.105	58498	53.1	0.160
47288	72.7	0.050	58501	53.2	0.145
47380	11.7	0.350	58503	87.4	0.110
47381	13.4	0.460	58505	87.1	0.120
47459	10.3	0.333	68003	117.0	0.130
47460	81.0	0.080	68150	121.1	0.030
47524	28.6	0.280	68387	150.8	0.060
56012	73.4	0.050	68489	150.5	0.045
57064	38.1	0.120	68491	150.5	0.045
57066	22.9	0.165	69039	154.0	0.040
57191	28.6	0.120			

[1]Definition of site-classification criteria is given in table 1.

Table 3.—*Strong-motion stations on alluvium (SC-III, S_D)[1] used in regression analyses of PHA*

[PHA, mean peak horizontal acceleration. Owner: USGS, U.S. Geological Survey; CDMG, California Division of Mines and Geology. Location: BSMT, basement; GRND, ground level; TOE, toe of dam]

Station No.	Owner	Station name	Location
1103	USGS	BERKELEY—2168 SHATTUCK, EAST	BSMT
1116	USGS	SAN FRANCISCO—CSUSF, THORTON HALL	GRND
1226	USGS	LIVERMORE—VA HOSPITAL, BLDG. 62	BSMT
1227	USGS	PALO ALTO—VA HOSPITAL, BLDG. 1	BSMT
1230	USGS	MENLO PARK—VA HOSPITAL, BLDG. 37	GRND
1239	USGS	SAN FRANCISCO—TRANSAMERICA TOWER	BSMT
1265	USGS	DEL VALLE DAM	TOE
1439	USGS	RICHMOND—BULK MAIL CENTER	GRND
1446	USGS	SAN FRANCISCO—STANDARD OIL BUILDING	BSMT
1474	USGS	BEAR VALLEY #5—CALLENS RANCH	GRND
1479	USGS	BEAR VALLEY #10—WEBB RESIDENCE	GRND
1481	USGS	BEAR VALLEY #12—WILLIAMS RANCH	GRND
1575	USGS	HOLLISTER—CITY HALL ANNEX	BSMT
1601	USGS	STANFORD UNIVERSITY—SLAC TEST LAB	GRND
1652A	USGS	ANDERSON DAM—DOWNSTREAM	GRND
1652C	USGS	ANDERSON DAM—TOE	TOE
1656	USGS	HOLLISTER—DIFFERENTIAL ARRAY (SMA)	GRND
1675	USGS	SAN FRANCISCO—1295 SHAFTER	GRND
1678	USGS	SAN FRANCISCO—GOLDEN GATE BRIDGE	GRND
1686	USGS	FREMONT—EMERSON COURT	GRND
1687	USGS	CALAVERAS RESERVOIR—SOUTH	GRND
1689	USGS	DUBLIN—FIRE STATION	GRND
1695	USGS	SUNNYVALE—COLTON AVENUE	GRND
46173	CDMG	BITTERWATER—COALINGA ROAD	GRND
47125	CDMG	CAPITOLA—FIRE STATION	GRND
47179	CDMG	SALINAS—JOHN & WORK	GRND
47288	CDMG	SAN BENITO	GRND
47380	CDMG	GILROY #2—HIGHWAY 101 MOTEL	GRND
47381	CDMG	GILROY #3—SEWAGE PLANT	GRND
47459	CDMG	WATSONVILLE—TELEPHONE BUILDING, N.W.	GRND
47460	CDMG	GREENFIELD—POLICE STATION	GRND
47524	CDMG	HOLLISTER—GLORIETTA WAREHOUSE, F.F.	GRND
56012	CDMG	LOS BANOS	GRND
57064	CDMG	FREMONT—MISSION SAN JOSE	GRND
57066	CDMG	AGNEWS—AGNEWS STATE HOSPITAL	GRND
57191	CDMG	HALLS VALLEY—GRANT PARK	GRND
57355	CDMG	SAN JOSE—GREAT WESTERN BUILDING, SOUTH	BSMT
57356	CDMG	SAN JOSE—TOWN PARK TOWERS, SOUTH	GRND
57357	CDMG	SAN JOSE—SANTA CLARA COUNTY BLDG., S.W.	BSMT
57382	CDMG	GILROY #4—SAN YSIDRO SCHOOL	GRND
57425	CDMG	GILROY #7—MANTELLI RANCH	GRND
57458	CDMG	TRACY—SEWAGE PLANT	GRND
57476	CDMG	GILROY—OLD FIREHOUSE	GRND
57502	CDMG	MILPITAS—2-STORY BUILDING, EAST	GRND
57504	CDMG	COYOTE LAKE DAM—DOWNSTREAM	GRND
57528	CDMG	LIVERMORE—FAGUNDES RANCH	GRND
57562	CDMG	SAN JOSE—3-STORY BUILDING, EAST	GRND
57563	CDMG	SAN JOSE—SANTA TERESA HILLS	GRND
58000	CDMG	BERKELEY—UCB, STADIUM GROUNDS	GRND
58065	CDMG	SARATOGA—14675 ALOHA	GRND
58224	CDMG	OAKLAND—TITLE & TRUST BUILDING, N.E.	GRND
58233	CDMG	LOWER CRYSTAL SPRINGS DAM—DOWNSTREAM	GRND
58235	CDMG	SARATOGA—SCHOOL GYM, SHEAR WALL, NO.	GRND
58261	CDMG	SO. SAN FRANCISCO—KAISER MEDICAL CENTER	BSMT
58393	CDMG	HAYWARD—MUIR SCHOOL (APEEL #2E)	GRND
58394	CDMG	SAN BRUNO—U.S. POSTAL BUILDING, CENTER	GRND
58462	CDMG	HAYWARD—6-STORY OFFICE BUILDING, CENTER	BSMT
58483	CDMG	OAKLAND—24-STORY BUILDING, WEST	GRND
58490	CDMG	SAN BRUNO—6-STORY OFFICE BUILDING	GRND
58492	CDMG	CONCORD—8-STORY BUILDING, CENTER	GRND
58496	CDMG	BERKELEY—2-STORY HOSPITAL	BSMT
58498	CDMG	HAYWARD—BART STATION, PARKING LOT	GRND
58501	CDMG	HAYWARD—BART ELEVATED SECTION, BENT 132	GRND
58503	CDMG	RICHMOND—3-STORY GOVERNMENT BLDG., E.	BSMT
58505	CDMG	RICHMOND—CITY HALL, PARKING LOT	GRND
68003	CDMG	OLEMA—POINT REYES RANGER STATION	GRND
68150	CDMG	NAPA—NAPA COLLEGE	GRND
68387	CDMG	SANTA ROSA—5-STORY BUILDING, WEST	GRND
68489	CDMG	SANTA ROSA—14-STORY BUILDING, CENTER	GRND
68491	CDMG	SANTA ROSA—HENDLEY & TUPPER	GRND
69039	CDMG	BODEGA HEAD—DORAN BEACH	GRND

[1]Definition of site-classification criteria is given in table 1.

km from the seismogenic rupture zone, this preliminary model tended to overestimate PHA, whereas for distances greater than 80 km the opposite effect was observed. Between these two distances the residuals showed a gradual transition from one trend to the other. Upon further analysis it became clear that this bias was caused by the presence of a zone of nearly constant acceleration between distances of about 50 and 80 km from the seismogenic rupture zone.

In order to model the observed behavior, a second regression analysis was performed in which the distance limits defining the zone of constant acceleration were included as regression coefficients. The only constraint imposed in this analysis was that PHA remain constant between these two distance limits. This resulted in the following tripartite attenuation relationship:

$$\begin{aligned} \ln \text{PHA} &= 1.876 - 1.03 \ln [R_S + 7.79], && R_S \leq 50.6 \text{ km}; \\ &= -2.313, && 50.6 < R_S < 79.1 \text{ km}; \\ &= 3.223 - 1.24 \ln [R_S + 7.79], && R_S \geq 79.1 \text{ km}; \end{aligned} \quad (1)$$

where PHA is the arithmetic mean of the two horizontal components of peak ground acceleration in fractions of gravity (g = 981 cm/s), and R_S is the closest distance to the zone of seismogenic rupture in kilometers. The standard error of estimate, $\sigma_{\ln \text{PHA}}$, associated with this model was 0.406. This relationship together with its supporting data is plotted in figure 1. This figure, which is plotted in terms of a linear rather than a logarithmic distance scale to accentuate the larger distances, clearly shows the existence of a zone of nearly constant acceleration between distances of about 50 and 80 km.

A comparison of equation (1) with empirical attenuation relationships available in 1990 was made by Campbell (1991). Because of what was then considered unusual attenuation characteristics exhibited by the earthquake, most of these attenuation relationships were found to underpredict systematically the accelerations by as much as a factor of 1.5 to 3 at distances greater than about 50 km. However, they all accurately predicted the accelerations at distances of 50 km and less. Similar behavior had been previously observed during the 1987 Whittier Narrows, California, earthquake (Campbell, 1988) and was subsequently observed during the 1992 Landers, California, earthquake (Campbell and Bozorgnia, 1994a)

An analysis of residuals conducted by Campbell (1991) using equation (1) indicated that there was a strong dependence of the residuals on azimuth. This dependence is summarized in table 4. Sites located northwest of the epicenter at azimuths of 320° to 350° (measured clockwise from north with respect to the epicenter) were found to have median accelerations that were 19 percent higher, and sites located north and northeast of the epicenter at azimuths of 350° to 030° had median accelerations that were 29 percent lower than those given by equation (1). The rate of attenuation of PHA was found to be lower toward the northwest and higher toward the northeast as compared to the average rate of attenuation given by equation (1). These differences were found to be significant at the 90 percent confidence level.

Based on the above results, a third regression analysis was performed in which the rate of attenuation was allowed to vary as a function of azimuth. Since there was an insufficient number of strong-motion recordings with which to

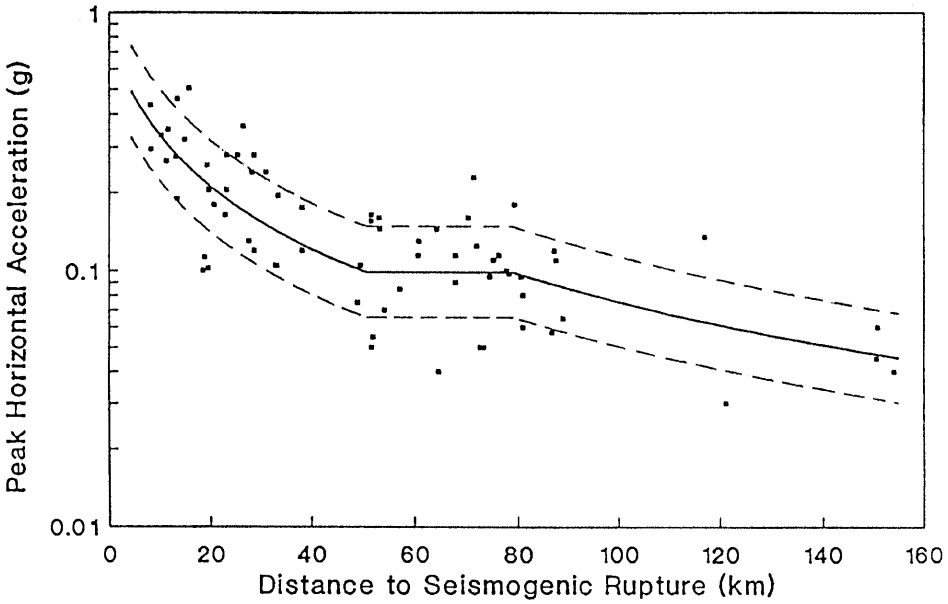

Figure 1.—Attenuation relationship for the earthquake developed by Campbell (1991): solid line, median; dashed lines, one standard error bounds; solid squares, recorded values of mean peak horizontal acceleration.

Table 4.—*Summary of relative azimuthal effects for PHA*

[PHA, mean peak horizontal acceleration; —, no value]

Azimuth (° clockwise from N.)	Direction from epicenter	Relative factor	
		Median	68% confidence interval
1989 Loma Prieta earthquake (this study)			
350–030	Northeast	1.00	0.73–1.36
320–350	Northwest	1.68	1.19–2.38
1992 Landers earthquake (Campbell and Bozorgnia, 1994a)			
175–240	Southwest	1.00	—
240–300	West	1.29	—
300–015	Northwest	1.62	—
115–175	Southeast	1.59	—

constrain the rate of attenuation at some azimuths and distances, the abundant observations of MMI on alluvium were used to supplement the limited strong-motion data in these regions. The procedure for doing this is discussed below. The resulting attenuation relationship is given by the expression,

$$
\begin{aligned}
\ln \mathrm{PHA} &= \ln \mathrm{PHA}_1, && 270^\circ \le \theta < 340^\circ \\
&= W \ln \mathrm{PHA}_1 + (1-W) \ln \mathrm{PHA}_2, && 340^\circ \le \theta < 360^\circ; \\
&= \ln \mathrm{PHA}_2, && 000^\circ \le \theta < 060^\circ; \\
&= W \ln \mathrm{PHA}_2 + (1-W) \ln \mathrm{PHA}_3, && 060^\circ \le \theta < 095^\circ; \\
&= \ln \mathrm{PHA}_3, && 095^\circ \le \theta < 195^\circ; \\
&= W \ln \mathrm{PHA}_3 + (1-W) \ln \mathrm{PHA}_4, && 195^\circ \le \theta < 210^\circ; \\
&= \ln \mathrm{PHA}_4, && 210^\circ \le \theta < 255^\circ; \\
&= W \ln \mathrm{PHA}_4 + (1-W) \ln \mathrm{PHA}_1, && 255^\circ \le \theta < 270^\circ;
\end{aligned}
\qquad (2)
$$

where

$$
\begin{aligned}
\ln \mathrm{PHA}_i &= 2.899 - 1.0 \ln (R_S + 31.6) - 0.00585\, R_S, && i = 1; \\
&= 1.845 - 1.0 \ln (R_S + 11.0) - 0.00373\, R_S, && i = 2; \\
&= 2.228 - 1.0 \ln (R_S + 16.2) - 0.00443\, R_S, && i = 3; \\
&= 2.899 - 1.0 \ln (31.6) - 0.00585\, R_S, && i = 4;
\end{aligned}
$$

$$W = \tfrac{1}{2}(1 + \cos \delta),$$

$$\delta = \frac{\pi(\theta - \theta_1)}{\theta_2 - \theta_1},$$

PHA and R_S are as defined in equation (1), θ_1 is source-to-site azimuth measured clockwise from north (assuming an epicentral location at 37.037° N. and 121.883° W.), θ_1 is the beginning azimuth for the specified range, θ_2 is the ending azimuth for the specified range, and W is an azimuthally dependent weighting factor. The standard error of estimate of this model is $\sigma_{\ln \mathrm{PHA}} = 0.297$, which corresponds to a 27 percent reduction in the standard error associated with equation (1). This relationship, along with its supporting data, is plotted in figures 2 through 6.

Equation (2) was developed from a nonlinear regression analysis in which the amplitude of PHA at $R_S = 0$, the assumed source of the radiated energy, was constrained to be constant at all azimuths. The range of azimuths used to define the various segments of the model were determined from the azimuthal dependence of PHA observed by Campbell (1991) and from maps of peak acceleration and MMI published by Maley and others (1989), Shakal and others (1989), and Stover and others (1990).

Intensity observations on alluvium compiled by Stover and others (1990) and C. Stover (written commun., 1991) were used to constrain the attenuation of PHA at distances beyond about 75 km, where the number of strong-motion recordings was limited. This was done through an iterative procedure in which azimuthally dependent estimates of R_S and PHA for MMI contours IV, V, VI, VII, and VIII were used to simultaneously develop an attenuation relationship for PHA and an earthquake-specific relationship between PHA and MMI (see next section). Initial estimates of PHA for MMI contours IV, V, and VI were taken from a relationship developed by Trifunac (1976), and those for MMI contours VII and VIII were obtained from a preliminary version of equation (2).

The steps involved in this iterative procedure are summarized as follows: (1) estimates of PHA and R_S for MMI contours IV, V, and VI were used in conjunction with the strong-motion recordings compiled for this study to develop an attenuation relationship for PHA, (2) estimates of PHA for distances associated with MMI contours IV through VIII obtained from the attenuation relationship developed in step 1 were used to develop a relationship between PHA and MMI, and (3) steps 1 and 2 were repeated until an acceptable level of convergence between the PHA attenuation relationship and the PHA-MMI relationship was obtained.

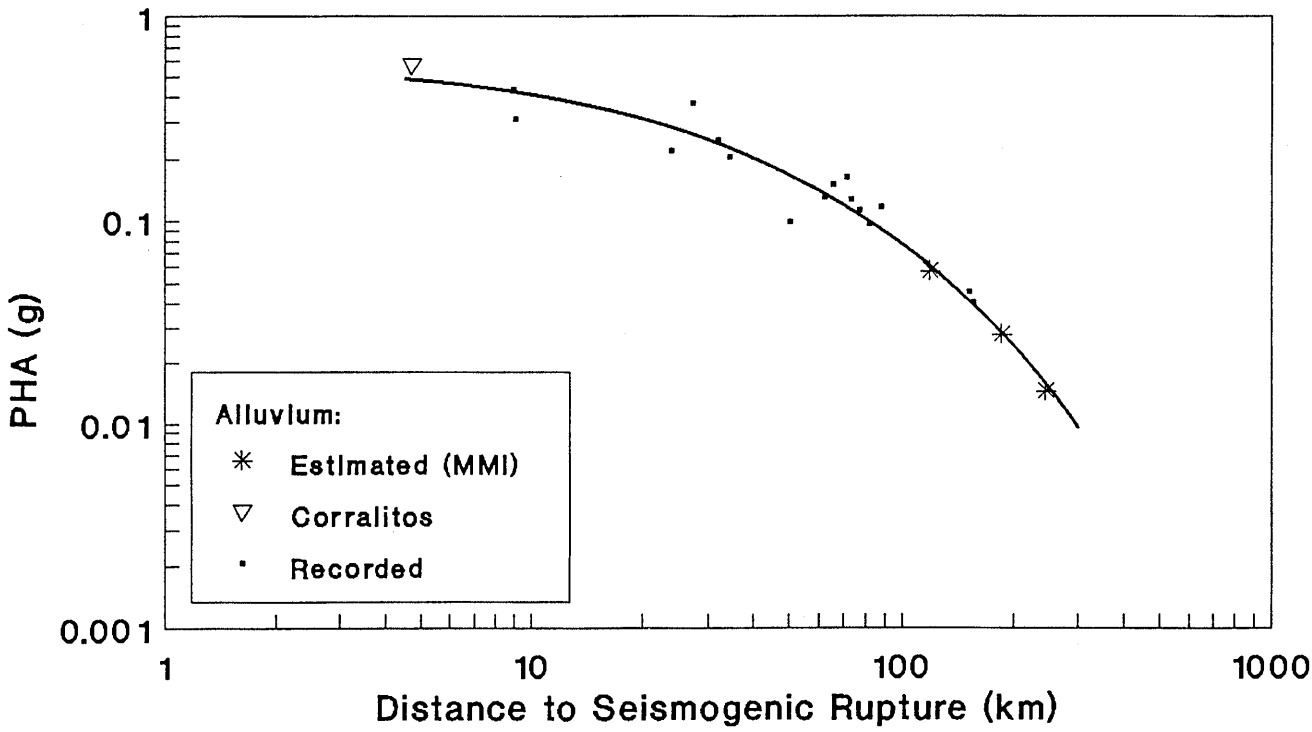

Figure 2.—Attenuation relationship developed in this study for alluvial sites located at epicenter-to-site azimuths of 270° to 340° (northwest direction) measured clockwise from north.

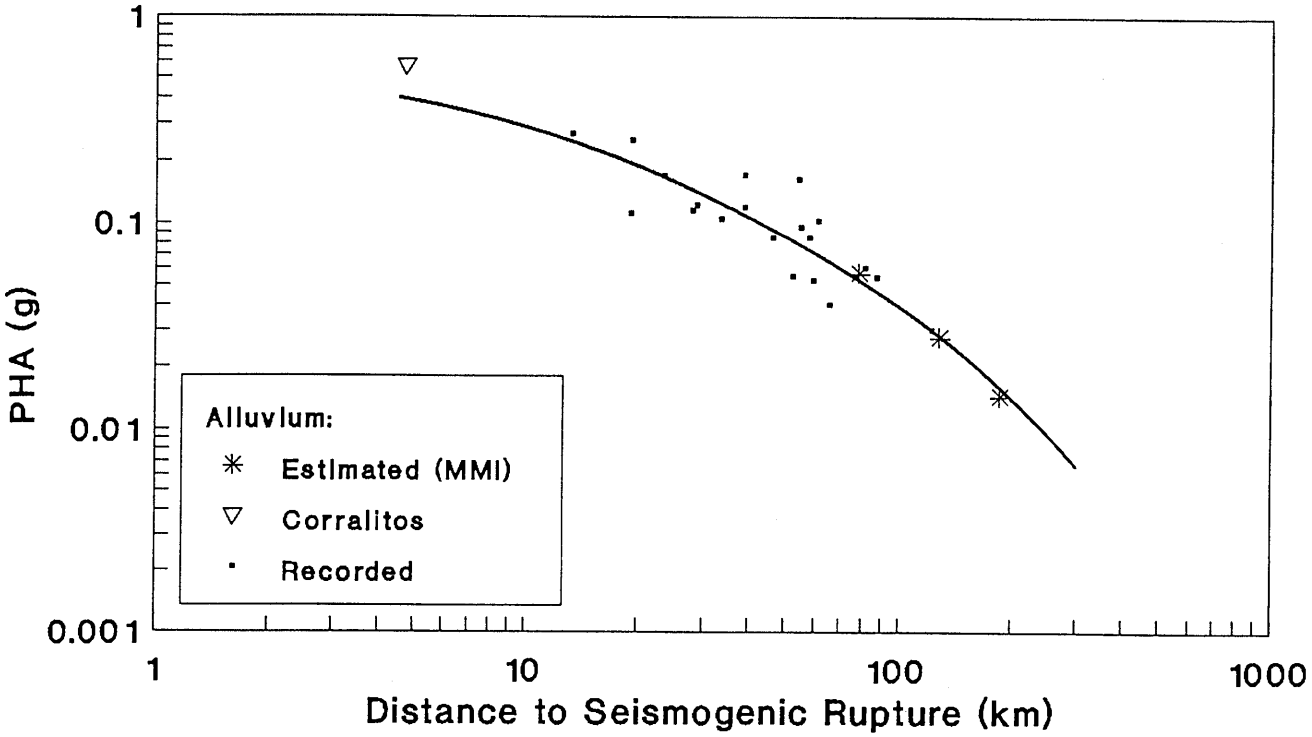

Figure 3.—Attenuation relationship developed in this study for alluvial sites located at epicenter-to-site azimuths of 000° to 060° (northeast direction) measured clockwise from north.

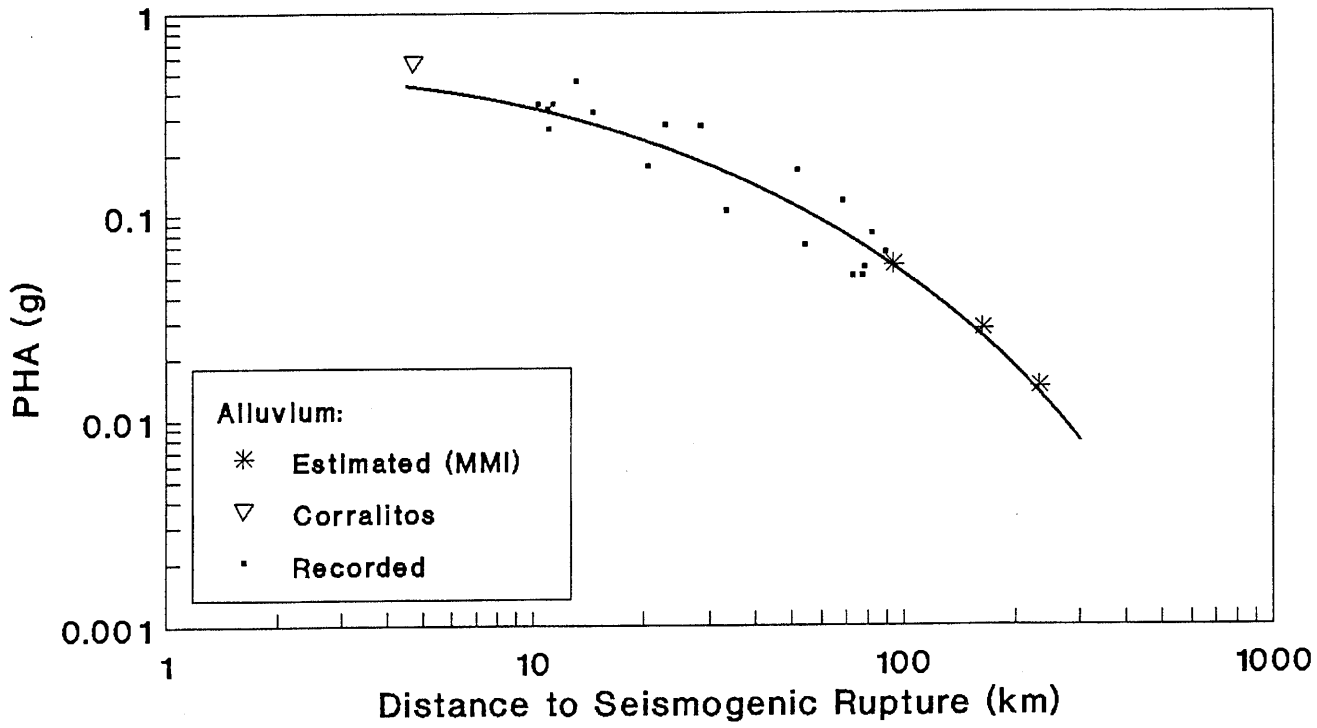

Figure 4.—Attenuation relationship developed in this study for alluvial sites located at epicenter-to-site azimuths of 095° to 195° (southeast direction) measured clockwise from north.

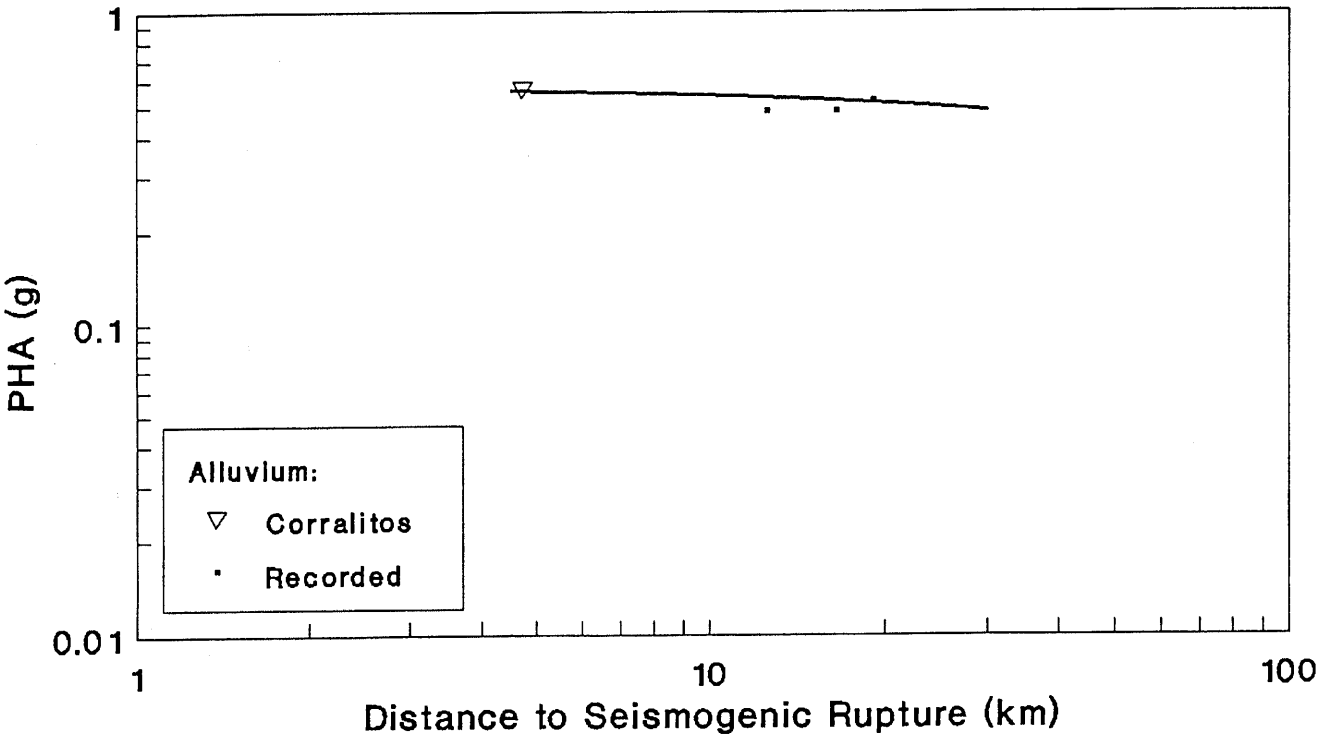

Figure 5.—Attenuation relationship developed in this study for alluvial sites located at epicenter-to-site azimuths of 210° to 255° (southwest direction) measured clockwise from north.

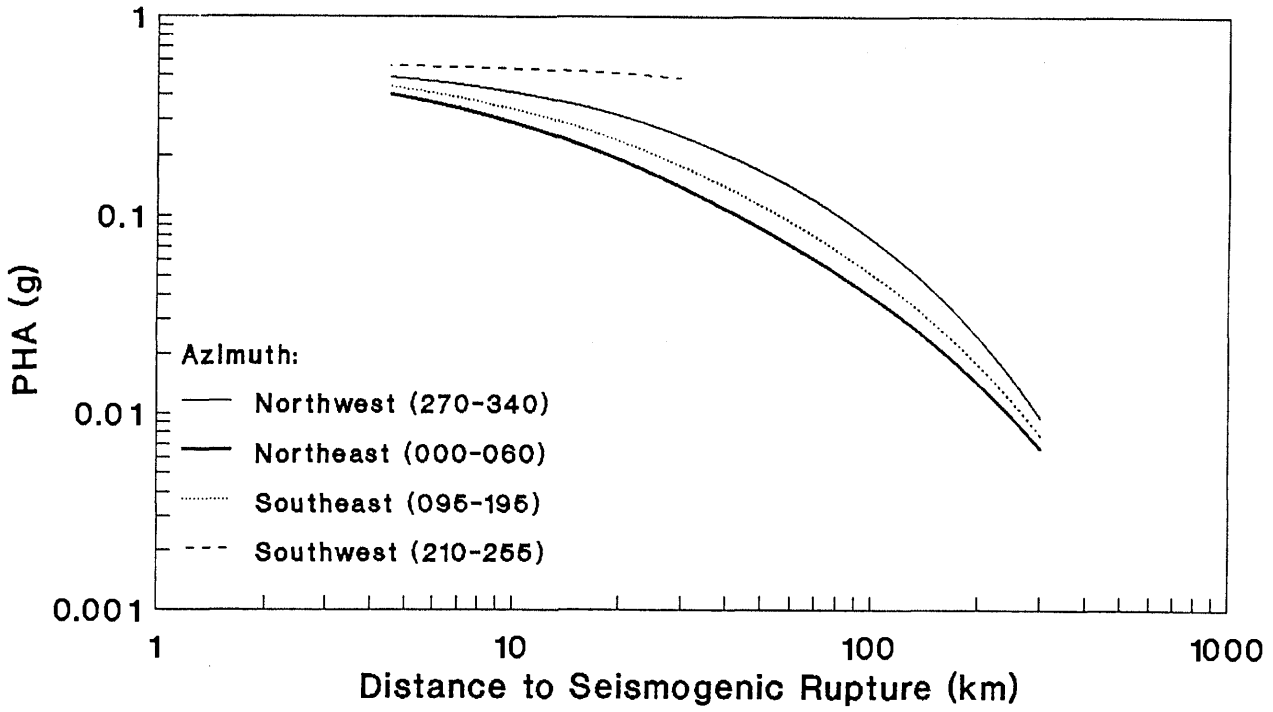

Figure 6.—Comparison of attenuation relationships developed in this study for alluvial sites for epicenter-to-site azimuths corresponding to the northwest, northeast, southeast, and southwest directions.

MODIFIED MERCALLI INTENSITY

The relationship between MMI and PHA obtained using the iterative procedure described in the previous section is given by the expression,

$$\text{MMI} = 8.76 + 0.637\ (\ln \text{PHA}) - 0.114\ (\ln \text{PHA})^2,$$

which is considered to be valid for accelerations ranging from 0.014 to 1.0 *g*. This relationship is plotted in figure 7, where it is compared to the relationship proposed by Trifunac (1976) for California earthquakes. The Trifunac relationship has been adjusted by +½ MMI to predict the value of PHA at the MMI contour rather than at the middle of the region between contours. Figure 7 indicates that estimates of MMI from equation (3) are consistently lower than those predicted by the Trifunac relationship. EQE International, Inc. (1995) found a similar discrepancy between observed and predicted intensities for the 1994 Northridge earthquake.

The standard error of estimate, (σ_{MMI}, associated with equation (3) is 0.107, indicating a remarkably strong correlation between PHA and the MMI contour value. However, for purposes of prediction, it is the error associated with the estimation of MMI at an individual observation site, not the error associated with a specific MMI contour that is of interest. An estimate of this latter error was obtained from the standard deviation of the computed differences between the integer representations of the observed and predicted intensities at each alluvial site for which there was an MMI observation (C. Stover, written commun., 1991). This analysis indicated that the standard error associated with the estimation of MMI at an individual site is about 0.55.

PEAK HORIZONTAL VELOCITY

Because there was an insufficient number of digitized recordings, it was not possible to develop an independent attenuation relationship for peak horizontal velocity for alluvial sites. Instead, the available processed recordings were used to develop the following relationship between PHV and PHA:,

$$\begin{aligned}
\ln \text{PHV} &= \ln \text{PHV}_1, && 095^\circ \le \Theta < 340^\circ \\
&= W \ln \text{PHV}_1 + (1-W) \ln \text{PHV}_2, && 340^\circ \le \Theta < 360^\circ \\
&= \ln \text{PHV}_2, && 000^\circ \le \Theta < 060^\circ; \\
&= W \ln \text{PHV}_2 + (1-W) \ln \text{PHV}_1, && 060^\circ \le \Theta < 095^\circ;
\end{aligned}$$

where (4)

$$\begin{aligned}
\ln \text{PHV}_i &= 4.720 + \ln \text{PHA}, && i = 1; \\
&= 4.551 + \ln \text{PHA}, && i = 2,
\end{aligned}$$

PHV is the arithmetic mean of the two horizontal components of peak ground velocity in centimeters per second, PHA is calculated by equation (2), and the standard error of estimate, $\sigma_{\ln \text{PHV}}$, is 0.305. The ratio of PHV to PHA given by equation (4) is between 94.7 and 112.1 cm/s/g, the lower estimate corresponding to sites located northeast of the epicenter. The higher ratios at sites located toward the southeast, west, and northwest are consistent with the effects of

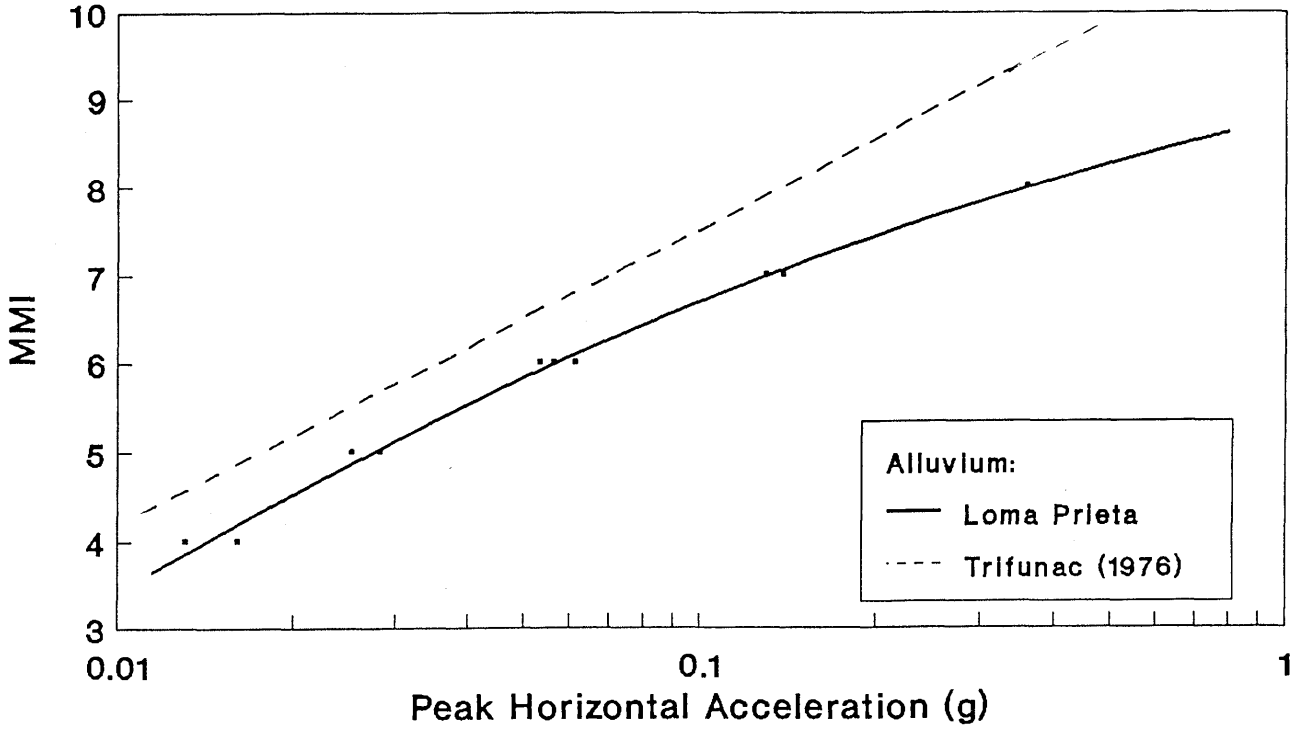

Figure 7.—Comparison of the relationship between the Modified Mercalli intensity (MMI) contour and mean peak horizontal acceleration (PHA) developed in this study for alluvial sites with a similar relationship developed by Trifunac (1976) for California earthquakes. The Trifunac relationship has been adjusted by +1/2 MMI to predict the value of PHA at the MMI contour rather than at the middle of the region between contours.

directivity and shear-wave radiation pattern that have a larger impact on the longer-period ground motions associated with PHV than on the shorter-period motions associated with PHA. The ratios given by Equation (4) are summarized in Table 5, where they are compared to PHV/PHA ratios recommended by Mohraz and Elghadamsi (1989).

EFFECT OF SURFICIAL GEOLOGY

An analysis of residuals was used to identify the potential effects of surficial geology on the observed values of PHA (Campbell, 1991). The residuals, which are referred to by the notation NR in the discussion that follows, were computed with respect to the predicted value of ln PHA from equation (1) and divided by $\sigma_{\ln PHA}$. A positive residual indicates that the recorded value is larger than that predicted by the model, and a negative residual indicates that the recorded value is smaller than that predicted by the model. Since the residuals have been normalized by $\sigma_{\ln PHA}$, an NR of ±1 represents a deviation of plus-and-minus one standard error between the recorded and predicted value of ln PHA. If the residuals are assumed to be normally distributed, NR be-

Table 5.—*Summary of PHV to PHA ratios for alluvium (SC-III, S_D)*[1]

[PHV, mean peak horizontal velocity; PHA, mean peak horizontal acceleration; *g*, acceleration of gravity; —, no value]

Azimuth (° clockwise from N.)	Soil depth (feet)	PHV/PHA ratio (cm/s/g)	
		Median	68% confidence interval
1989 Loma Prieta earthquake (this study)			
000–060	—	95	70–129
095–340	—	112	83–152
Mohraz and Elghadamsi (1989)			
—	<30	88	51–151
—	30–200	84	53–133
—	>200	133	90–196

[1]Definition of site-classification criteria is given in table 1.

comes an estimate of the standard normal variate. In this case a normalized residual of 0 corresponds to a recording that falls at the 50th percentile (the median) of the distribution of residuals, and normalized residuals of -1 and +1 correspond to recordings that fall at the 16th percentile and 84th percentile of this distribution, respectively. The correspondence between the site classification criteria given below and those recommended for building-code and engineering applications by Borcherdt (1994), Borcherdt and Glassmoyer (1994), and the International Conference of Building Officials (1996) is given in table 1.

ALLUVIUM

A plot of NR versus R_S for alluvium (SC-III, S_D) is displayed in figure 8. There is no visible trend in this plot. This is expected since these recordings were used to develop the relationship. The diamonds in this figure represent recordings from embedded sites, primarily from basements of buildings. A hypothesis test indicated that the embedded recordings had a mean residual close to zero, no different from the mean residual of the ground-level and free-field recordings at the 90 percent confidence level. This test appears to contradict the results of previous studies which have found embedded sites to have smaller accelerations than nonembedded sites (see Campbell, 1987, 1988, 1989, 1990); however, the relatively large distances associated with many of these recordings has apparently minimized this effect (Campbell, 1987). Figure 9 shows the distribution of residuals with respect to R_S and azimuth. This plot indicates that distances greater than 80 km between azimuths of 000° and 160° and all distances between azimuths of 160° and 320° are poorly represented by the recordings.

A plot of NR versus azimuth is displayed in figure 10. This plot shows that there is a strong azimuthal bias in the residuals, with NR between azimuths of 320° and 350° biased toward positive values, representing an underestimation of PHA by the regression model, and those between azimuths of 350° and 030° biased toward negative values, representing an overestimation of PHA. The underestimation occurs at azimuths corresponding to San Francisco and Oakland, the overestimation at azimuths corresponding to Hayward and San Jose. This bias was accounted for in equation (2). Evidence presented later strongly suggests that this azimuthal bias is due to the combined effects of differences in attenuation, source directivity, and shear-wave radiation pattern. Stover and others (1990) found a similar azimuthal bias in reported values of MMI.

SOFT AND HARD ROCK

A plot of NR versus R_S for soft rock (SC-II, S_C) and hard rock (SC-Ib, S_B) is displayed in figure 11. This plot indicates that both soft-rock and hard-rock recordings at distances of 20 km and greater tend to have smaller accelerations than those recorded on alluvial sites. The effect is most significant for hard-rock sites. Hypothesis tests indicated that the mean residuals of both the soft-rock and hard-rock recordings at similar azimuths were significantly different from the mean residual of the alluvial recordings at the 90 percent confidence level. A simi-

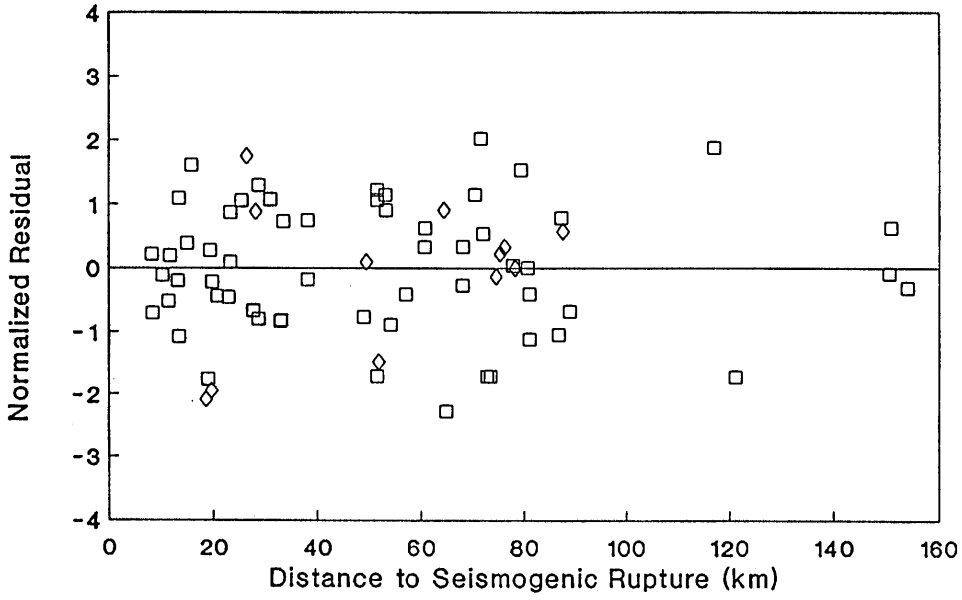

Figure 8.—Plot of normalized residuals versus closest distance to the seismogenic rupture zone for alluvial sites: squares, ground-level and free-field recordings; diamonds, embedded recordings.

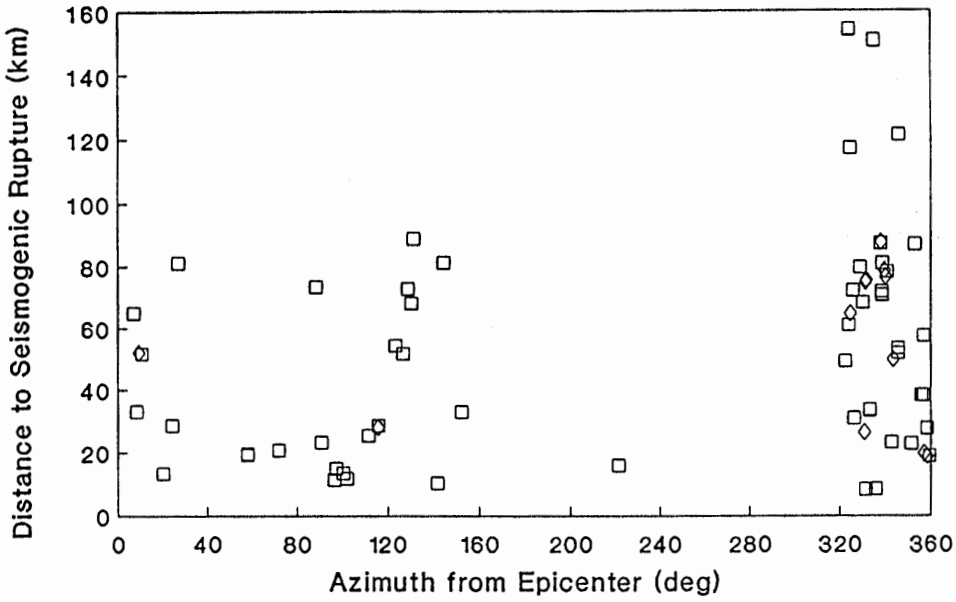

Figure 9.—Plot of closest distance to the seismogenic rupture zone versus epicenter-to-site azimuth measured clockwise from north for alluvial sites: squares, ground-level and free-field recordings; diamonds, embedded recordings.

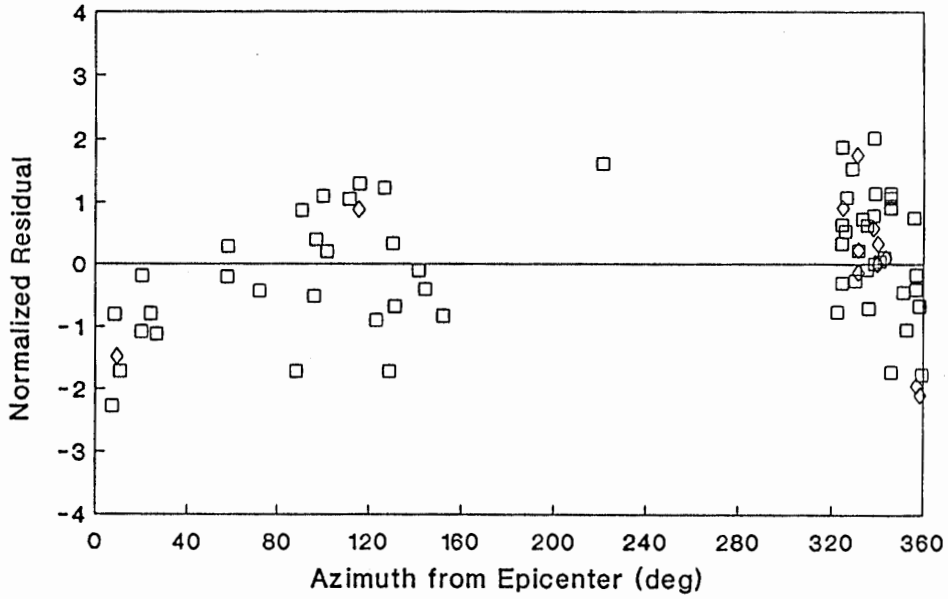

Figure 10.—Plot of normalized residuals versus epicenter-to-site azimuth measured clockwise from north for alluvial sites: squares, ground-level and free-field recordings; diamonds, embedded recordings.

lar effect was observed during the 1987 Whittier Narrows earthquake (Campbell, 1988).

Figure 12 is a plot of the distribution of residuals with respect to R_S and azimuth. This plot shows that, although rock recordings are fairly evenly distributed with respect to azimuth, there are few recordings at distances greater than 50 km except at azimuths corresponding to San Francisco and Oakland.

A plot of NR versus azimuth is displayed in figure 13. The number of recordings on rock is less than for alluvium, and their residuals are biased toward negative values. As a result, it is not obvious from this figure whether the rock recordings show a similar bias with azimuth. The residuals corresponding to azimuths of 320°to 350° do appear to be larger, on average, than those corresponding to azimuths of 350° to 030°, which lends qualitative

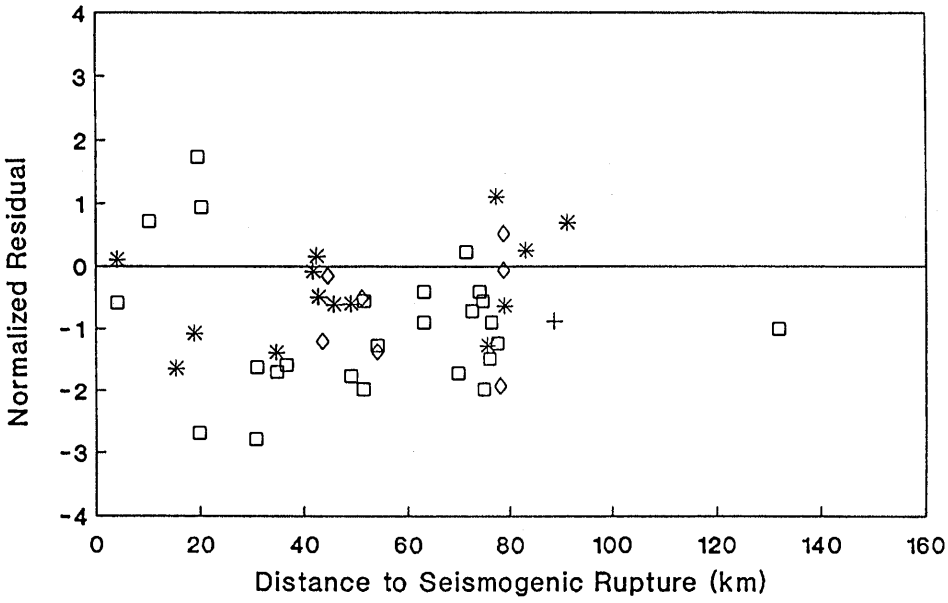

Figure 11.—Plot of normalized residuals versus closest distance to the seismogenic rupture zone for rock sites: asterisks, ground-level and free-field recordings on soft rock; crosses, embedded recordings on soft rock; squares, ground-level and free-field recordings on hard rock; diamonds, embedded recordings on hard rock.

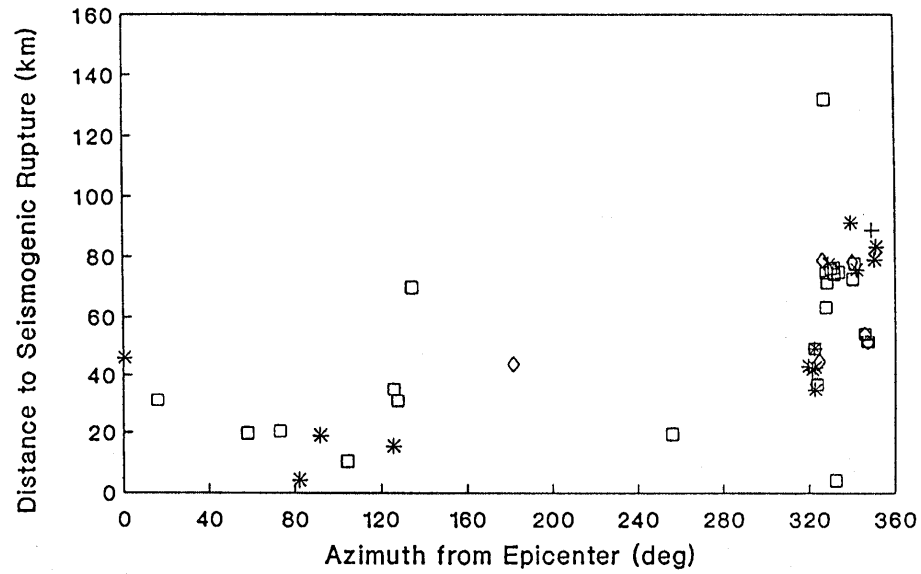

Figure 12.—Plot of closest distance to the seismogenic rupture zone versus epicenter-to-site azimuth measured clockwise from north for rock sites: asterisks, ground-level and free-field recordings on soft rock; crosses, embedded recordings on soft rock; squares, ground-level and free-field recordings on hard rock; diamonds, embedded recordings on hard rock.

support to the suggestion that this bias is a propagation effect and/or a source effect, and not a site effect.

BAY MUD

A plot of NR versus R_S for Bay mud (SC-IV, S_E) is displayed in figure 14. This plot shows that Bay mud sites have substantially larger accelerations than alluvial sites. As indicated in figures 15 and 16, all of these sites lie between azimuths of 320° and 350°. The analysis of the alluvial recordings indicated that these azimuths were associated with higher than average accelerations. Therefore, the large bias associated with these sites is probably caused by a combination of both azimuthal and site effects. A hypothesis test indicated that the mean residual

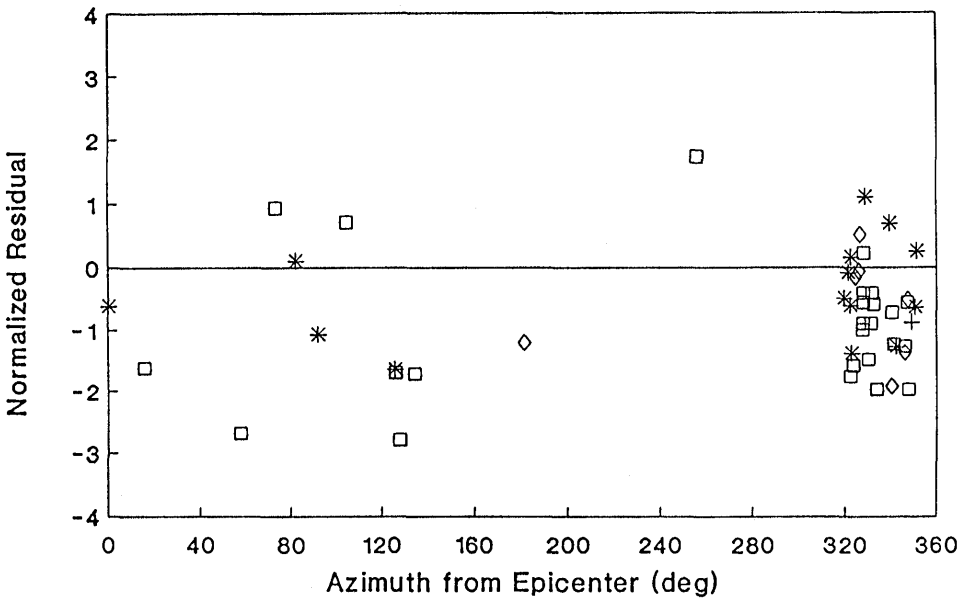

Figure 13.—Plot of normalized residuals versus epicenter-to-site azimuth measured clockwise from north for rock sites: asterisks, ground-level and free-field recordings on soft rock; crosses, embedded recordings on soft rock; squares, ground-level and free-field recordings on hard rock; diamonds, embedded recordings on hard rock.

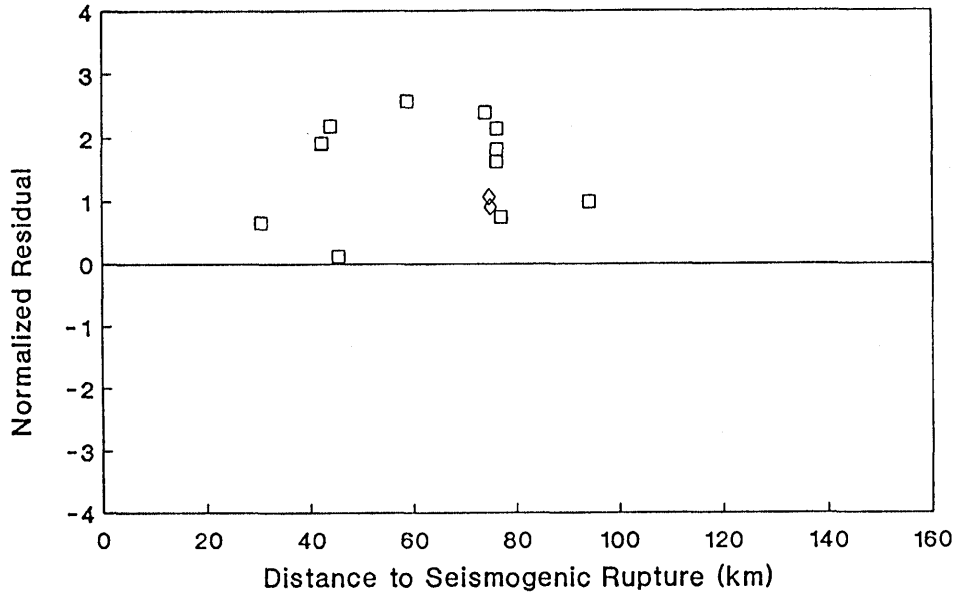

Figure 14.—Plot of normalized residuals versus closest distance to the seismogenic rupture zone for Bay mud sites: squares, ground-level and free-field recordings; diamonds, embedded recordings.

of the Bay mud recordings was significantly different from the mean residual of the alluvial recordings for similar azimuths at the 90 percent confidence level. Thus, the large amplitude bias associated with the Bay mud sites is statistically significant.

The effect of surficial geology on peak acceleration is summarized in table 6, where it is compared to similar low-strain site-amplification factors observed or predicted by others, as discussed in a later section. The median site factor from the empirical attenuation relationships is the geometric mean of those calculated for moment magnitudes (M_W) of 6.5 and 7.5. The 68 percent confidence interval from the empirical attenuation relationships was derived from the complete set of calculated values for both M_W 6.5 and 7.5 assuming a log-normal distribution. According to these results, PHA recorded at intermedi-

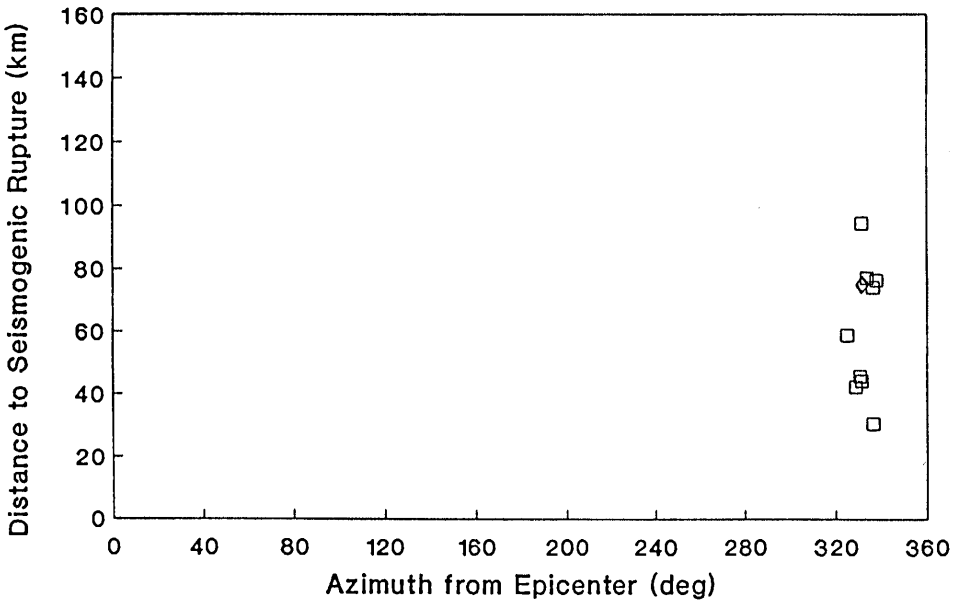

Figure 15.—Plot of closest distance to the seismogenic rupture zone versus epicenter-to-site azimuth measured clockwise from north for Bay mud sites: squares, ground-level and free-field recordings; diamonds, embedded recordings.

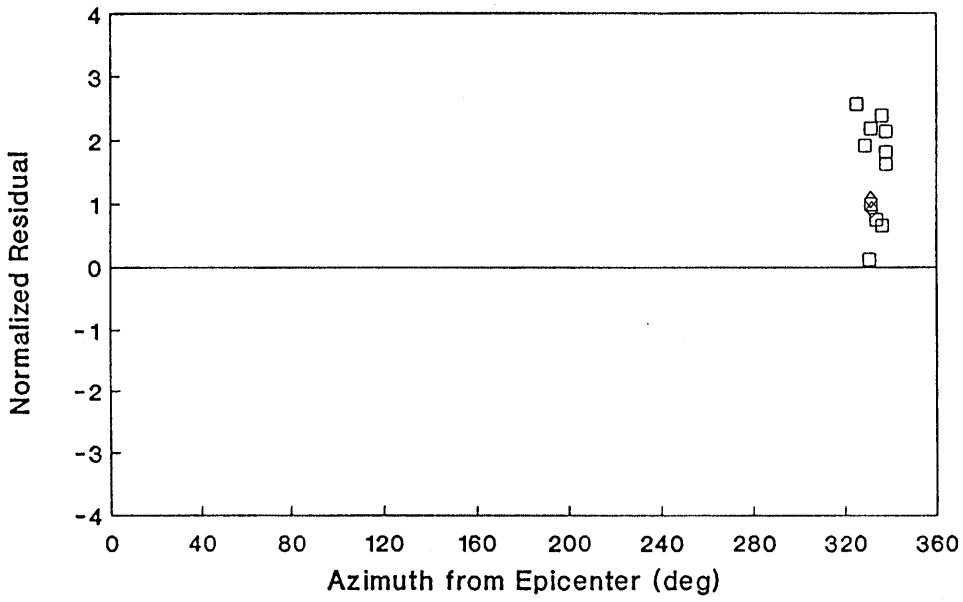

Figure 16.—Plot of normalized residuals versus epicenter-to-site azimuth measured clockwise from north for Bay mud sites: squares, ground-level and free-field recordings; diamonds, embedded recordings.

ate and far distances at all azimuths during the earthquake exhibited a strong dependence on site geology, with PHA on Bay mud (SC-IV, S_E), alluvium (SC-III, S_D), and soft rock (SC-II, S_C) being on average 2.76, 1.47, and 1.25 times, respectively, higher than that on hard, predominantly Franciscan rock (SC-Ib, S_B). These differences were all found to be significant at the 90 percent confidence level.

COMPARISON WITH PREVIOUS STUDIES

REGIONAL ATTENUATION

The zone of nearly constant ground motions observed in figure 1 between distances of about 50 to 80 km from the seismogenic rupture zone when recordings at all azimuths

Table 6.—*Summary of relative low-strain site-amplification factors for PHA and short-period response spectral acceleration*

[PHA, mean peak horizontal acceleration; g, acceleration of gravity; MW, moment magnitude; —, no value]

Reference	Site classification			
	Hard rock (SC-Ib, SB)	Soft rock (SC-II, SC)	Alluvium (SC-III, SD)	Soft soil (Bay mud) (SC-IV, SE)
1989 Loma Prieta earthquake (MW 6.9)				
This study (median)	0.80	1.00	1.18	2.21
This study (68% confidence interval)	0.53–1.21	0.73–1.37	0.78–1.78	1.62–3.02
Boore and others (1989)	1.002	1.002	1.13	2.81
Other earthquakes				
1987 Whittier Narrows (Campbell, 1988), MW 6.1	0.84	1.00	1.47	—
1992 Landers (Campbell and Bozorgnia, 1994a), MW 7.3	0.81	1.00	1.20	—
Empirical attenuation relationships; hard-rock PHA = 0.05 g (MW 6.5, 7.5)				
Abrahamson and Silva (1997)	—	1.00	1.15, 1.15	—
Boore and others (1997)3	0.77, 0.77	1.00	1.31, 1.31	—
Campbell and Bozorgnia (1994b), Campbell (1997)	0.79, 0.78	1.00	1.21, 1.34	—
Idriss (1991, 1993)	—	1.00	1.17, 1.17	3.26, 3.82
Sadigh and others (1997)	—	1.00	1.15, 1.34	—
MEDIAN	0.78, 0.78	1.00, 1.00	1.20, 1.26	3.26, 3.82
MEDIAN (all MW)	0.78	1.00	1.23	3.53
68% CONFIDENCE INTERVAL (all MW)	—	—	1.15–1.31	—
Building-code and engineering applications4				
Borcherdt (1994b), Borcherdt and Glassmoyer (1994)	0.77	1.00	1.23	1.54
Proposed 1997 UBC (International Conference of Building Officials, 1996)	0.83	1.00	1.33	1.75

1Definition of site-classification criteria is given in table 1.
2No distinction was made between soft rock and hard rock.
3Calculated for shear-wave velocities of 250, 510, and 1,070 m/s for alluvium, soft rock, and hard rock, respectively.
4Corresponds to hard-rock PHA of 0.075 g (International Conference of Building Officials, 1996) and 0.1 g (Borcherdt, 1994).

are combined is not as evident when these ground motions are segregated by azimuth as in figures 2 to 6. It appears that varying the rate of attenuation with azimuth, as was done in equation (2), can explain the geographic distribution of alluvial recordings better than simply varying the rate of attenuation with distance for all azimuths, as was done in equation (1). This observation is statistically confirmed by the 27 percent reduction in the standard error associated with equation (2).

The plot comparing the attenuation of PHA with azimuth (fig. 6) indicates that the highest accelerations and lowest rates of attenuation were located southwest of the epicenter in the direction of Santa Cruz and Capitola. This region is located on the hanging wall of the causative fault and is near a maximum in the shear-wave radiation pattern. As a result, this region was subject to strong amplification due to source effects. The next highest accelerations and lowest rate of attenuation was located northwest of the epicenter in the direction of San Francisco and Oakland. Seismic waves propagating in this direction were subject to amplification due to both source directivity and radiation pattern and were observed to have an unusually low rate of attenuation as a result of (1) high Q in the lower crust (Fletcher and Boatwright, 1991) and (2) critical reflections from velocity discontinuities or strong velocity gradients within the crust and from the base of the crust, or Moho (Catchings and Kholer, 1997).

The lowest accelerations and highest rates of attenuation were located northeast of the epicenter. This region is near a minimum in the shear-wave radiation pattern and has propagation paths that cross several faults and fault-bounded basins. As a result, seismic waves propagating in this direction were subject to increased attenuation due to scattering and abrupt changes in crustal velocity structure. Seismic waves propagating toward the southeast had acceleration amplitudes intermediate between those to the northwest and northeast. This region is near a maximum in the shear-wave radiation pattern and was possibly subject to source directivity (assuming bilateral rupture). However, these effects were either weaker than they were toward the northwest, and/or propagation to the southeast was subject to greater attenuation and scattering, possibly as a result of different crustal properties (see Catchings and Kholer, 1997).

Seismological observations of test explosions and aftershocks have indicated that critical reflections from within the crust and from the Moho result in a relatively low rate of attenuation along the San Francisco Peninsula beyond distances of a few tens of kilometers that is believed to be the cause of the relatively high ground motions in the San Francisco and Oakland areas during the main shock (see Somerville and Yoshimura, 1990; McGarr and others, 1991; Fletcher and Boatwright, 1991; Borcherdt and Glassmoyer, 1994; Somerville and others, 1994; Stevens and Day, 1994; Catchings and Kholer, 1997). Figures 2 to 6 generally support these observations; however, the sparse strong-motion data set is not sufficient to unequivocally confirm or refute the specific details of these observations.

Schneider and others (1993) used a band-limited, white-noise stochastic simulation model to assess the effects of source finiteness, crustal wave propagation, and site response on 23 strong-motion recordings located primarily along the San Francisco Peninsula. They compared a simple spherical spreading propagation model with a seismologically more rigorous model, which included both direct and critically reflected phases, and found that the two methods resulted in nearly the same estimates of uncertainty. They found that simple spherical spreading provided a good fit to the response spectra computed from recordings at fault distances between 1 and 80 km, consistent with the results of this study, and concluded that the effects of the crustal structure could easily be accommodated by other parameters in the model.

LOCAL SITE CONDITIONS

As demonstrated in table 6, the relative site amplification factors obtained in this study are consistent with those derived for the earthquake by Boore and others (1989), Plafker and Galloway (1989), and Borcherdt and Glassmoyer, 1992, 1994); for the 1987 Whittier Narrows earthquake by Campbell (1988); and for the 1992 Landers earthquake by Campbell and Bozorgnia (1994a). They are also consistent with site factors predicted by empirical attenuation relationships developed by Campbell and Bozorgnia (1994b) and Boore and others (1997), assuming a hard-rock PHA of 0.05 *g*. Although not shown in table 6, the relative amplification factors developed in this study are also qualitatively consistent with site factors determined from recordings in the San Francisco Bay region of nuclear explosions in Nevada as well as with regional variations in intensity for the 1906 San Francisco earthquake (Borcherdt and Gibbs, 1976). All of these results are biased toward recordings obtained at relatively large distances and/or low values of PHA and, therefore, represent relatively low in-situ strains.

Also shown in table 6 for comparison are the relative low-strain site-amplification factors for short-period spectral accelerations recommended for building-code and engineering applications by Borcherdt (1994), Borcherdt and Glassmoyer (1994), and the International Conference of Building Officials (1996). These site factors represent hard-rock (SC-Ib, S_B) accelerations of 0.1 g for the Borcherdt study and 0.075 *g* for the International Conference of Building Officials study. The recommended site factors are very similar to those observed and predicted from past earthquakes, indicating a reasonable empirical basis for these recommendations.

Empirical analyses by Idriss (1991, 1993), Campbell and Bozorgnia (1994b), Abrahamson and Silva (1997), Campbell (1997), and Sadigh and others (1997) have shown that PHA and short-period spectral site-amplification factors become significantly smaller at near-source distances, consistent with the general trend of the amplitude-dependent amplification factors recommended by Borcherdt (1994), Borcherdt and Glassmoyer (1994), and the International Conference of Building Officials (1996). Table 7 compares relative site-amplification factors between alluvium (SC-III, S_D) and soft rock (SC-II, S_C) predicted from these studies with those recommended for building-code and engineering applications for hard-rock accelerations ranging from 0.05 to 0.4 *g*. For those studies which do not distinguish between soft and hard rock, rock has been classified as soft rock, consistent with the mean shear-wave velocity of 618 m/s determined for strong-motion recording sites classified as generic rock by Boore and Joyner (1997). The soft-rock PHA corresponding to a given value of hard-rock PHA was estimated from the attenuation relationships of Campbell and Bozorgnia (1994b) and Campbell (1997).

The results in table 7 indicate that the amplitude-dependent amplification factors recommended for use in scaling short-period response spectral acceleration for building-code and engineering applications have a weaker dependence on cyclical strain than that predicted for PHA and, therefore, short-period spectral acceleration, by empirical attenuation relationships. Borcherdt (1994) described his recommended site factors as being based directly on Loma Prieta strong-motion recordings for low-amplitude rock accelerations and on theoretical dynamic site-response analyses for higher amplitude rock accelerations. As demonstrated in table 6, the use of Loma Prieta observations to determine the low-strain amplification factors has resulted in factors that are consistent with a large number of other empirical observations. However, the results in table 7 indicate that, although the trend with amplitude is similar, the amplification factors recommended for building-code and engineering applications for hard-rock accelerations of 0.1 *g* and larger are consistently higher than those predicted from empirical attenuation relationships. This latter observation is independent of the assumption of whether a generic rock site is classified as either soft rock or hard rock.

It is possible that the above discrepancy is the result of an intentional built-in conservatism in the recommended amplification factors, a bias in the theoretical site-response analyses that were used to calculate the high-strain dependence of these factors, and/or a bias in the way that the empiri-

Table 7.—*Summary of amplitude-dependent site-amplification factors for PHA and short-period response spectral acceleration for alluvium (SC-III, S_D) relative to soft rock (SC-II, S_C)*[1]

[PHA, mean peak horizontal acceleration; g, acceleration of gravity; MW, moment magnitude; —, no value]

Reference	PHA on hard rock (SC-Ib, SB)				
	0.05 g	0.1 g	0.2 g	0.3 g	0.4 g
Empirical attenuation relationships (MW 6.5, 7.5)					
Abrahamson and Silva (1997)	1.15, 1.15	1.02, 1.02	0.89, 0.89	0.82, 0.82	0.78, 0.78
Boore and others (1997)	1.31, 1.31	—	—	—	—
Campbell and Bozorgnia (1994b), Campbell (1997)	1.21, 1.34	1.12, 1.23	1.01, 1.11	0.95, 1.03	0.88, 0.96
Idriss (1991, 1993)	1.17, 1.17	1.06, 1.05	0.96, 0.95	0.91, 0.91	0.88, 0.87
Sadigh and others (1997)	1.15, 1.34	1.02, 1.15	0.91, 0.99	0.85, 0.91	0.82, 0.86
MEDIAN	1.20, 1.26	1.05, 1.11	0.94, 0.98	0.98, 0.91	0.84, 0.87
MEDIAN (all MW)	1.23	1.08	0.96	0.90	0.85
68% CONFIDENCE INTERVAL (all MW)	1.15–1.31	1.01–1.16	0.89–1.04	0.83–0.97	0.79–0.91
Building-code and engineering applications					
Borcherdt (1994), Borcherdt and Glassmoyer (1994)	1.23	1.23	1.17	1.00	0.90
Proposed 1997 UBC (International Conference of Building Officials, 1996)	1.332	1.273	1.17	1.09	1.00

1Definition of site-classification criteria is given in table 1.
2Corresponds to a hard-rock PHA of 0.075 g.
3Corresponds to average of hard-rock PHA of 0.075 g and 0.15 g.

cal attenuation relationships were developed. The possibility of the last consideration is demonstrated by the empirical predictions of Campbell and Bozorgnia (1994b) and Campbell (1997). These relationships were developed specifically to accommodate an independent scaling of site amplification with distance, thereby minimizing any bias in these factors imposed by arbitrary constraints. The results in table 7 show that the amplification factors predicted by these relationships are greater than those predicted by the other attenuation relationships, but generally consistent with those recommended for building-code and engineering applications.

MODEL VERIFICATION

The validity of the ground-motion models developed in this study was tested by comparing 37 estimates of PHA, PHV, and MMI derived from equations (2) through (4) with values observed on alluvium at sites located within about 250 km of the seismogenic rupture zone (table 8). These sites were specifically selected to sample a wide range of distances and azimuths. A few sites located on Bay mud were included in the comparison to demonstrate the difference between expected and observed ground motions on soft soils located along the margins of San Francisco Bay. Because the MMI-PGA relationship predicts the MMI contour for a given value of PHA, only the integer part of the calculated MMI should be compared with the observed value of MMI. For example, calculated intensities of 6.3 and 6.7 are comparable to an observed MMI of VI (6). To make this comparison easier in table 8, the value of the calculated MMI that should be compared to the observed MMI is given in parentheses after the calculated value.

The following adjustments were made to the predicted ground motions for Bay mud sites located in San Francisco and Redwood City to account for the presence of soft soils. Estimates of PHA from equation (2) were adjusted by the relative difference between peak accelerations recorded on soft soils (SC-IV, S_E) and those recorded on alluvium (SC-III, S_D) based on charts given by Seed and Idriss (1982) and Idriss (1990). Estimates of PHV from equation (4) were increased by a factor of 1.7 based on site-amplification factors developed by Campbell (1992). Estimates of MMI from equation (3) were increased by one intensity unit based on the expected difference in intensity between firm soils (Ground-Shaking Unit L) and soft soils (Ground-Shaking Unit J) recommended by Evernden and Thomson (1988). As discussed below, predictions at several other localities were also adjusted to reflect the unusually large ground motions and intensities observed at these locations during the earthquake.

Strong-motion recordings obtained during the earthquake clearly showed that sites located on Bay mud had, on average, significantly higher ground motions than those located on alluvium or rock (see Boore and others, 1989; Campbell, 1991; Borcherdt and Glassmoyer, 1992, 1994). There were, however, some notable exceptions to these observations. For example, accelerograms recorded on Bay mud at Foster City and near the Dumbarton Bridge had peak accelerations similar to those recorded on nearby alluvial sites.

Table 8.—*Comparison of predicted and observed values of MMI, PHA, and PHV*

[MMI, Modified Mercalli intensity; PHA, mean peak horizontal acceleration; PHV, mean peak horizontal velocity; R_S, closest distance to seismogenic rupture zone, Pred., predicted; Obs., observed or recorded; —, no value reported]

Location	R_S	MMI		PHA (*g*)		PHV (cm/s)	
	(km)	Pred.[1]	Obs.	Pred.	Obs.	Pred.	Obs.
Corralitos	5	8.4 (8)	8	0.56	0.57	50	51
Los Gatos	6	8.2 (8)	8	0.46	—	52	—
Watsonville	11	7.9 (8)	8	0.33	0.33	37	44
Santa Cruz	20	8.3 (8)	8	0.51	0.50	57	—
Hollister	28	8.4 (8)	8	0.26	0.27	36	47
Oakland (Bay mud, Merritt Sand)	72	7.9 (8)	7-8	0.17	0.22	22	29
Oakland (alluvium)	72	6.8 (6)	6-7	0.11	—	13	—
San Francisco (Bay mud)	75	7.8 (7)	7-8	0.17	0.15	21	18
San Francisco (alluvium)	75	6.8 (6)	6-7	0.11	0.11	12	14
Gilroy	11	7.9 (7)	7	0.32	0.27	36	34
Morgan Hill	15	7.6 (7)	7	0.23	—	22	—
San Jose	19	7.5 (7)	7	0.20	0.16	19	19
Palo Alto	31	7.6 (7)	7	0.24	0.29	27	33
Salinas	32	7.3 (7)	7	0.17	0.10	19	13
Redwood City (alluvium)	35	7.5 (7)	7	0.22	—	25	—
Redwood City (Bay mud)	35	8.5 (8)	—	0.29	0.25	42	45
Fremont	40	7.1 (7)	7	0.14	0.12	15	9
San Mateo	51	7.2 (7)	7	0.16	—	18	—
San Bruno	61	7.1 (7)	6-7	0.14	0.13	15	15
San Leandro	61	7.0 (7)	6-7	0.13	—	15	—
Hayward	53	7.0 (7)	6	0.14	0.16	15	13
Livermore	58	6.3 (6)	6	0.07	0.07	7	—
Los Banos	74	6.3 (6)	6	0.07	0.05	8	—
Walnut Creek	79	6.3 (6)	6	0.07	0.07	7	9
Tracy	79	5.9 (5)	6	0.05	0.06	5	—
Greenfield	81	6.2 (6)	6	0.07	0.08	8	—
Richmond	88	6.6 (6)	6	0.09	0.12	10	16
Napa	125	5.8 (5)	6	0.05	0.03	5	—
Stockton	105	5.4 (5)	5-6	0.04	—	6	—
Modesto	95	5.6 (5)	5	0.04	—	4	—
Santa Rosa	152	5.6 (5)	5	0.04	0.05	5	—
Sacramento	160	4.6 (4)	4-5	0.02	—	2	—
Fresno	170	4.8 (4)	3-5	0.02	—	3	—
Coalinga	150	5.1 (5)	4	0.03	—	3	—
Paso Robles	172	4.7 (4)	4	0.02	—	3	—
Ukiah	240	4.2 (4)	4	0.02	—	2	—
Santa Maria	250	3.7 (3)	4	0.01	—	1	—
Marysville	220	3.7 (3)	3	0.01	—	1	—

[1]Value in parentheses indicates number to be compared with observed value.

There were also several sandy sites that exhibited amplifications comparable to those on Bay mud. One such site—a two-story office building in downtown Oakland—is founded on Merritt Sand, a Pleistocene deposit of saturated dune sand that overlies older bay sediments. These observations together with those noted above have led some investigators (see Shakal and others, 1990; Hanks and Brady, 1991) to suggest that the response of the entire soil column above bedrock, not simply the response of Bay mud and other surficial soft sediments, was responsible for the observed amplification at many of these sites. As discussed previously, several investigators have suggested that critical reflections from within the crust and from the Moho were at least partly responsible for the high ground motions observed in San Francisco and Oakland. However, as discussed below, these critical reflections cannot totally explain the unusual pattern of ground motion and damage observed in parts of San Francisco and Oakland during the mainshock.

MMI observations by Plafker and Galloway (1989) and E.V. Leyendecker (oral commun., 1992) indicate that damage on firm soils on the San Francisco Peninsula north of San Bruno were generally consistent with an MMI of VI, and that areas of saturated fill and Bay mud along the northern and eastern margins of San Francisco were consistent with an MMI of VII with isolated pockets of VIII and IX. The areas of higher intensity coincide with areas of relatively high ground motions observed during postearthquake seismological investigations (Boatwright and others, 1991a, b; Seekins and Boatwright, 1994). In contrast, Stover and others (1990) assigned a uniform MMI of VII to most of the San Francisco Peninsula. E.V. Leyendecker (oral commun., 1992) indicates that this assessment by Stover and others was somewhat conservative and does not reflect the distribution of damage observed from his field reconnaissance.

Recorded ground motions in downtown Oakland on Merritt Sand were nearly as large as those recorded at nearby sites on Bay mud at the Oakland Harbor Wharf and at Emeryville. Yet, other nearby sites in east Oakland and Berkeley had ground motions significantly smaller than these. Damage in downtown Oakland and along the eastern margin of San Francisco Bay where saturated artificial fill and Bay mud predominate was found to be generally consistent with an MMI of VII with isolated pockets of VIII and IX (Plafker and Galloway, 1989; Stover and others, 1990; E.V. Leyendecker, oral commun., 1992). These observations are consistent with the high ground motions and intensities observed on similar sites in San Francisco.

The lower ground motions recorded in Berkeley appear to be inconsistent with both the MMI of VII generally assigned to this area by Stover and others (1990) and the MMI of VI assigned to the area further north near Richmond, where somewhat higher ground motions were recorded. After reviewing his notes, E.V. Leyendecker (oral commun., 1992) suggested that, in his opinion, the area north of downtown Oakland should have been assigned an MMI of VI, more consistent with ground motions and damage observed in east Oakland and Richmond.

Based on the above observations, we adjusted the predicted ground motions for sites located on saturated artificial fill and Bay mud, including those sites located along the northern and northeastern margins of the San Francisco Peninsula, and for sites located on Merritt Sand in downtown Oakland and near Alameda (south of Oakland) to be consistent with the increased ground shaking expected on soft soil.

The region around the city of Hollister was another area that exhibited unusually high ground motions during the earthquake. Stover and others (1990) assigned an MMI of VIII to this area, whereas damage at comparable distances in this same general vicinity was found to be more consistent with an MMI of VII or less. Steidl and others (1991) and Wald and others (1991) were unable to account for these larger than expected ground motions in their seismological models of the main shock and suggested that site effects may have been responsible for the higher ground motions in this area. Because of the strong empirical and theoretical evidence that indicated unusually high site amplification in this area, the predicted ground motions for sites located in the Hollister region were adjusted to be consistent with the increased ground shaking expected on soft soil. This adjustment produces estimates of PHA, PHV, and MMI that are consistent with those observed in the area (table 8).

In conclusion, the comparison shown in table 8 indicates that the ground-motion models developed in this study accurately predict both the peak ground-motion parameters and the Modified Mercalli intensities observed throughout the central California region during the earthquake over a wide range of azimuths and distances.

ACKNOWLEDGMENTS

Dave Hampson, formerly with the U.S. Geological Survey and now with EQE International, Inc., assisted in developing the geologic descriptions of the strong-motion recording sites used in this study. Glen Reagor of the U.S. Geological Survey provided a digital database of MMI observations collected by the USGS. Klaus Jacob of Lamont-Doherty Geological Observatory, Roger Borcherdt of the U.S. Geological Survey, and several anonymous reviewers provided insightful comments that significantly improved the manuscript. The study was initiated at the U.S. Geological Survey and was completed at Dames & Moore and EQE International. The author would like to thank these organizations for their support.

REFERENCES CITED

Abrahamson, N.A., and Silva, W.J., 1997, Empirical response spectral attenuation relations for shallow crustal earthquakes: Seismological Research Letters, v. 68, no. 1, p. 94-127.

Boatwright, J., Fletcher, J.B., and Fumal, T.E., 1991a, A general inversion scheme for source, site, and propagation characteristics using multiply recorded sets of moderate-sized earthquakes: Bulletin of the Seismological Society of America, v. 81, p. 1754-1782.

Boatwright, J., Seekins, L.C., Fumal, T.E., Liu, H.-P., and Mueller, C.S., 1991b, Ground motion amplification in the Marina District: Bulletin of the Seismological Society of America, v. 81, p. 1980-1997.

Boore, D.M., and Joyner, W.B., 1997, Site amplification for generic rock sites: Bulletin of the Seismological Society of America, v. 87, p. 327-341.

Boore, D.M., Seekins, L., and Joyner, W.B., 1989, Peak accelerations from the 17 October 1989 Loma Prieta earthquake: Seismological Research Letters, v. 60, p. 151-166.

Boore, D.M., Joyner, W.B., and Fumal, T.E., 1997, Equations for estimating horizontal response spectra and peak acceleration from western North American earthquakes—a summary of recent work: Seismological Research Letters, v. 68, no. 1, p. 128-153.

Borcherdt, R.D., 1994, Estimates of site-dependent response spectra for design (methodology and justification): Earthquake Spectra, v. 10, p. 617-653.

Borcherdt, R.D., and Gibbs, J.F., 1976, Effects of local geological conditions in the San Francisco Bay region on ground motions and the intensities of the 1906 earthquake: Bulletin of the Seismological Society of America, v. 66, p. 467-500.

Borcherdt, R.D., and Glassmoyer, G., 1992, On the characteristics of local geology and their influence on ground motions generated by the Loma Prieta earthquake in the San Francisco Bay region, California: Bulletin of the Seismological Society of America, v. 82, no. 2, p. 603-641.

———1994, Influences of local geology on strong and weak ground motions recorded in the San Francisco Bay region and their implications for site-specific building-code provisions, *in* Borcherdt, R.D., ed., The Loma Prieta, California, earthquake of October 17, 1989—strong ground motion: U.S. Geological Survey Professional Paper 1551-A, p. 77-108.

Brady, A.G., and Mork, P.N., 1990, The Loma Prieta, California, earthquake, October 18 (GMT), 1989, processed strong-motion records, volume 1: U.S. Geological Survey Open-File Report 90-247.

Brady, A.G., and Shakal, A.F., 1994, Strong-motion recordings, *in* Borcherdt, R.D., ed., The Loma Prieta , California, earthquake of October 17, 1989—strong ground motion: U.S. Geological Survey Professional Paper 1551-A, p. 9-38.

Campbell, K.W., 1981, Near-source attenuation of peak horizontal acceleration: Bulletin of the Seismological Society of America, v. 71, p. 2039-2070.

———1987, Predicting strong ground motion in Utah, *in* Gori, P.L., and Hays, W.W., eds., Assessment of regional earthquake hazards and risk along the Wasatch Front, Utah: U.S. Geological Survey Open-File Report 87-585, v. II, p. L1-L90.

———1988, The Whittier Narrows, California, earthquake of October 1, 1987—preliminary analysis of peak horizontal acceleration: Earthquake Spectra, v. 4, p. 115-137.

———1989, Empirical prediction of near-source ground motion for the Diablo Canyon Power Plant site, San Luis Obispo County, California: U.S. Geological Survey Open-File Report 89-484.

———1990, Empirical prediction of near-source soil and soft-rock ground motion for the Diablo Canyon Power Plant site, San Luis Obispo County, California: Evergreen, Colorado, report prepared for Lawrence Livermore National Laboratory by Dames & Moore.

———1991, An empirical analysis of peak horizontal acceleration for the Loma Prieta, California, earthquake of 18 October 1989: Bulletin of the Seismological Society of America, v. 81, p. 1838-1858.

———1992, Recommended models for predicting strong ground motion and MMI in the San Francisco Bay area: Evergreen, Colorado, report prepared for EQE International Inc. By Dames & Moore.

———1997, Empirical near-source attenuation relationships for horizontal and vertical components of peak ground acceleration, peak ground velocity, and pseudo-absolute acceleration response spectra: Seismological Research Letters, v. 68, no. 1, p. 154-179.

Campbell, K.W. and Bozorgnia, Y., 1994a, Empirical analysis of strong ground motion from the 1992 Landers, California, earthquake: Bulletin of the Seismological Society of America, v. 84, no. 3, p. 573-588.

———1994b, Near-source attenuation of peak horizontal acceleration from worldwide accelerograms recorded from 1957 to 1993, *in* Fifth U.S. National Conference on Earthquake Engineering, Proceedings, Chicago, 1994: Berkeley, California, Earthquake Engineering Research Institute, v. III, p. 283-292.

Catchings, R.D., and Kholer, W.M., 1997, Reflected seismic waves and their effect on strong shaking during the 1989 Loma Prieta, California, earthquake: Bulletin of the Seismological Society of America, v. 80, no. 5, p. 1401-1416.

California Strong Motion Instrumentation Program, 1991a, Plots to accompany tapes LOMAPRIETA89-IG (phase 1 data) and LOMAPRIETA89-G (phases 2 & 3 data), processed strong-motion data from the Loma Prieta earthquake of 17 October 1989, ground-response records: Sacramento, California, Division of Mines and Geology, Strong Motion Instrumentation Program Report No. OSMS 91-06.

———1991b, Plots to accompany tapes LOMAPRIETA89-IB1, -IB2, -IB3 (phase 1 data) and LOMAPRIETA89-IIB1, -IIB2, -IIIB (phases 2 & 3 data), processed strong-motion data from the Loma Prieta earthquake of 17 October 1989, building records: Sacramento, California, Division of Mines and Geology, Strong Motion Instrumentation Program Report No. OSMS 91-07.

———1991c, Plots to accompany tapes LOMAPRIETA89-IL (phase 1 data) and LOMAPRIETA89-L (phases 2 & 3 data), processed strong-motion data from the Loma Prieta earthquake of 17 October 1989, lifeline records: Sacramento, California, Division of Mines and Geology, Strong Motion Instrumentation Program, Report No. OSMS 91-08.

EQE International, Inc., 1995, The Northridge earthquake of January 17, 1994—preliminary report of data collection and analysis; part A, damage and inventory data: Irvine and Pasadena, California, report prepared for the Governorís Office of Emergency Services of the State of California, by EQE International, Inc. and the Geographic Information Systems Group of the Governorís Office of Emergency Services.

Evernden, J.F., and Thomson, J.M., 1988, Predictive model for important ground motion parameters associated with large and great earthquakes: U.S. Geological Survey Bulletin 1838,

Fletcher, J.B., and Boatwright, J., 1991, Source parameters of Loma Prieta aftershocks and wave propagation characteristics along the San Francisco Peninsula from a joint inversion of digital seismograms: Bulletin of the Seismological Society of America, v. 81, p. 1783-1812.

Fumal, T.E., 1991, A compilation of the geology and measured and estimated shear-wave velocity profiles at strong-motion stations that recorded the Loma Prieta, California, earthquake: U.S. Geological Survey Open-File Report 91-311.

Hanks, T.C., and Brady, A.G., 1991, The Loma Prieta earthquake, ground motion, and damage in Oakland, Treasure Island, and San Francisco: Bulletin of the Seismological Society of America, v. 81, p. 2019-2047.

Housner, G.W., 1990, Competing against time, Thiel Jr., C.C., ed., report to Governor George Deukmejian from The Governor's Board of Inquiry on the 1989 Loma Prieta Earthquake: Sacramento, California, State of California, Office of Planning and Research.

International Conference of Building Officials, 1996, Suggested revisions to the 1994 editions of the uniform codes (submittals for 1996): Whittier, California.

Idriss, I.M., 1990, Response of soft soil sites in earthquakes, in Duncan, J.M., ed., H. Bolton Seed Memorial Symposium, Berkeley, California, 1990: Berkeley, University of California Press, v. 2, p. 273-289.

———1991, written communication to Thomas F. Blake, Newberry Park, California.

———1993, Procedures for selecting earthquake ground motions at rock sites: Gaithersburg, Maryland, National Institute of Standards and Technology, Report no. NIST GCR 93-625.

Maley, R., Acosta, A., Ellis, F., Etheredge, E., Foote, L., Johnson, D., Porcella, R., Salsman, M., and Switzer, J., 1989, U.S. Geological Survey strong-motion records from the northern California (Loma Prieta) earthquake of October 17, 1989: U.S. Geological Survey Open-File Report 89-568.

McGarr, A.F., Celebi, M., Sembera, E.D., Noce, T.E., and Mueller, C.S., 1991, Ground motion at the San Francisco International Airport from the Loma Prieta earthquake sequence, 1989: Bulletin of the Seismological Society of America, v. 81, no. 5, p. 1923-1944.

Mohraz, B., and F.E. Elghadamsi, 1989, Earthquake ground motion and response spectra, *in* Naeim, F., ed., The seismic design handbook (Structural Engineering Series): New York, Van Nostrand Reinhold, chapter 2, p. 32-80.

More, J.J., Garbow, B.S., and Hilstrom, K.E., 1980, User guide for MINPACK-1: Argonne, Illinois, Argonne National Laboratory, Report no. ANL-80-74.

Plafker, G., and Galloway, J.P., 1989, Lessons learned from the Loma Prieta, California, earthquake of October 17, 1989: U.S. Geological Survey Circular 1045.

Sadigh, K., Chang, C.-Y., Egan, J.A., Makdisi, F., and Youngs, R.R., 1997, Attenuation relationships for shallow crustal earthquakes based on California strong motion data: Seismological Research Letters, v. 68, no. 1, p. 180-189.

Schneider, J.F., Silva, W.J., and Stark, C., 1993, Ground motion model for the 1989 M 6.9 Loma Prieta earthquake including effects of source, path, and site: Earthquake Spectra, v. 9, p. 251-287.

Seed, H.B., and Idriss, I.M., 1982, Ground motions and soil liquefaction during earthquakes, *in* Agbabian, M.S., ed., Engineering Monographs on Earthquake Criteria, Structural Design, and Strong Motion Records: Berkeley, California, Earthquake Engineering Research Institute.

Seekins, L.C., and Boatwright, J., 1994, Ground motion amplification, geology, and damage from the 1989 Loma Prieta earthquake in the City of San Francisco: Bulletin of the Seismological Society of America, v. 84, p. 18-30.

Shakal, A., Huang, M., Reichle, M., Ventura, C., Cao, T., Sherburne, R., Savage, M., Darragh, R., and Petersen, C., 1989, CSMIP strong-motion records from the Santa Cruz Mountains (Loma Prieta), California, earthquake of 17 October 1989: Sacramento, California, Division of Mines and Geology, Strong Motion Instrumentation Program, Report no. OSMS 89-06.

Shakal, A.F., DeLisle, M.J., Reichle, M.S., and Darragh, R.B., 1990, Strong ground shaking from the Loma Prieta earthquake of 17 October 1989, and its relation to near surface geology in the Oakland area, *in* McNutt, S.R., and Sydnor, R.H., eds., The Loma Prieta (Santa Cruz Mountains) California, earthquake of 17 October 1989: Sacramento, California, Division of Mines and Geology, Special Report 104.

Somerville, P., and Yoshimura, J., 1990, The influence of critical MOHO reflections on strong ground motions recorded in San Francisco and Oakland during the 1989 Loma Prieta earthquake: Geophysical Research Letters, v. 17, p. 1203-1206.

Somerville, P.G., Smith, N.F., and Graves, R.W., 1994, Effect of critical reflections from the Moho on the attenuation of strong ground motion, *in* Borcherdt, R.D., ed., The Loma Prieta, California, earthquake of October 17, 1989—strong ground motion: U.S. Geological Survey Professional Paper 1551-A, p. 67-75.

Steidl, J.H., Archuleta, R.J., and Hartzell, S.H., 1991, Rupture history of the 1989 Loma Prieta, California, earthquake: Bulletin of the Seismological Society of America, v. 81, p. 1573-1602.

Stevens, J.L., and Day, S.M., 1994, Simulation of strong ground motion, *in* Borcherdt, R.D., ed., The Loma Prieta, California, earthquake of October 17, 1989—strong ground motion: U.S. Geological Survey Professional Paper 1551-A, p. 53-60.

Stover, C.W., Reagor, G.R., Baldwin, F.W., and Brewer, L.R., 1990, Preliminary isoseismal map for the Santa Cruz (Loma Prieta), California, earthquake of October 18, 1989 UTC: U.S. Geological Survey Open-File Report 90-18.

Trifunac, M.D., 1976, A note on the range of peak amplitudes of recorded accelerations, velocities and displacements with respect to the Modified Mercalli intensity scale: Earthquake Notes, v. 47, no. 1, p. 9-24.

U.S. Geological Survey Staff, 1990. The Loma Prieta, California, earthquake—an anticipated event: Science, v. 247, p. 286-293.

Wald, D.J., Helmberger, D.V., and Heaton, T.H., 1991, Rupture model of the 1989 Loma Prieta earthquake from the inversion of strong-motion and broadband teleseismic data: Bulletin of the Seismological Society of America, v. 81, p. 1540-1572.

EARTH STRUCTURES AND ENGINEERING CHARACTERIZATION OF GROUND MOTION

ATTENUATION OF VERTICAL AND HORIZONTAL RESPONSE SPECTRA OF THE LOMA PRIETA EARTHQUAKE

By Yousef Bozorgnia, Exponent Failure Analysis Associates, Menlo Park, Calif.; and
Mansour Niazi, Berkeley Geophysical Consultants, Berkeley, Calif.

CONTENTS

ABSTRACT

Ground motion attenuation relationships of vertical and horizontal response spectra for the Loma Prieta earthquake are developed through analyses of the ground motion at 53 sites within a 100 km radius of the source. The analyses are performed on the spectral ordinates for 16 incremental periods ranging from 0.05 to 2.0 seconds. The response spectra are modeled empirically for site conditions characterized by rock and by stiff soil. Data analysis is performed by the application of a nonlinear multivariate regression procedure allowing for distance and site factor as independent variables. Variation of the vertical-to-horizontal (V/H) spectral ratios with wave frequency and distance shows the same behavior as observed previously in the widely separated geographic regions of northeastern Taiwan and east-central Iran. The predicted ratios at sites underlain by stiff soil are generally higher than the commonly used value of two-thirds at high frequencies (>5 Hz) in the near-source region (R<30 km) but reduce to one-half or less at longer periods and farther distances. This behavior is also observed at rock sites; however, it is somewhat less pronounced.

With a faster attenuation of spectral ordinates at higher frequencies, the shape of the response spectrum is found to change with distance. As expected, the spectral attenuation with distance is generally higher for the vertical spectrum than for the horizontal spectrum. The difference is particularly significant at the higher frequency end of the spectrum.

Site amplification factors for stiff soil with respect to rock vary between 1.17 and 1.72 for the horizontal spectrum and between 1.01 and 1.81 for the vertical spectrum. Spectral amplifications at four sites underlain by soft soil and artificial fill are also evaluated. This is done by a comparison of the observed spectra with those predicted for rock sites at corresponding distances. As expected, the resulting amplification factors at soft-soil sites show significant increase relative to those at sites underlain by rock.

INTRODUCTION

The earthquake was the strongest event to occur on this segment of the San Andreas fault since the great San Francisco earthquake of 1906. It caused loss of life and considerable damage in the region, including the collapse of the Cypress section of Interstate Highway 880. The details of source geometry and extent of damage are given in U.S. Geological Survey (1989a), Earthquake Engineer Research Institute (1990), and Housner (1990). The epicentral region was well instrumented, including over a hundred accelerographs which provided an important suite of high-quality triaxial accelerograms. The behavior of the peak ground acceleration (PGA) has previously been studied by Boore and others (1989), Campbell (1991), and Niazi and others (1992). Despite some differences on the interpretation of the results, these studies suggest that the observed horizontal PGA for this earthquake exceeded previous model predictions.

The purpose of this study is to extend the analysis of PGA to the response spectra and to assess the intensity of vertical ground motion in the frequency range of engineering interest. Both vertical and horizontal response spectra are analyzed, and the results are given for sites characterized by rock and by stiff soil.

DATA SOURCE

The database consists of the pseudovelocity response spectra (PSV) calculated at 5 percent of critical damping at 53 sites within 100 km distance of the source as shown in figure 1. Site geology at 22 sites is characterized as rock, 27 as stiff soil (alluvial sites), and 4 as soft soil (Bay mud and artificial fill). The majority of the stations are maintained by the Strong Motion Instrumentation Program (SMIP) project of the California Department of Conservation (Shakal and others, 1989; Huang and others, 1990), and by the U.S. Geological Survey Strong Motion Program (U.S. Geological Survey, 1989b). The spectral ordinates used in this study have been calculated and published by these agencies from bandpass filtered accelerograms.

The analysis is performed at 16 incremental periods ranging between 0.05 and 2.0 s. Vertical PSV's are directly used in the analysis. For the horizontal PSV's , the arithmetic mean of the ordinates derived for the two horizontal components are entered. This is consistent with the previous studies by Niazi and Bozorgnia (1992a) and Campbell (1993). In total, nearly 2,500 spectral ordinates are analyzed. Table 1 gives a list of recording stations used in this study and their site geology. The distances are from the vertical projection of the rupture on the Earth's surface and have been discussed by Boore and others (1989) and Niazi and others (1992). The vertical and horizontal spectral ordinates at periods 0.1 and 0.5 s are also given in table 1.

DATA ANALYSIS

Data analysis was performed by the application of a multiregression procedure (SAS, 1985) with distance and

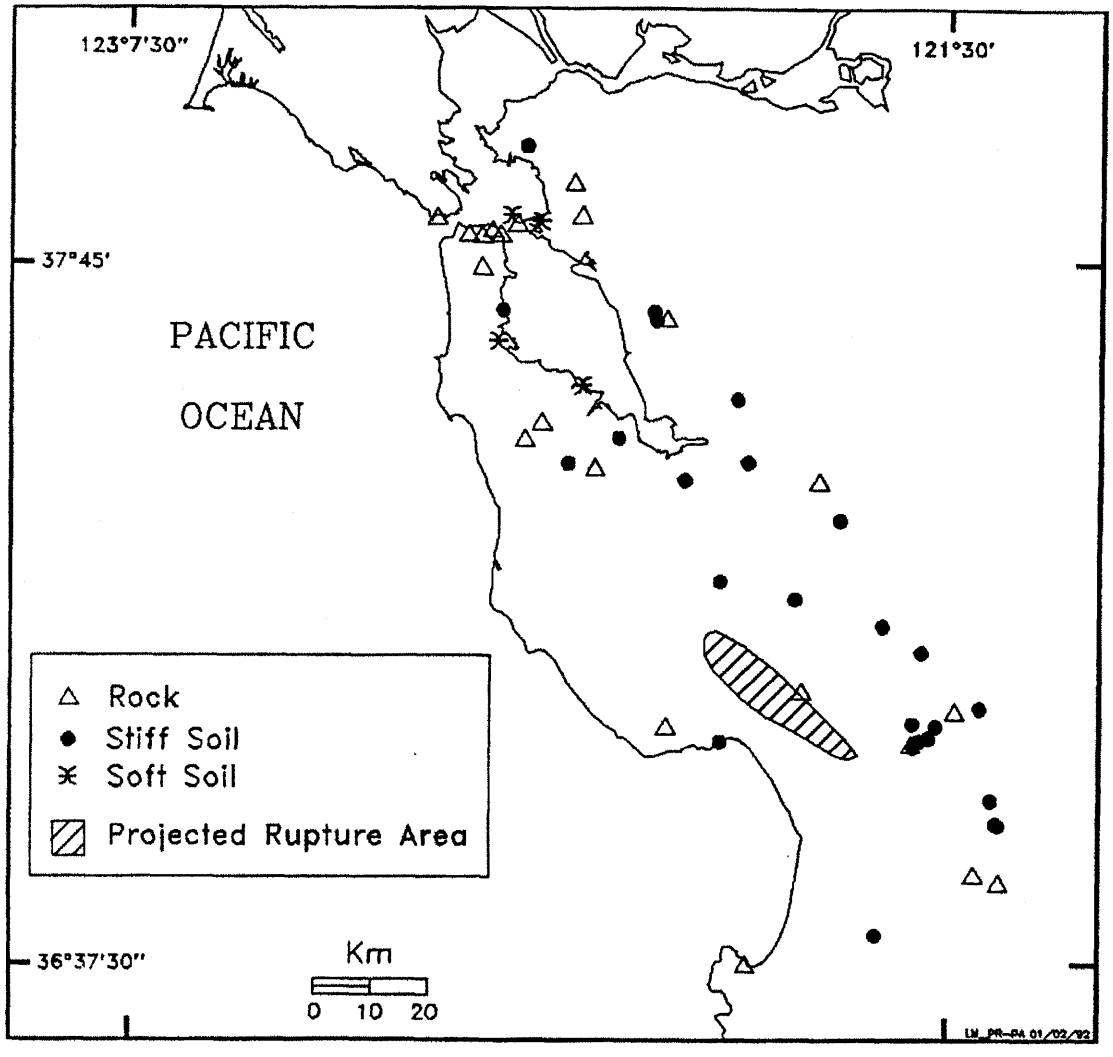

Figure 1.—Locations of 53 recording sites considered in this study. The shaded area is the surface projection of the rupture plane (Boore and others, 1989; Niazi and others, 1992).

Table 1.—*Recording stations used in this study*

Recording stations	Distance (km)	ROCK (**)	Vertical PSV at period 0.1 s (in/s)	Vertical PSV at period 0.5 s (in/s)	HOR. PSV at period 0.1 s (in/s)	HOR. PSV at period 0.5 s (in/s)
Corralitos	0.1	1	5.230	13.600	4.325	37.400
Capitola	8.6	0	8.880	6.610	4.675	24.800
Gilroy#1	10.5	1	1.750	6.670	5.965	26.700
Gilroy G C	10.9	0	2.250	4.770	4.485	18.900
Saratoga	11.7	0	4.720	7.740	4.030	18.500
Gilroy#2	12.1	0	3.070	5.320	3.145	21.850
Gilroy Cm Bldg	12.3	0	2.810	5.270	2.130	18.500
Santa Cruz	12.5	1	8.980	3.880	4.730	12.750
San Js. St.Te.	13.2	0	4.950	6.040	4.545	13.500
Gilroy#3	14.0	0	3.640	7.000	5.980	26.800
Gilroy#4	15.8	0	2.250	3.290	2.545	27.250
Gilroy#6	19.0	1	1.370	3.650	1.825	7.585
Anderson D.ds	20.0	0	1.629	6.276	2.474	16.185
Coyote L ds	21.7	0	1.490	4.960	1.670	11.115
Gilroy#7 MR	24.3	0	1.550	1.630	2.510	18.850
Hollister AP	25.4	0	2.256	4.000	2.042	21.642
Agnews SH	27.0	0	1.240	5.130	1.510	8.340
Sunnyv. Colt.	27.5	0	1.742	3.407	2.029	13.096
Hollister CH	27.8	0	2.058	4.000	1.492	19.407
Hollister W.H	28.3	0	1.750	4.640	2.005	29.150
Hollister S&P	28.3	0	2.610	4.920	1.995	28.400
Halls Valley	29.3	0	.843	6.980	.962	9.725
SAGO Vault	29.9	1	.612	1.796	.570	3.352
Salinas	31.4	0	1.520	2.670	.901	6.235
Milpitas 2s	31.4	0	1.290	2.980	1.035	9.860
Sago S	34.1	1	.467	3.610	.579	5.005
Stanford SLAC	35.0	1	1.885	6.043	2.099	17.526
Calveras Res.	36.1	0	1.026	1.603	.900	4.352
Menlo Park VA	36.5	0	2.696	2.701	1.719	12.268
Woodside	38.7	0	.388	2.000	.597	6.790
Fremont Msj	42.0	0	1.450	4.460	1.185	7.750
Monterey CH	42.7	1	.434	1.480	.783	3.335
U Crystal #7	46.5	1	.681	3.070	.977	6.615
U Crystal 10	46.6	1	.298	3.060	.700	9.290
Foster City	47.3	*	1.650	4.500	1.895	23.900
Hayward JMS	53.6	0	1.250	1.790	1.565	9.830

(*) Sites specified by an asterisk (*) are on soft soil.

(**) Site parameter ROCK is 1 for rock sites and 0 for stiff-soil sites.

Table 1.—Continued

Recording stations	Distance (km)	ROCK (**)	Vertical PSV at period 0.1 s (in/s)	Vertical PSV at period 0.5 s (in/s)	HOR. PSV at period 0.1 s (in/s)	HOR. PSV at period 0.5 s (in/s)
Hayward CSUHFF	56.0	1	.496	2.590	.831	3.740
Hayward BART	57.1	0	.972	3.640	2.240	5.970
SFO	63.2	*	.474	3.750	1.940	21.150
S SF Si.Pt.	67.6	1	.274	2.390	.657	3.775
SF Dim Hights	75.9	1	.409	3.200	.903	7.200
Piedmont Jr.H	77.2	1	.236	1.730	.628	5.745
SF Rincon Hill	78.5	1	.328	2.590	.825	4.445
Oaklnd O Har W	78.8	*	.705	4.360	1.830	18.400
Yerba Buena I	79.5	1	.230	2.090	.425	3.320
SF Pac Hights	80.5	1	.198	2.220	.409	2.980
SF Tel Hill	80.9	1	.234	1.870	.536	4.145
Tresure I	81.7	*	.113	.574	.937	9.700
Presidio	81.9	1	.462	3.780	1.096	11.520
LBL #1	83.2	1	.245	2.980	.547	6.025
SF Cliff House	83.2	1	.385	4.460	.600	6.685
Pt. Bonita	87.5	1	.240	1.700	.539	5.625
Richmond CH	92.0	0	.373	2.370	.915	6.615

(*) Sites specified by an asterisk (*) are on soft soil.
(**) Site parameter ROCK is 1 for rock sites and 0 for stiff-soil sites.

site geology as independent variables. Hence, as seen in equation (1), the site parameter "s" would allow an adjustment for site geology of PSV for stiff soil relative to rock.

$$\ln (\mathrm{PSV}) = a + d * \ln (R + c) + s * \mathrm{ROCK} + \varepsilon (0, \sigma^2) \quad (1)$$

In this equation R is distance in kilometers, PSV is pseudovelocity spectral ordinate in inches/second, ROCK is a site variable which has a value of 1 for rock and 0 for stiff soil, and a, c, d, and s are regression parameters. The input to the regression is confined only to the information at 49 sites characterized by either rock or stiff soil. The four soft-soil sites are used later for the evaluation of the amplification due to soft soil material. In equation (1) ε represents random error with zero mean and σ^2 variance.

A nonlinear regression procedure (SAS, 1985) is applied to the spectral ordinates at each of the 16 frequencies. A subjective weighting method is introduced to compensate for the concentration of the observations within specific distance bins. Because the employed methodology and the set up is similar to the one used in the study of PGA behavior by Niazi and others (1992), for further detail the reader is referred to that study.

DISTANCE-DEPENDENT RESPONSE SPECTRA

The numerical results for the regression parameters derived for the horizontal and vertical components are given in tables 2 and 3, respectively, as functions of period. Figure 2 shows the attenuation of the 5 percent damped vertical and horizontal response spectra at a period of 0.1 s for sites with stiff soil geology. The observed spectral ordinates for stiff soil sites are also marked in figure 2. Figures 3 and 4 show the attenuation of spectra at 0.5 and 1.0 s, respectively. It is evident from figures 2 through 4 that the magnitude of the vertical and horizontal spectral ordinates are comparable at the short period (0.1 s), while at the longer periods the horizontal spectra exceed those for vertical motion. This is due to the fact that the vertical ground motion is in general enriched in the higher frequency waves relative to the horizontal component. Thus, at the short period end of the spectrum, the vertical motion is pronounced. At longer periods, however, the vertical motion does not contain enough energy to strongly excite a long-period oscillator; therefore, as shown in fig-

Table 2.—*Computed parameters of regression analysis for horizontal response spectra*

	T(s)	a	c	d	s	sigma
1	0.05	2.882	7.666	-0.924	-0.266	0.372
2	0.075	3.791	9.437	-1.008	-0.264	0.369
3	0.10	4.877	13.094	-1.147	-0.268	0.400
4	0.11	5.330	14.990	-1.196	-0.316	0.425
5	0.15	6.118	16.377	-1.257	-0.323	0.433
6	0.20	5.870	12.974	-1.113	-0.378	0.391
7	0.28	5.331.	6.570	-0.932	-0.203	0.427
8	0.30	5.290	6.324	-0.908	-0.164	0.418
9	0.40	6.020	8.871	-0.997	-0.268	0.422
10	0.50	4.799	3.177	-0.657	-0.380	0.416
11	0.60	4.621	1.619	-0.576	-0.477	0.402
12	0.70	4.351	0.780	-0.480	-0.455	0.449
13	0.80	3.847	0.118	-0.337	-0.500	0.451
14	1.00	3.624	0.548	-0.267	-0.379	0.503
15	1.50	4.560	3.882	-0.529	-0.546	0.576
16	2.00	3.575	1.577	-0.308	-0.528	0.543

Table 3.—*Computed parameters of regression analysis for vertical response spectra*

	T(s)	a	c	d	s	sigma
1	0.05	5.289	12.473	-1.577	-0.486	0.479
2	0.075	7.106	18.134	-1.804	-0.596	0.464
3	0.10	6.898	14.182	-1.688	-0.573	0.471
4	0.11	5.938	10.265	-1.461	-0.563	0.453
5	0.15	6.600	12.728	-1.513	-0.579	0.552
6	0.20	5.449	5.624	-1.224	-0.432	0.521
7	0.28	4.479	4.757	-0.954	-0.225	0.356
8	0.30	4.494	6.413	-0.939	-0.138	0.347
9	0.40	4.380	11.148	-0.803	-0.283	0.421
10	0.50	2.884	1.510	-0.460	-0.046	0.336
11	0.60	3.078	4.145	-0.451	-0.094	0.470
12	0.70	2.774	1.738	-0.379	-0.013	0.481
13	0.80	2.506	0.544	-0.301	-0.041	0.437
14	1.00	2.520	0.322	-0.222	-0.240	0.436
15	1.50	3.634	9.837	-0.527	-0.200	0.462
16	2.00	3.327	7.806	-0.479	-0.209	0.576

ures 3 and 4, the amplitude of the vibration in the horizontal direction exceeds that of the vertical motion.

Figure 5 shows the empirically predicted median horizontal response spectra at 10, 20, 40 and 60 km distances from the source, derived from equation (1) by the substitution of the numerical values of the regression, as listed in table 2. Figure 5*A* shows the attenuation of response spectra for stiff soil and 5*B* is for rock. Figure 6 shows similar plots for vertical response spectra based on the coefficients listed in table 3. Figure 6*A* shows the predicted median response spectra at sites underlain by stiff soil and 6*B* shows the same for rock. It should be noted that within the distance range of $R<30$ km, predictions for rock sites are not as tightly constrained as for soil sites, by virtue of fewer recordings (see table 1).

Figures 5 and 6 show that the shape of response spectra (for both vertical and horizontal components) is distance dependent; that is, as distance from the source increases, the spectra gradually become depleted from higher frequency waves in a relative sense. This is evident since the medium between the source and recording site is a dynamic system which acts as a low-pass filter. The suggested distance dependence of the shape of the response spectrum clearly indi-

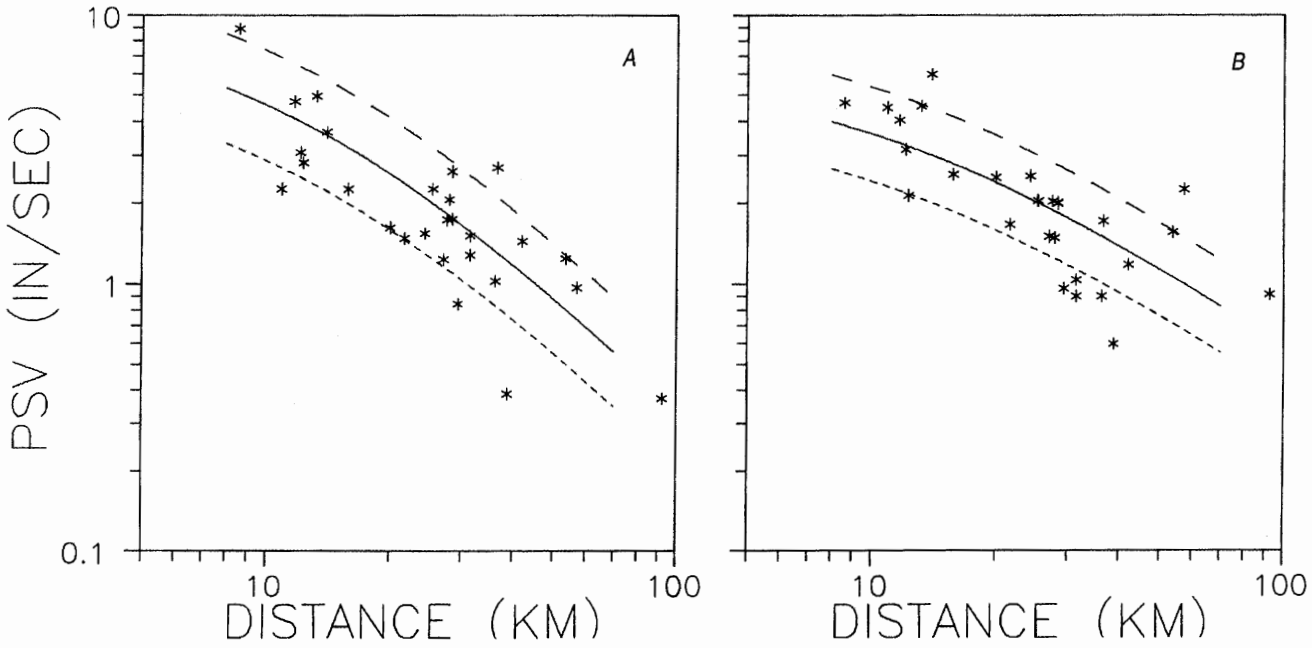

Figure 2.—Attenuation of 5 percent damped vertical (*A*) and horizontal (*B*) response spectra at a period of 0.1 s for stiff soil sites. Solid curve is for the median spectrum. One standard deviation band is shown by the dashed curves. The observed spectral ordinates are also marked.

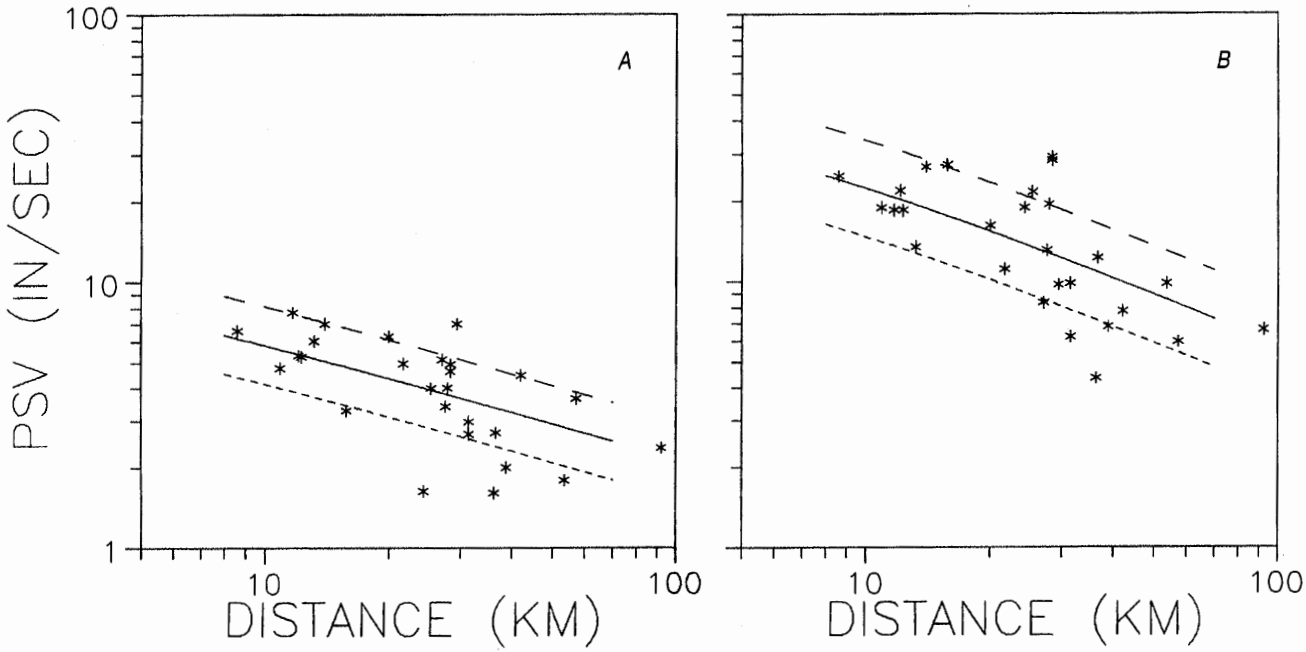

Figure 3.—Attenuation of 5 percent damped vertical (*A*) and horizontal (*B*) spectra at a period of 0.5 s for stiff soil sites. Solid curve is for the median spectrum. One standard deviation band is shown by the dashed curves. The observed spectral ordinates are also marked.

cates that scaling of a standard spectral shape with a single parameter, such as PGA, is not justified. This was also noted by Krawinkler and others (1991) regarding the horizontal spectrum.

Comparison of figures 5*A*and 5*B* shows that the spectral ordinates at stiff-soil sites are generally larger than those at rock sites. This is also true for vertical spectra (fig. 6), except, by different factors. It is also evident from tables 2 and 3 where the site parameter "s" for soil sites is negative for both horizontal and vertical spectra. The resulting amplification factor at stiff-soil sites relative to rock varies between 1.17 and 1.72 for the horizontal spectrum and between 1.01 and 1.81 for the vertical spectrum. Application of the regression procedure to equation (1) at discrete periods results in a site parameter "s" as a function of the wave period. The model adopted in this study, however, does not allow evalu-

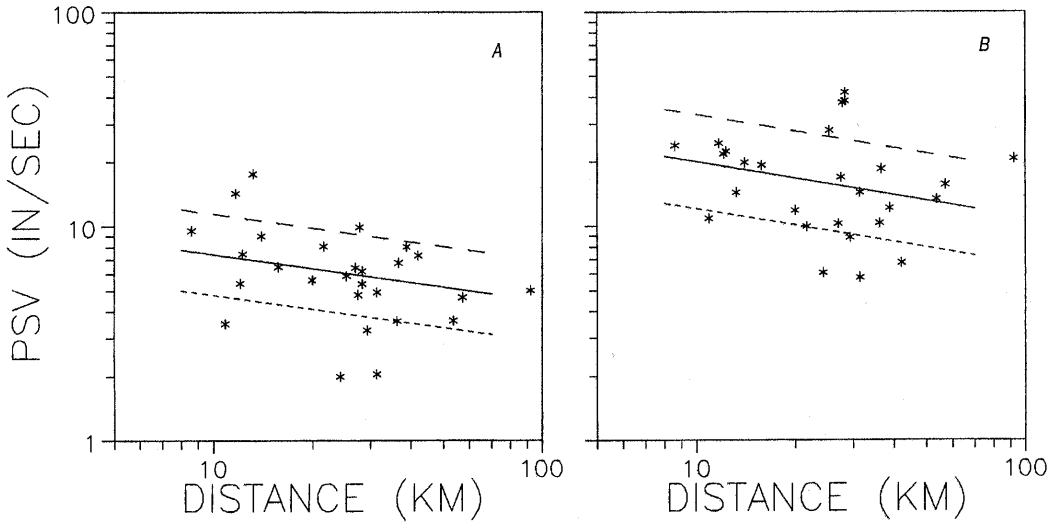

Figure 4.—Attenuation of 5 percent damped vertical (*A*) and horizontal (*B*) spectra at period 1.0 s for stiff soil sites. Solid curve is for the median spectrum. One standard deviation band is shown by the dashed curves. The observed spectral ordinates are also marked.

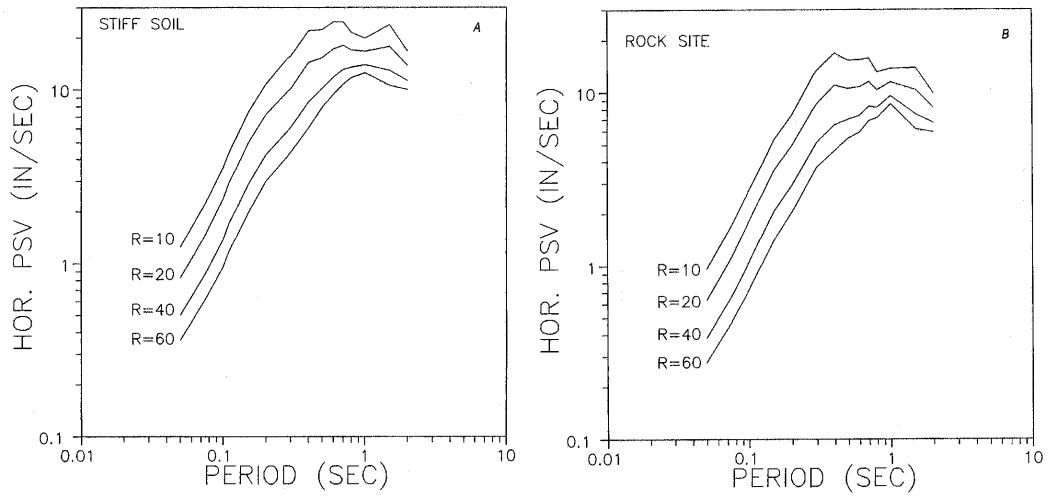

Figure 5.—Attenuation of 5 percent damped spectra: Median horizontal response spectra at distances *R*=10, 20, 40, 60 km from the surface projection of the rupture plane for (*A*) stiff soil and (*B*) rock sites.

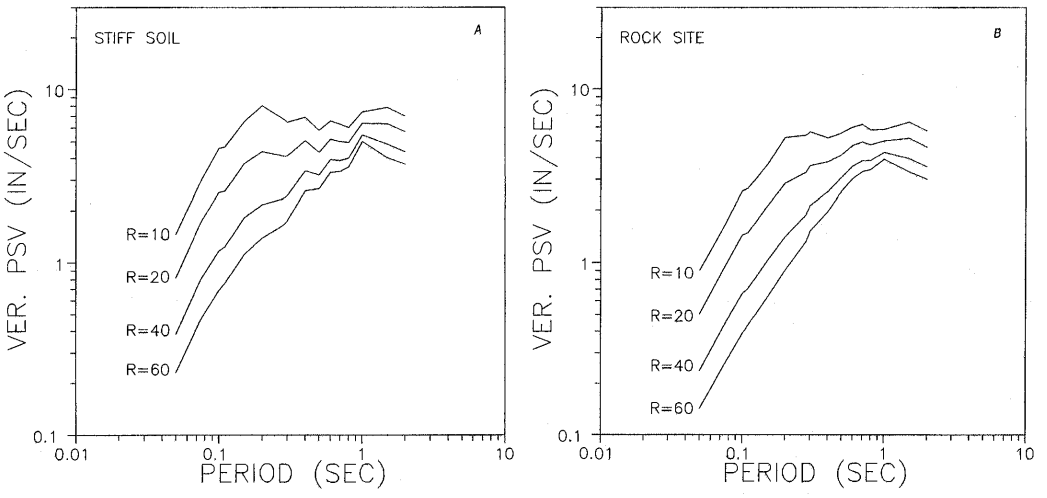

Figure 6.—Attenuation of 5 percent damped spectra: Median vertical response spectra at distances *R*=10, 20, 40, 60 km from the surface projection of the rupture plane for (*A*) stiff soil and (*B*) rock sites.

ation of distance dependence of the parameter "s,"unless, as explained below, independent analyses are performed on the subsets of data collected at rock and soil sites, separately. It is of interest to note that for the vertical spectrum the site amplification factor "s" generally tends to decrease with period, whereas for the horizontal spectrum the trend is reversed, especially for periods longer than about 0.3 s (see tables 2 and 3).

UNIFORM GEOLOGY MODELS

The regression coefficients of tables 2 and 3, and the resulting empirical spectra of figures 5 and 6 are all based on the analyses of the entire data for both stiff soil and rock sites combined. Next, the data files are split into two subsets, one containing stiff-soil data and the other rock data. By doing so we search for possible bias in the predictions at stiff-soil sites which may be introduced by the observations at rock sites and vice versa. As already explained, there are 22 rock sites and 27 sites characterized by stiff soil in the data. Application of the regression procedure given in equation (1), without the soil classification term, to the two data subsets, results in four sets of independent regression coefficients which may somewhat differ from those listed in tables 2 and 3. The resulting empirical models of horizontal and vertical pseudoacceleration spectra (PSA) obtained from the two procedures are compared in figures 7 and 8, respectively.

Figure 7*A* compares the horizontal acceleration spectra for the subset of data observed at stiff-soil sites (dashed curves) and for the combined data (solid curves) at 10, 20, 40 and 60 km. Figure 7*B* shows the same comparison at rock sites. Corresponding plots for the vertical component are shown in figure 8, in which again figure 8*A* compares the predictions of stiff-soil observations with those of the combined data and figure 8*B* compares those of rock observations and the entire data. It is noted that the largest separation between the dashed and solid curves occurs at near-source distances of up to 10 km, where very few observations exist, especially for rock sites. To provide a scale for the comparison, in each example we have also plotted the mean plus sigma (84.1 percent probability) of predictions at 10 km distance for the combined set. In comparison with one sigma, even the largest observed differences between the prediction results are thus relatively small and the models based on the entire data are confirmed.

VERTICAL-TO-HORIZONTAL SPECTRAL RATIOS

Using the regression parameters of tables 2 and 3, vertical-to-horizontal ratios (V/H) of the predicted response spectra at four given distances of 10, 20, 40 and 60 km are derived and shown in figure 9. It is clear from figure 9 that V/H spectral ratio is distance—as well as frequency—dependent. The highest ratios are observed for the high-frequency motion in the near-source region (Niazi and Bozorgnia, 1992b). At more distant sites, the spectral ratios decrease apparently due to a faster rate of attenuation for the

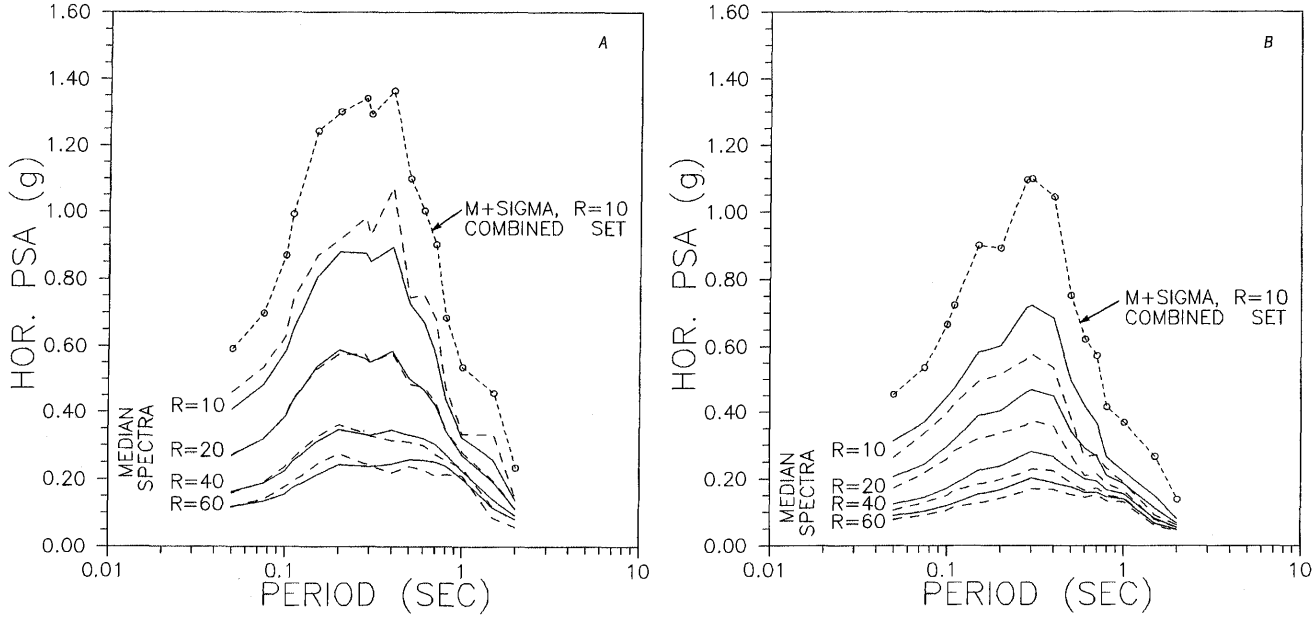

Figure 7.—Comparison of the results of two regression analyses on the spectral ordinates: median horizontal response spectra at distances R=10, 20, 40, 60 km for (*A*) stiff soil and (*B*) rock sites. Solid curves are for the application of equation (1) to the combined soil and rock data and assigning proper value for variable "ROCK." Dashed curves are for the analysis of (*A*) soil data only and (*B*) rock data only. The 84th percentile spectra for R=10 km of the combined analysis are also shown.

high-frequency-rich vertical motion as compared to the low-frequency horizontal component.

The observed variation with frequency and distance at stiff-soil sites (fig. 9*A*) shows similar behavior as those reported previously at stiff-soil sites in widely separated geographic regions of northeastern Taiwan and east-central Iran (Niazi and Bozorgnia, 1992a). Spectral ratios generally exceed the commonly used value of two-thirds at periods shorter than 0.2 s, particularly at near-source distances of $R < 30$ km. The ratios, however, fall below one-half at longer periods for all distances; that is, the use of two-thirds factor would likely result in overconservatism at long periods. Spectral

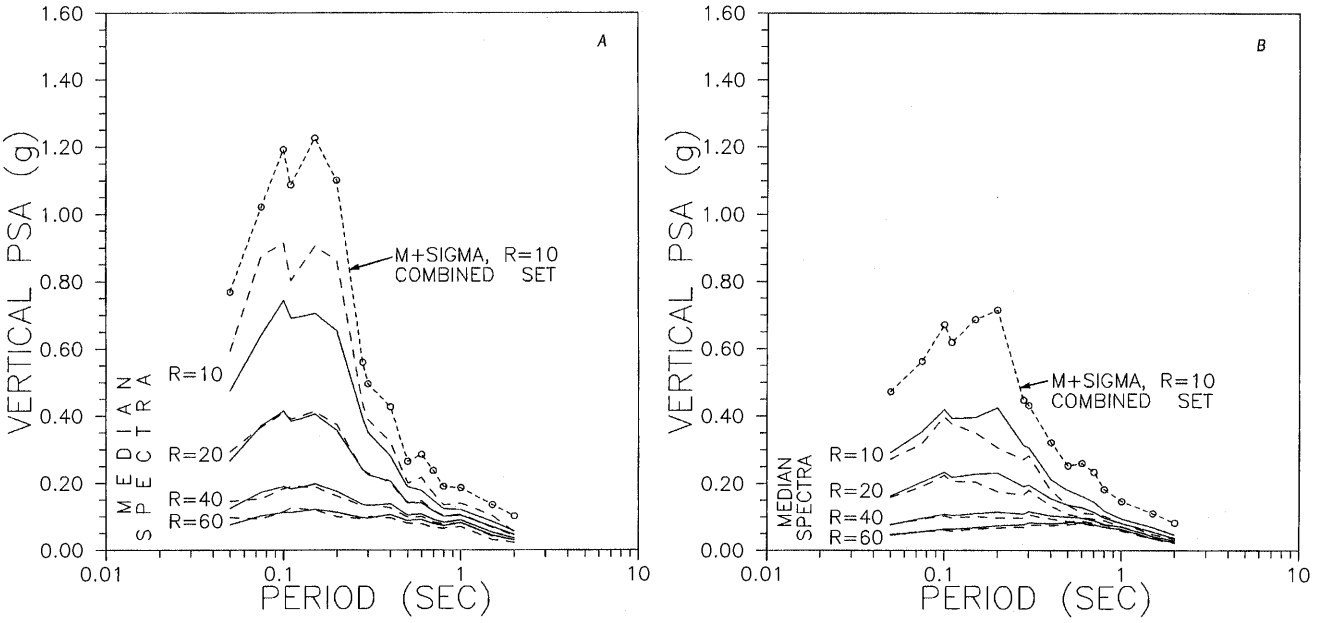

Figure 8.—Comparison of the results of two regression analyses on the spectral ordinates: Median vertical response spectra at distances R=10, 20, 40, 60 km for (*A*) stiff soil and (*B*) rock sites. Solid curves are for the application of equation (1) to the combined soil and rock data and assigning proper value for variable "ROCK." Dashed curves are for the analysis of (*A*) soil data only and (*B*) rock data only. The 84th percentile spectrum for R=10 km of the combined analysis is also shown.

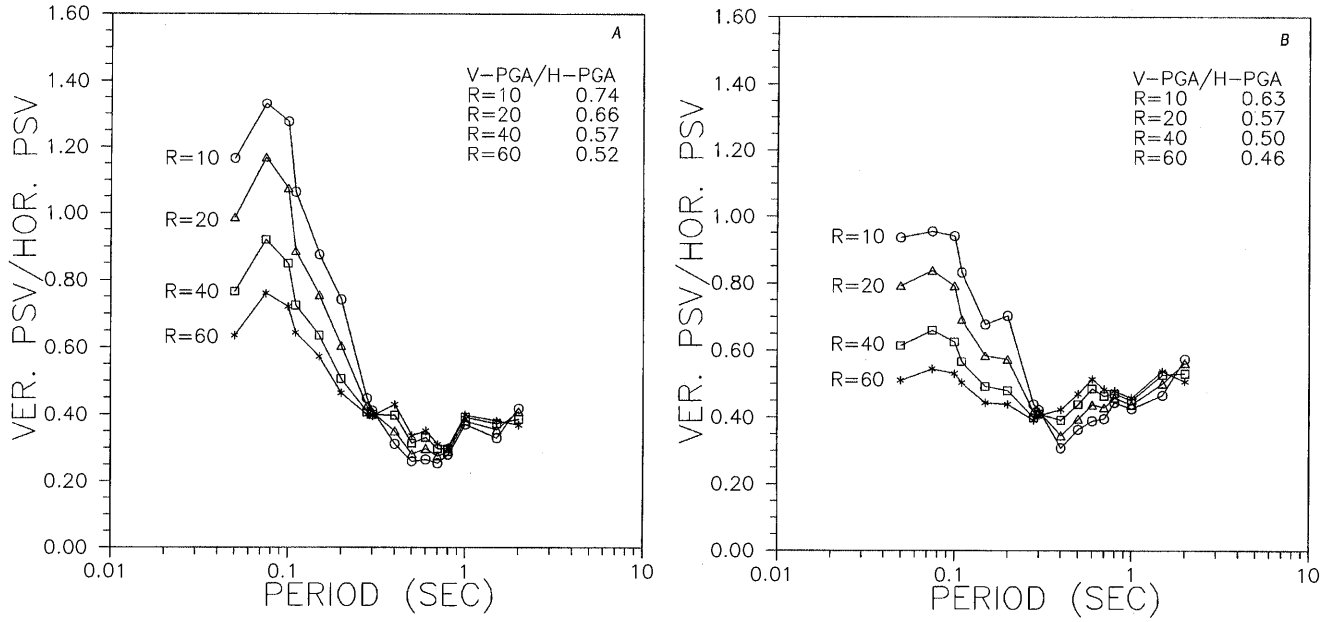

Figure 9.—Ratio of predicted vertical to horizontal spectral ordinates at distances R=10, 20, 40, and 60 km from the source at (*A*) stiff soil and (*B*) rock sites. Regression was performed on the combined soil and rock data set. The ratios of vertical to horizontal PGA's are also given (Niazi and others, 1992).

ratios for different distances converge to a common point at a period of about 0.3 s, where the ratio becomes independent of distance at a value of 0.4.

The same behavior is also observed at rock sites (fig. 9*B*), however, not as pronounced as for soil. The V/H spectral ratios at stiff-soil sites are larger than those at rock sites for periods shorter than 0.4 s, and slightly less for longer periods. The predicted values of the V/H ratio of PGA for this earthquake are also listed in the insets of figures 9A and 9B for the corresponding site geology. These values are based on the empirical predictions of Niazi and others (1992).

We offer the following preliminary explanation for the observed variation of the V/H spectral ratio. Since the vertical motion is enriched in higher frequencies, it will be attenuated at a faster pace. The behavior of V/H spectral ratio is due to the combination of two factors. The first factor is the differential attenuation of higher frequency P waves (predominantly vertical) relative to shear waves. The second factor is the ray geometry, whereby at short distances the high-frequency P waves have a larger vertical component than shear waves, owing to a near-vertical incidence and alignment of particle motion with the direction of propagation.

The V/H spectral behavior observed in several regions, over a wide range of peak accelerations, therefore appears to be real. The existence of deep sedimentary cover (stiff soil) apparently accentuates this behavior. Whether the nonlinear response of the soil has an influence is not clear. Observations by Darragh and Shakal (1991) of the main shock and several aftershocks at the Treasure Island site clearly demonstrate that horizontal response at sites underlain by soft sedimentary material and artificial fill is modified substantially by the nonlinear behavior of the soil. However, the same authors failed to detect a similar effect at the Gilroy#2 station with stiff-soil geology.

SPECTRAL AMPLIFICATION OF SOFT SOIL

In order to evaluate site amplification at stations underlain by soft soil, the observed response spectra at four sites with soft-soil geology are compared with the predictions of our empirical results at rock sites, computed at corresponding distances. These four sites are denoted by asterisk (*) in table 1. Figure 10 shows the result of this comparison at individual sites for both horizontal and vertical components. The observed site amplifications of horizontal spectra, as seen in figure 10A, show similar features at the four sites considered here. Spectral ratios show a gentle negative trend approximately up to the 0.2-s period. For the Oakland Wharf, Treasure Island, and Foster City sites, amplification peaks occur at 0.6-0.7-s and 1.5-s periods. For the San Francisco Airport (SFO), these peaks occur at shorter periods, implying a thinner soft-soil column.

The peak horizontal spectral amplification varies between 4.5 and 7 at these four sites. Darragh and Shakal (1991) also found a peak Fourier spectral ratio of 4 for the strong phase of the horizontal motion at Treasure Island relative to the neighboring rock site at Yerba Buena Island. However, they also noted that the observed site response is systematically higher for smaller magnitude aftershocks.

Site amplification for the vertical component (figure 10*B*) is generally smaller than that of horizontal component. Except for the 1.5-s peak at the Oakland Wharf with an ampli-

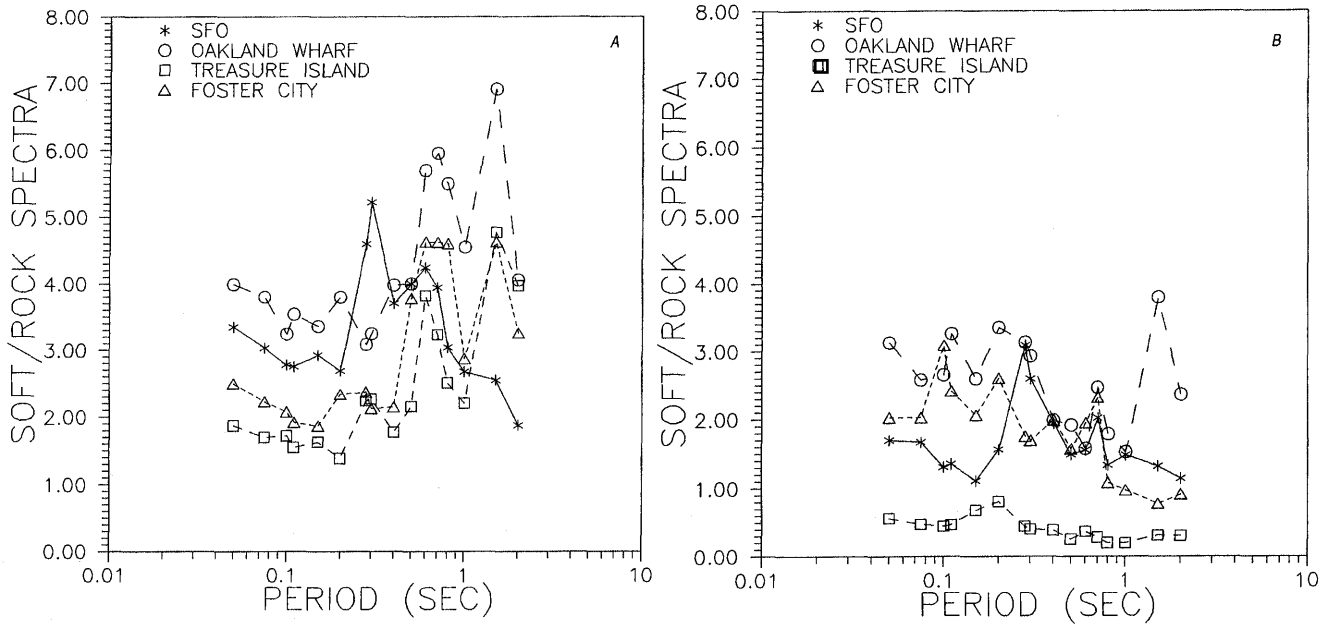

Figure 10.—Ratio of observed spectra at soft-soil sites over predicted spectra at rock sites for (*A*) horizontal and (*B*) vertical ground motion.

fication factor of 3.8, peak amplifications occur predominantly at periods shorter than 0.3 s. As already reported by Niazi and others (1992), the vertical component at the Treasure Island site shows deamplification rather than amplification.

DISCUSSION OF RESULTS

Previous studies of a more extensive database recorded at SMART-1 array, Taiwan (Niazi and Bozorgnia, 1989a, 1989b, 1992a), showed, for the first time, a strong dependence of V/H spectral ratios on both distance and wave frequency. Some of the suggestions emerging from that study are as follows:

1.The shape of the response spectra for both vertical and horizontal components of the ground motion, and their ratio, is distance—as well as magnitude—dependent.

2.The V/H spectral ratio at the high-frequency end of the spectrum shows a substantial increase relative to the standard two-thirds value. The increase is particularly significant at near-source distances.

3.At low frequencies and far-field distances, the spectral ratios reduce significantly, such that the two-thirds ratio would become conservative.

Most of these suggestions, with the exception of the magnitude-scaling effects (inapplicable to a single earthquake) also apply to the Loma Prieta observations. A study of the magnitude-scaling effect on this ratio requires simultaneous analysis of several earthquakes over a broad range of magnitude.

Table 3 shows that in general the short-period end of the vertical response spectrum is characterized by higher values of the attenuation parameter d, site amplification parameter s, and to some extent the distance saturation parameter (depth term) c. However, the absolute value of d tends to decrease almost monotonically down to a value of 0.22 at 1 Hz. Below 1 Hz, the long-period noise may become significant. The correlation of attenuation with frequency is expected as a consequence of intrinsic attenuation and scattering. There may also be a slight possibility of a tradeoff between c and d parameters. For the horizontal motion, a similar trend is observed in the variation of the attenuation parameter d and the depth term c; however, vertical motion attenuates much faster at periods below 0.2 s than the horizontal motion (see tables 2 and 3). The same differential attenuation between vertical and horizontal motions was also observed in the analysis of the SMART-1 data below 0.2 s (Niazi and Bozorgnia, 1992a). However, the SMART-1 data showed much higher attenuation at periods above 0.2 s than Loma Prieta for both vertical and horizontal components. Tables 2 and 3 show a tendency for the site-amplification factor to decrease with period for the vertical spectrum but to increase for the horizontal component, especially for periods longer than about 0.3 s.

As recognized by previous investigators, the effects of the vertical ground motion on the response of structures may not always be neglected. For example, as Newmark and Hall (1982) indicated, columns and walls in compression, beams, and other horizontal elements are particularly vulnerable to the vertical component of ground motion. Other examples include the effects on the seismic response of multistory frames (Anderson and Bertero, 1973), concrete gravity dams (Chakrabarti and Chopra, 1973), and reinforced concrete highway bridges (Saadeghvaziri and Foutch, 1991).

In the estimation of near-source vertical ground motion so far, reliance has been placed on the extrapolation of far-field information due to the scarcity of high-quality observations close to the source. Recent studies of SMART-1 data as well as observations of the 1978 Tabas, Iran, and the Loma Prieta earthquakes made it possible to quantify the range of distances and frequencies where the vertical ground motion is pronounced.

ACKNOWLEDGMENTS

The authors wish to thank the U.S. Geological Survey and California Department of Conservation for providing the accelerograms used in this study. Copyright release provided by John Wiley & Sons, Ltd, is also acknowledged.

REFERENCES

Anderson, J.W., and Bertero,V.V., 1973, Effects of gravity loads and vertical ground acceleration on the seismic response of multistory frames, *in* Proceedings of the Fifth World Conference on Earthquake Engineering, Rome, p. 2914-2923.

Boore, D.M., Seekins, L., and Joyner,W.B., 1989, Peak accelerations from the 17 October 1989 Loma Prieta earthquake: Seismological Research Letters, v. 60, no. 4, p.151-166.

Campbell, K.W., 1991, An empirical analysis of peak horizontal acceleration for the Loma Prieta, California earthquake of October 18, 1989: Bulletin of the Seismological Society of America, v. 81, no. 5, p. 1838-1858.

———1993, Empirical prediction of near-source ground motion from large earthquakes, *in* International workshop on earthquake hazard and large dams in Himalaya.

Chakrabarti, P., and Chopra, A.K. 1973, Hydrodynamic pressures and response of gravity dams to vertical earthquake component: Earthquake Engineering and Structural Dynamics, v. 1, p. 325-335.

Darragh, R.B., and Shakal, A.F., 1991, The site response of two rock and soil station pairs to strong and weak ground motion: Bulletin of the Seismological Society of America, v. 81, no. 5, p. 1885-1899.

Earthquake Engineering Research Institute, 1990, Loma Prieta Earthquake Reconnaissance Report, Supp. Earthquake Spectra, v. 6.

Housner, G.W., 1990, Competing against time; report to Governor G. Deukmejian, Board of Inquiry on the 1989 Loma Prieta earthquake: The State of California, Office of Planning and Research, Sacramento.

Huang, M.J., Cao, T.Q.,Vetter, U.R., and Shakal, A.F.,1990, Third interim set of CSMIP processed strong-motion records from the Santa Cruz Mountains (Loma Prieta), California, earthquake of 17 October 1989: California Strong Motion Instrumentation Program, California Department of Conservation, Division of Mines and Geology, Report No. OSMS 90-05.

Krawinkler, H., Nasser, A., and Rahnama, M., 1991, Damage potential of Loma Prieta ground motions: Bulletin of the Seismological Society of America, v. 81, no. 5, p.2048-2069.

Newmark, N.M., and Hall, W.J., 1982, Earthquake spectra and design: Earthquake Engineering Research Institute.

Niazi, M., and Bozorgnia, Y.,1992a, Behavior of near-source vertical and horizontal response spectra over SMART-1 array, Taiwan: Earthquake Engineering and Structural Dynamics, v. 21, p. 37-50.

———1992b, Vertical response spectra of Loma Prieta earthquake as functions of distance and site geology: Seismological Research Letters, v. 63, no. 1.

———1989a, Behavior of vertical ground motion parameters in the nearfield: Seismological Research Letters, v. 60, no. 1, January-March 1989.

———1989b, Empirical modeling of site specific response spectra for Lotung, Taiwan, *in* Proceedings of International Association of Seismology and Physics of the Earth's Interior, Istanbul, August 1989.

Niazi, M., Mortgat, C.P., and Schneider, J.F., 1992, Attenuation of peak ground acceleration in Central California from observations of the October 17, 1989 Loma Prieta earthquake: Earthquake Engineering and Structural Dynamics, v. 21, p. 493-507.

Saadeghvaziri, M.A., and Foutch, D.A., 1991, Dynamic behavior of R/C highway bridges under the combined effect of vertical and horizontal earthquake motions: Earthquake Engineering and Structural Dynamics, v. 20, p. 535-549.

SAS, 1985, User's Guide; Statistics, Version 5: SAS Institute, Cray, N.C.

Shakal, A., Huang, M., Reichle, M., Ventura, C., Cao, T., Sherburne, R., Savage, M., Darragh, R., and Petersen, C., 1989, CSMIP strong-motion records from the Santa Cruz Mountains (Loma Prieta), California, earthquake of 17 October 1989, Report No. OSMS 89-06: California Strong Motion Instrumentation Program, California Department of Conservation, Division of Mines and Geology.

U.S. Geological Survey, 1989a, Loma Prieta, California earthquake: an anticipated event: Science, v. 247, p. 286-293.

———1989b, Strong-motion records from the Northern California (Loma Prieta) earthquake of October 17, 1989: U.S. Geological Survey Open-File Report 89-568.

☆ U.S. GOVERNMENT PRINTING OFFICE: 1998 — 773-051 / 20126 Region No. 8